The *eta7/csn3-3* auxin response mutant of Arabidopsis defines a novel function for the CSN3 subunit of the COP9 signalosome

A DISSERTATION
SUBMITTED TO THE FACULTY OF THE GRADUATE SCHOOL
OF THE UNIVERSITY OF MINNESOTA
BY

He Huang

IN PARTIAL FULFILLMENT OF THE REQUIREMENTS
FOR THE DEGREE OF
DOCTOR OF PHILOSOPHY

Advised by: Dr. William M. Gray

July. 2012

Acknowledgements

This research was supported by the NIH (National Institutes of Health) Foundation and the Plant Biological Sciences (PBS) Program Summer Fellowship.

I would like to give my great thanks to my advisor Dr. William Gray for his enormous and exceptional guidance and support during my Ph.D. thesis research and training. He deeply impresses me as a creative, passionate and diligent scientist and has been a role model for my career path. I'd also like to appreciate him for his patience and guidance on helping me with scientific writings and presentations.

I would like to thank members of my advisory committee, Dr. Jerry Cohen, Dr. Neil Olszewski, Dr. Fumiaki Katagiri, Dr. Min Ni and Dr. Carolyn Silflow for their valuable suggestions and support for my research. In particular, Dr. Jerry Cohen generously provided the Mixer-Mill vibration mill for homogenizing plant tissues. Dr. Neil Olszewski gave me valuable suggestions at each joint-lab meeting. Dr. Fumiaki Katagiri generously provided me the HPB vector. Dr. Min Ni generously provided the Red/Far Red light incubator.

I'd like to thank members in Dr. William Gray's lab who have supported my research in many ways and given good suggestions about my research, particularly thank Dr. Wenjing Zhang for patiently teaching me to use the FPLC system. I'd also like to acknowledge the Plant Biological Sciences (PBS) Program for offering me the opportunity to study here and assisting me through my Ph.D. training. I would appreciate people in the department who have been great help to me. In particular, Dr. Nora Plesofsky and Dr. Robert Brambl generously provided the Transphor Electrophoresis

Unit. Dr. Debby Samac generously provided the BioTek FL600 Fluorescence Microplate Reader.

I'd like to give special thanks to my parents, Jianli and Kelin; my friends and colleagues, Yun, Xiaodong, Xiaoqing, Wenjing and Xing. Their care and support to me has been an important part of my life here in Minnesota.

Others' contribution to this work: Dr. Marcel Quint mapped the *csn1-10* and *csn3-3* mutation. Dr. William Gray developed the CSN1 and CSN3 antibodies. Dr. Xing-Wang Deng from Yale University generously provided the CSN1, CSN3 and CUL4 antibodies. Dr. Lucia Strader from Washington University in St. Louis generously provided the IAA28-myc construct and transgenic plants.

Dedication

This dissertation is dedicated to my beloved parents, Jianli and Kelin. Without their unconditional love, care and motivation, I will never achieve my goals.

Abstract

The COP9 signalosome (CSN) is an eight subunit protein complex conserved in all higher eukaryotes. In *Arabidopsis thaliana*, the CSN regulates plant auxin response by removing the ubiquitin-like protein NEDD8/RUB1 from the CUL1 subunit of the $SCF^{TIR1/AFB}$ ubiquitin-ligase (deneddylation). Previously described null mutations in any CSN subunit resulted in the pleiotropic *cop/det/fus* phenotype and caused seedling lethality, hampering the study of CSN functions in plant development. In a genetic screen to identify enhancers of the auxin response defects conferred by the *tir1-1* mutation, we identified a viable *csn* mutant of subunit 3 (CSN3), designated *eta7/csn3-3*. In comparison with *eta6/csn1-10*, which was identified in the same enhancer screen (Zhang et al., 2008), both *csn3-3* and *csn1-10* enhanced the auxin response defects of *tir1-1*. Similar to *csn1-10*, *csn3-3* also confers several phenotypes associated with impaired auxin signaling, including auxin resistant root growth and diminished auxin responsive gene expression. Surprisingly however, unlike *csn1-10* as well as other previously characterized *csn* mutants, *csn3-3* plants are not defective in either the CSN-mediated deneddylation of CUL1 or in $SCF^{TIR1/AFB}$ mediated degradation of Aux/IAA proteins. These findings suggest that *csn3-3* is an atypical *csn* mutant that defines a novel CSN or CSN3-specific function. Consistent with this possibility, I observed dramatic differences in double mutant interactions between *csn3-3* and other auxin signaling mutants compared to *csn1-10*. Lastly, unlike other *csn* mutants, assembly of the CSN holocomplex was unaffected in *csn3-3* plants. However, I detected a small CSN3-containing protein complex (sCSN3c) that was altered in *csn3-3* plants. I hypothesize that

in addition to its role in the CSN as a cullin deneddylase, CSN3 functions in a smaller protein complex that is required for proper auxin signaling. Analyses on the purification of sCSN3c suggested that it is not likely a dimer of CSN3, or a CSN subcomplex. My data resulting from sCSN3c purification using various chromatographic steps provide useful information necessary for identifying the components of the complex.

Table of Contents

List of Figures

Chapter One: Literature Review

I. The Ubiquitin/proteasome system (UPS)

In eukaryotic cells, the ubiquitin/proteasome system (UPS) selectively degrades many short-lived proteins, including cell-cycle regulators, transcription factors, tumor suppressors, etc (Hershko and Ciechanover, 1998). Therefore, the UPS is essential for a variety of basic cellular and developmental processes. On one hand, the UPS is the major protein quality control mechanism in eukaryotes. It plays a housekeeping role in removing abnormal proteins and fine-tunes the homeostasis of the existing protein pool. On the other hand, the UPS also contributes to the cellular regulation and redirects growth and development, by removing short-lived regulatory proteins or rate-limiting enzymes in response to internal or external changes (Smalle and Vierstra, 2004).

Ubiquitin (Ub) is a small peptide consisting of 76 amino acids and is extremely conserved in all higher eukaryotes (Smalle and Vierstra, 2004). Free Ub can be covalently attached to a UPS substrate protein through an ATP-dependent conjugation cascade, which requires the activity of a ubiquitin-activating enzyme (E1), a ubiquitin-conjugating enzyme (E2) and a ubiquitin ligase (E3) (Pickart, 2001). As illustrated in **Figure 1**, the E1 utilizes ATP and binds Ub directly via a thiol-ester bond between the glycine at the Ub C-terminus and a cysteine in the E1. This activated Ub then will be transferred to a cysteine in an E2 by forming a Ub-E2 intermediate. Both groups of E1s and E2s don't have many isoforms (e.g. the *Arabidopsis thaliana* genome contains 2 E1

genes and 37 E2 genes) and thus have limited impact on substrate specificity (Vierstra, 2003; Smalle and Vierstra, 2004).

The substrate specificity is instead determined by the E3 ubiquitin ligase, which recruits the Ub-E2 intermediate to the proximity of the target protein (Smalle and Vierstra, 2004). Consequently, E3s form a more diverse family (~1300 genes encoding E3 components in *Arabidopsis thaliana*) and therefore make the E1-E2-E3 cascade into a hierarchical structure (Pickart, 2001; Gagne et al., 2002; Smalle and Vierstra, 2004). With the help of an E3 enzyme, the Ub-E2 intermediate will deliver Ub to the substrate by forming an isopeptide bond between the C-terminal glycine of Ub and one or more lysl ε-amino groups of the target protein (Hershko and Ciechanover, 1998; Smalle and Vierstra, 2004). In some cases only one Ub is attached (mono-ubiquitination). In most cases, however, a polymer of Ubs is added to the substrate protein through the reiteratively attachment of Ub to the Lys residue of the previously bound Ub. Ub is mostly attached to the lysine of position 48 (K48), as well as other positions including K6, 11, 27, 29 and 63 (Smalle and Vierstra, 2004). Phosphorylation of the substrate is frequently required for the recognition by E3s in animals (Deshaies, 1999), but in plants it is not always a prerequisite. For instance, substrates of the $SCF^{TIR1/AFB}$ E3 ligase don't undergo phosphorylation (Tian et al., 2003), while rice SCF^{GID2} E3 ligase recognizes the phosphorylated SLR1 for its degradation (Sasaki et al., 2003).

Proteins with a polyubiquitin chain will be recognized by the 26S proteasome for degradation. The 26S proteasome is a 2.5MDa molecular machine consisting of ~35 subunits. It contains two kinds of subcomplexes, the barrel-shaped 20S protease core

(CP) and the 19S regulatory particle (RP) capping at one or both ends of the 20S protease core (Voges et al., 1999; Smalle and Vierstra, 2004). Proteins with a poly Ub chain will be recognized by the 19S RP and unfolded in an ATP-dependent manner to enter into the 20S CP for degradation (Voges et al., 1999).

It is noteworthy that non-degradative functions of ubiquitination also exist. In *Saccharomyces cerevisiae*, DNA damage will trigger the mono-ubiquitination at the K164 residue of the DNA-replication processivity factor PCNA (for proliferating cell nuclear antigen), which then promotes the interaction between PCNA and the translesion polymerase for DNA repair (Hoege et al., 2002; Stelter and Ulrich, 2003; Haracska et al., 2004). It has also been found that the budding yeast Ub E2 enzyme Rad6 (Ubc2) mono-ubiquitinates the K123 residue on histone H2B, the process of which is a prerequisite for the methylation of histone H3 (Sun and Allis, 2002; Welchman et al., 2005). Ubiquitin is also implicated in the plasma-membrane internalization step and in the endosomal sorting process: mono-ubiquitination of a G-protein coupled receptor in *Saccharomyces cerevisiae* is sufficient to signal receptor internalization (Leitner et al.; Terrell et al., 1998; Welchman et al., 2005); in Arabidopsis, the polyubiquitination of the K63 residue of PIN2, an auxin efflux carrier protein, is required for the endocytosis of PIN2 (Leitner et al., 2012).

Ubiquitination can be reversed by deubiquitinating enzymes (DUBs). DUBs specifically recognize the Ub moiety and cleave the peptide bond between the C-terminal glycine within the Ub and its attached peptides (Komander et al., 2009). DUBs can be divided into two groups based on sequence homology: ubiquitin carboxy-terminal

hydrolases (UCH) and ubiquitin processing proteases (UBPs) (Wing, 2003). Functions of DUBs are to process ubiquitin precursors (Callis et al., 1995; Wing, 2003), to edit and disassemble poly Ub chains for recycling free Ub, to reverse the effects of ubiquitination, etc (Amerik et al., 1997; Doelling et al., 2001; Wing, 2003). It has been proposed that DUBs rescue proteins that have been mistakenly ubiquitinated (Lam et al., 1997; Wing, 2003; Nijman et al., 2005). About 30 mammalian DUBs have been reported in the literature describing their regulatory roles in a variety of pathways and processes (Nijman et al., 2005). In *Arabidopsis*, at least 30 genes have been found to encode potential DUBs (Smalle and Vierstra, 2004). For instance, the ubiquitin-specific protease UBP14 in Arabidopsis is essential during early plant development, with the T-DNA insertion mutant of *AtUBP14* exhibiting the embryonic lethal phenotype (Doelling et al., 2001).

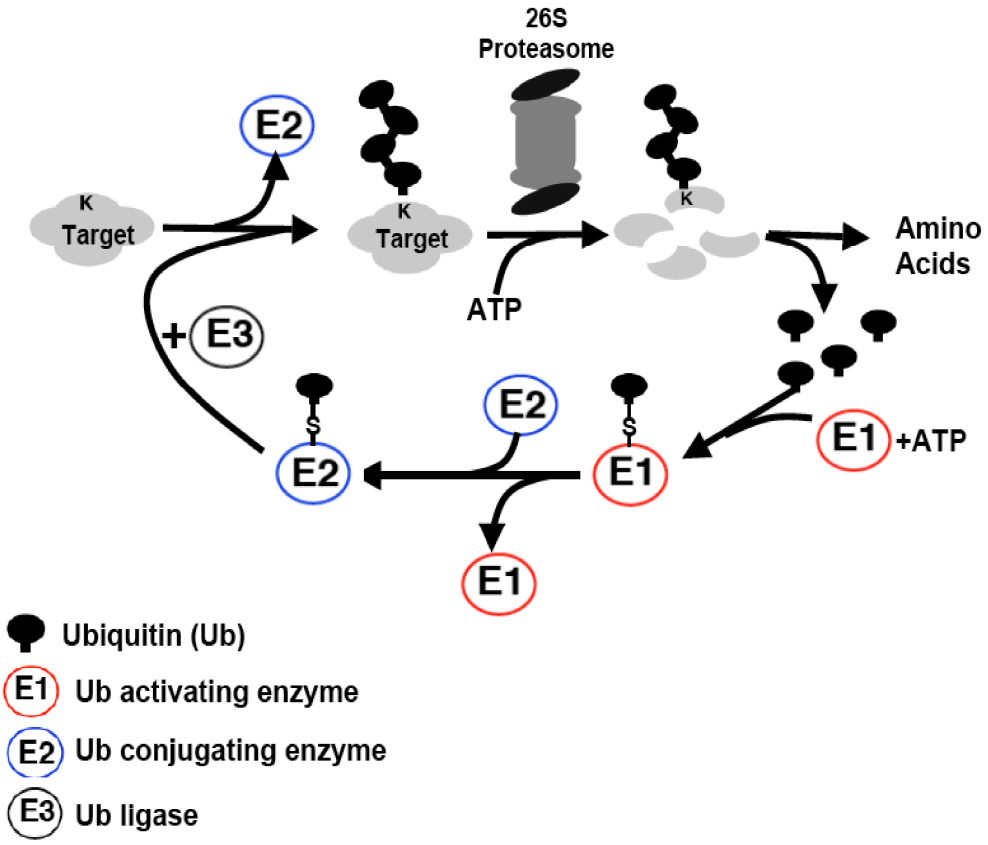

Figure 1. The ubiquitin/proteasome pathway.
The E1 ubiquitin activating enzyme activates ubiquitin (Ub) in an ATP-dependent manner, forming a thiol-ester bond between a cysteine residue within the E1 and the glycine residue of the Ub C-terminus. The E2 ubiquitin conjugating enzyme takes over the Ub molecule from the E1 and, with the help of the E3 ubiquitin ligase, conjugates Ub to a lysine residue of the substrate protein. Reiteration of these reactions results in the generation of a polyubiquitin chain. Proteins with the polyubiquitin chain will then be recognized and degraded by the 26S proteasome.

II. Ubiquitin E3s: CRLs and the SCF E3 ligase

The large number of E3 ubiquitin ligases can be divided into several groups based on their compositions and mechanism of action: the HECT domain E3s (for Homology to E6AP C Terminus), the APC E3 ligase (for anaphase-promoting complex) and the RING (for Real Interesting New Gene)/U-box domain E3s (Cyr et al., 2002; Peters, 2002; Smalle and Vierstra, 2004; Bosu and Kipreos, 2008). The HECT E3s accept Ub from their cognate E2s and form a Ub-E3 thiol-ester intermediate using a Cys residue within the C-terminal HECT domain. They then pass on the Ub to the substrate proteins interacting with their N-terminal domains. Therefore the HECT E3s have dual functions in both substrate recruiting and Ub conjugation, different from other E3s that function only as a docking site for the target substrate (Pickart, 2001). The APC E3 ligase is a high molecular mass protein complex containing at least 11 subunits and is essential for degrading cyclins (Peters, 2002). The RING domain E3 is named after its signature RING-finger motif, while the U-Box domain E3 is considered a non-canonical RING domain E3 due to the structural similarity (Cyr et al., 2002). Some RING domain E3s can function as a single subunit enzyme, typified by the well-studied mammalian Cbl protein family (Joazeiro et al., 1999), while more often RING domain E3s function as part of a multisubunit ubiquitin ligase with the scaffolding proteins of the cullin family (Cyr et al., 2002).

The largest known group of E3 ligases is the cullin-RING ubiquitin ligase family (CRLs). As illustrated in **Figure 2A**, CRLs are composed of a cullin (CUL) protein, a RING H2 finger protein (RING), a substrate-recognition subunit (SRS) and, with the

exception of CUL3-based CRLs, an adaptor protein that links the SRS to the cullin protein (Bosu and Kipreos, 2008). There are at least 5 cullin proteins in animals (CUL1~CUL5). The *Arabidopsis* genome also encodes multiple putative cullin proteins including CUL1, CUL2, CUL3a, CUL3b and CUL4, among which CUL2 is a paralog of CUL1 rather than an ortholog of animal CUL2 (Shen et al., 2002; Bosu and Kipreos, 2008). Each cullin nucleates multi-subunit protein complexes with different SRSs and adaptor proteins to degrade specific targets, resulting in a complex regulation of various biological processes (Bosu and Kipreos, 2008; Merlet et al., 2009).

The SCF (for Skp1-Cdc53/CUL1-F-box) E3 ubiquitin ligase is the archetype of CRLs (Petroski and Deshaies, 2005). As illustrated in **Figure 2B**, in *Arabidopsis*, the SCF ligase is composed of four subunits: the cullin protein, CUL1, functions as a scaffold protein and binds the RING H2 finger protein RBX1 with its C-terminus. The adaptor protein ASK1 (for Arabidopsis SKP1-LIKE) recruits one F-box protein (FBP) to the N-terminus of CUL1 (Patton et al., 1998; Gray et al., 1999; Zheng et al., 2002b). All the SCF E3s share the CUL1-RBX1 protein core, while they use different FBPs to recognize different target proteins for ubiquitination.

Mutants affecting CUL1 or RBX1, often exhibit severe growth defects and seedling lethality in *Arabidopsis*, suggesting their prominent role in maintaining different SCF E3s (Hobbie et al., 2000; Lechner et al., 2002; Hellmann et al., 2003). The adaptor protein ASK has 21 homologs in *Arabidopsis*, among which the ASK1 has the highest level of expression, ubiquitous expression pattern and is essential for male meiosis (Yang et al., 1999; Farras et al., 2001; Zhao et al., 2003). ASK2 is highly related to ASK1 based

on sequence and is also expressed in all tissues, suggesting some functional redundancy (Zhao et al., 2003). Indeed, the *ask1ask2* double mutation affects embryo development, which has never been seen in either single mutant (Liu et al., 2004). However, the embryo defects in the *ask1ask2* double mutant are not as severe as in the CUL1 null mutant, suggesting other ASK proteins may also contribute to the SCF function in embryo development (Liu et al., 2004).

It is noteworthy that the Arabidopsis genome encodes ~700 putative FBPs (Gagne et al., 2002). Several FBPs, including TIR1 (Dharmasiri et al., 2005a; Kepinski and Leyser, 2005), SLY1 (Dill et al., 2004), COI1 (Xu et al., 2002), FKF1 (Imaizumi et al., 2005), ORE9 (Woo et al., 2001) and UFO (Samach et al., 1999), have been shown to be essential for various developmental processes. Protein-protein interaction studies of CUL1, ASK and FBP families in Arabidopsis have shown that some members of ASK proteins interact specifically with members of the FBPs and the interaction between CUL1 and FBPs also have some degree of specialization (Risseeuw et al., 2003). By employing specific FBPs, plant SCF E3 ubiquitin ligases play pivotal roles in a variety of growth and developmental processes, including hormone responses, photomorphogenesis, cell division/organ development, self-incompatibility, abiotic/biotic stress responses and circadian rhythms (Smalle and Vierstra, 2004; Lechner et al., 2006).

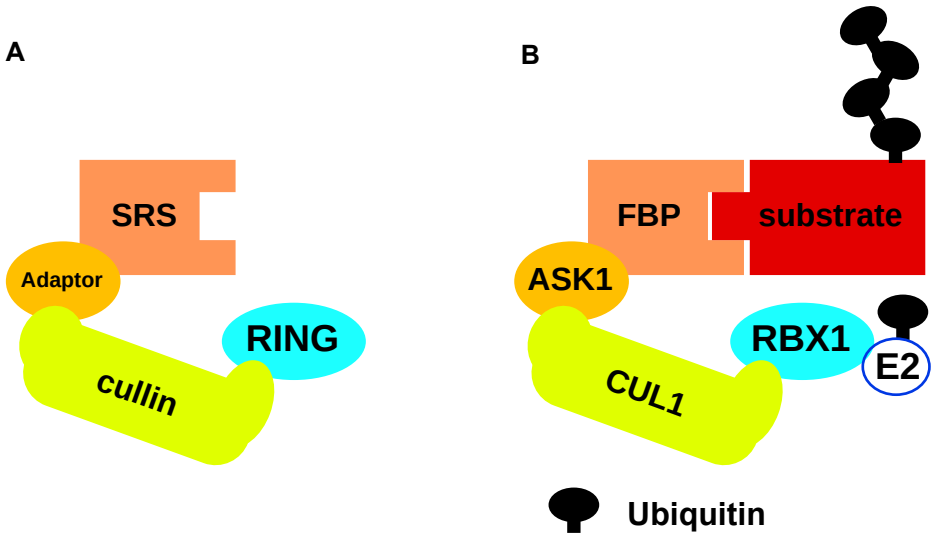

Figure 2. Compositions of the cullin-RING ubiquitin ligase (CRL) and SCF.
(A) Composition of a CRL. A cullin protein and a RING domain containing protein forms the protein scaffold, while an adaptor protein brings a substrate-recognition subunit (SRS) to the N-terminus of the cullin protein.
(B) Scheme of a SCF E3 ubiquitin ligase in Arabidopsis, showing the CUL1-RBX1 core, the adaptor protein ASK1 and an F-box protein (FBP) as the SRS. Ubiquitin E2 enzyme interacts with RBX1 and conjugates ubiquitin to the substrate.

III. Auxin signaling and $SCF^{TIR1/AFB}$

The phytohormone auxin (indole-3-acetic acid or IAA) regulates numerous plant developmental processes, by modulating expression of auxin-responsive genes (Abel and Theologis, 1996) to control cell division (Wong et al., 1996), expansion (Gray et al., 1998) and differentiation (Lur and Setter, 1993). To "turn on" auxin responsive genes, a group of transcriptional repressors called Aux/IAA proteins must be targeted by the SCF^{TIR1} and SCF^{AFB} E3 ubiquitin ligases in an auxin-dependent manner, and degraded by the 26S proteasome (Gray et al., 2001; Maraschin et al., 2009) and **Figure 3**).

Aux/IAAs and ARFs

Two groups of proteins are essential to auxin-mediated gene expression: short-lived transcriptional repressor Aux/IAA proteins and ARF transcription factors. Aux/IAA proteins are encoded by one of the most thoroughly characterized auxin-responsive gene families (the other two are *SAURs* and *GH3s*), expressions of which are up regulated within minutes of auxin treatment (Abel and Theologis, 1996).

There are 29 putative Aux/IAA genes in *Arabidopsis*. Most of them contain four conserved domains (domain I through IV), while some lack one or more of the conserved domains (Remington et al., 2004). Domain II functions as the degron for Aux/IAAs, which destabilizes the protein by interacting with the TIR1/AFB F-box proteins (Gray et al., 2001; Ramos et al., 2001). Gain-of-function mutations in the conserved domain II of Aux/IAAs, as seen in the *axr2/IAA7* and *axr3/IAA17* mutants, stabilize the protein and result in defects in auxin responses, suggesting the negative role of Aux/IAAs in auxin

signaling (Nagpal et al., 2000; Gray et al., 2001; Ouellet et al., 2001). Domains III and IV have been shown to mediate the dimerization between Aux/IAA and ARF proteins (Kim et al., 1997; Ulmasov et al., 1999a). The negative regulatory role of Aux/IAA proteins is probably accomplished by recruiting a co-repressor through its domain I. For instance, the TOPLESS (TPL) transcriptional repressor physically interacts with IAA12/BDL, through the association between the EAR motif within TPL and the IAA12 domain I (Szemenyei et al., 2008). Genetic data further confirmed that TPL is required for IAA12's suppression on the ARF5/MP transcriptional activity (Szemenyei et al., 2008). A subset of Aux/IAAs (e.g. IAA7 and 17) is also proposed to contain a second repression domain (Li et al., 2011a; Li et al., 2011b).

ARFs are transcription factors that bind specifically to the TGTCTC auxin response elements (AuxREs) within the promoter region of auxin responsive genes (Ulmasov et al., 1995). Binding of ARFs can either activate or repress expression of those auxin response genes (Ulmasov et al., 1995; Ulmasov et al., 1999b). ARFs have a conserved N-terminal DNA binding domain (DBD) followed by either an activation domain (AD) or a repression domain (RD). All the ARFs, except for ARF3, 13 and 17, also contain a conserved C-terminal domain (CTD), which is homologous to domains III and IV of the Aux/IAA proteins and functions in the ARF-ARF or ARF-Aux/IAA dimerization (Kim et al., 1997; Okushima et al., 2005; Guilfoyle and Hagen, 2007).

Truncated ARFs possessing only DBD and AD will constitutively bind AuxREs and activate the reporter gene, while the association of Aux/IAAs to the CTD of full length ARFs represses the transcriptional activity (Tiwari et al., 2003; Tiwari et al.,

2004). Interestingly, among 23 ARFs encoded by the *Arabidopsis* genome, only 5 have been shown to be as transcriptional activators when transiently expressed in protoplasts with reporter genes (Ulmasov et al., 1999b; Tiwari et al., 2003; Wilmoth et al., 2005), thus raising the question if the Aux/IAA suppression on ARF repressors functions positively in regulating gene expression. However, results from yeast two-hybrid and plant protoplast assays also suggest that interactions between ARF activators and Aux/IAAs are much stronger than ARF repressor-Aux/IAA interactions (Hardtke et al., 2004; Guilfoyle and Hagen, 2007). Therefore, a model has been established in which Aux/IAAs preferentially heterodimerize with ARF activators to repress the transcriptional activities of ARFs upon the downstream auxin response genes (Ulmasov et al., 1997; Tiwari et al., 2004), with the help of a co-repressor (e.g. TPL) (Szemenyei et al., 2008)

$SCF^{TIR1/AFB}$ in auxin signaling

As mentioned above, auxin triggers the degradation of Aux/IAA repressors through the ubiquitin/proteasome pathway. The $SCF^{TIR1/AFB}$ E3 ubiquitin ligase is the major component in plant auxin signaling. The F-box protein TIR1 (TRANSPORT INHIBITOR RESPONSE 1) of the $SCF^{TIR1/AFB}$ ubiquitin ligase is an auxin receptor, targeting Aux/IAAs for ubiquitination upon binding auxin (Dharmasiri et al., 2005a; Kepinski and Leyser, 2005; Tan et al., 2007). Mutations in SCF^{TIR1} subunits, such as *axr6/cul1* and *tir1-1*, cause the stabilization of Aux/IAAs and result in auxin response defects, including deficient embryogenesis/seedling development, increased resistance to

the auxin-induced root growth inhibition and reduced lateral root initiation (Hobbie et al., 2000; Gray et al., 2001; Hellmann et al., 2003; Quint et al., 2005). The N-terminal F-box domain of TIR1 is responsible for interacting with ASK1 to form the SCF^{TIR1} ubiquitin ligase as well as for the interaction with Aux/IAAs, while its 18 leucine-rich repeat (LRRs) domain is solely responsible for auxin reception and target recruitment (Ruegger et al., 1998; Dharmasiri et al., 2005a; Kepinski and Leyser, 2005; Tan et al., 2007). Pull down experiments using GST-IAA7 show that auxin enhances the TIR1-Aux/IAA interaction and directly binds to the TIR1-IAA7 complex (Dharmasiri et al., 2005a; Kepinski and Leyser, 2005). A more recent in vitro auxin binding assay using recombinantly expressed TIR1 (with ASK1) and IAA7 also indicates TIR1 and IAA7 alone lack the capability to directly bind auxin, whereas the TIR1-IAA7 complex binds auxin in much higher affinity (Calderon Villalobos et al., 2012). Additionally, the crystal structure of the TIR1-ASK1 complex with auxin and the IAA7 degron peptide indicate that both TIR1 and Aux/IAA function as co-receptors for auxin (Tan et al., 2007). The auxin binding does not induce significant conformational changes of the hormone receptors. Instead auxin serves as a 'molecular glue' by filling in the hydrophobic cavity at the TIR1-Aux/IAA interface and stabilizes the TIR1-Aux/IAA interaction (Tan et al., 2007).

The mechanism of auxin perception is the first example of small-molecule regulation of an SCF E3 ubiquitin ligase by facilitating the substrate-SCF interactions. Similar mechanisms have also been found in other SCF-mediated processes in plants, typified by several other hormone response signaling pathways. In the perception of

gibberellin (GA), the GA molecule binds directly to the GID1 receptor and enhances the interaction between GID1 and DELLA repressors, which are then targeted for ubiquitination by the SCF^{SLY1} ubiquitin ligase (Dill et al., 2004; Murase et al., 2008). Thus the GA-activated GID1 functions as a 'ubiquitination chaperon' that stimulates the substrate recognition by SCF^{SLY1} (Murase et al., 2008). In the case of jasmonate (JA), the JAZ proteins are also degraded by SCF^{COI1} in a JA-dependent manner (Chini et al., 2007; Thines et al., 2007). The crystal structure analyses also indicate that COI and JAZ serves as co-receptors for JA and that JA fills in the COI open pocket to facilitate the COI1-JAZ interaction (Sheard et al., 2010).

Besides TIR1, there are other proteins that have been shown as alternative auxin co-receptors. A group of F-box proteins called AFBs (for auxin-signaling F-box protein, AFB1 to 5) have been found related to TIR1. They exhibit 50-70% sequence identity to TIR1 and also interact with Aux/IAAs in an auxin-dependent manner (Dharmasiri et al., 2005b; Greenham et al., 2011). None of the *tir1* or *afb* single mutants exhibit severe auxin-regulated phenotypes. However, the *tir1afb2afb3* and *tir1afb1afb2afb3* mutants are seedling lethal and exhibit similar phenotype as seen in the *bdl/iaa12* mutant, in which the IAA12 protein is stabilized due to the gain-of-function mutation (Dharmasiri et al., 2005b; Mockaitis and Estelle, 2008). This strongly suggests the functional redundancy between the TIR1 and AFB proteins. Interestingly, several lines of evidence also suggest the functional specialization among TRI1/AFB proteins. For instance, TIR1 and AFB2 have a stronger interaction with Aux/IAAs than AFB1 and AFB3 (Parry et al., 2009; Greenham et al., 2011). AFB4 has also been shown to have a negative role in regulating

plant auxin responses (Greenham et al., 2011). Comparison between TIR1-IAA7 and AFB5-IAA7 suggest they have differential auxin binding affinities (Calderon Villalobos et al., 2012). When TIR1 is paired with different Aux/IAAs to form the auxin co-receptor complexes, they also exhibit a wide range of auxin-binding affinities (Calderon Villalobos et al., 2012).

To summarize the molecular mechanism of plant auxin signaling (**Figure 3**), in the absence of auxin, Aux/IAAs dimerize with ARFs to suppress their transcriptional activation of auxin response genes. When plants receive the auxin signal, the auxin molecule promotes the interaction between the F-box protein (TIR1 or AFB) and Aux/IAAs. Aux/IAAs will then be ubiquitinated and degraded through the ubiquitin-proteasome pathway. Consequently, this releases ARFs from repression of their transcriptional activities, resulting in the expression of auxin responsive genes and auxin-regulated responses in plants.

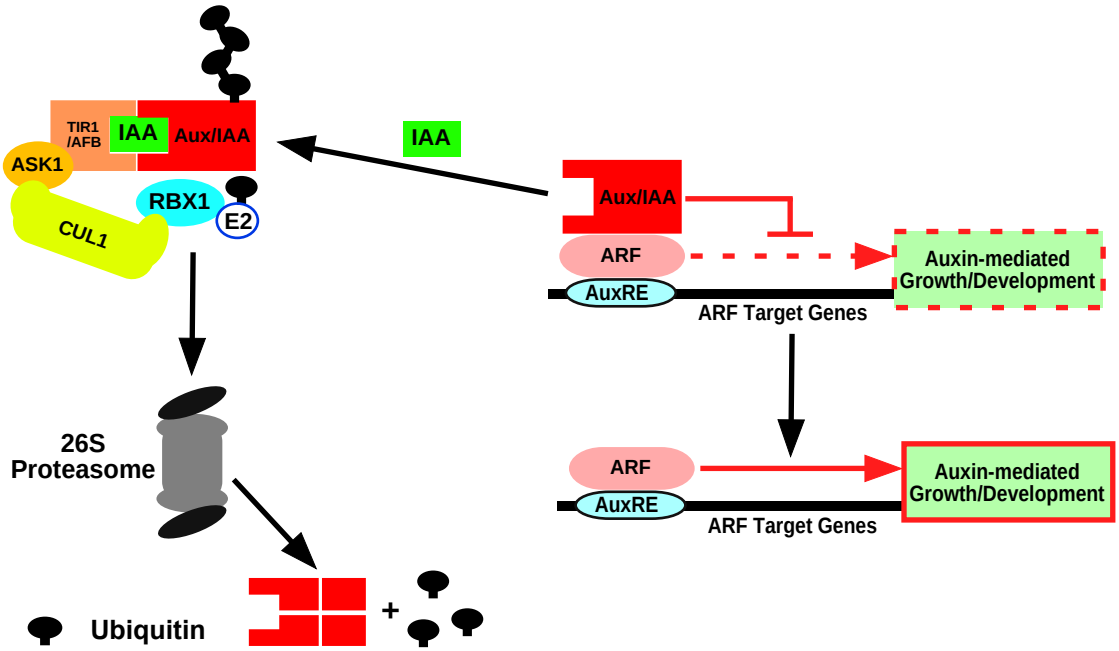

Figure 3. The model of auxin signaling in Arabidopsis.
The ARF transcription factor regulates the expression of auxin response genes by binding to the auxin-responsive elements (AuxRE) within their promoter region. The heterodimerization of Aux/IAAs with ARFs suppresses the ARF transcriptional activity. In the presence of auxin, the Aux/IAAs is recruited by TIR1/AFB to the $SCF^{TIR1/AFB}$ E3 ligase for ubiquitination. Polyubiquitinated Aux/IAAs will be degraded by the 26S proteasome, releasing the Aux/IAA suppression on ARFs. Consequently, the expression of the ARF target genes will be switched on.

IV. Regulation of CRL activity

The activity of CRLs can be regulated in different ways, including neddylation/deneddylation, inhibitory sequestration of the cullin protein by CAND1, turnover of substrate-recognition subunits (SRSs) and the dimerization of CRLs (Petroski and Deshaies, 2005; Bosu and Kipreos, 2008). The following section will emphasize neddylation and CAND1-mediated regulation on CRLs.

Positive regulation of CRLs: cullin neddylation and CRL dimerization

One of the best characterized posttranslational controls of SCF complexes, as well as other CRLs, is a process called neddylation, in which a ubiquitin-like protein NEDD8 (for Neural precursor cell Expressed Developmentally Down-regulated protein 8, also known as RUB in yeast and *Arabidopsis*, for related to ubiquitin) is covalently conjugated to a conserved Lys residue of the cullin subunit (CUL1 in SCF) (del Pozo et al., 1998; del Pozo et al., 2002; Dharmasiri et al., 2003; Pan et al., 2004). Genetic, biochemical and structural analyses have shown that neddylation activates CRLs and is essential for CRL-mediated proteolysis (Wu et al., 2000; Dharmasiri et al., 2007; Duda et al., 2008; Saha and Deshaies, 2008).

The neddylation process is similar to ubiquitination and also requires an E1-E2-E3 enzymatic cascade. Human protein APP-BP1 and UBA3 are required for NEDD8 activation, while UBC12 is the E2 enzyme that conjugates NEDD8/RUB to the cullin protein (Liakopoulos et al., 1998; Gong and Yeh, 1999). Analogously, as illustrated in **Figure 4**, the AXR1 and ECR1 proteins of *Arabidopsis* also form a heterodimer and

activate the RUB protein (del Pozo et al., 2002), while RCE1 acts as the E2 enzyme that conjugates NEDD8/RUB to the CUL1 in the SCF complex (Dharmasiri et al., 2003). In *Arabidopsis*, the RBX1 protein of the SCF complex functions as a neddylation E3 by bridging RCE1 with CUL1 (Gray et al., 2002; Dharmasiri et al., 2003) and **Figure 4**). Another protein called DCN1 (for defective in cullin neddylation) is also found to promote the neddylation of CUL3 in *C. elegans* and CUL1/Cdc53 in budding yeast (Kurz et al., 2005) and has been shown to be a scaffold-like E3 ligase for cullin neddylation *in vitro* (Kurz et al., 2008). However, a loss-of –function mutant of an *Arabidopsis* DCN1 homolog gene (AAR3) doesn't have obvious defects in the SCF^{TIR1}–mediated degradation of Aux/IAAs or in the expression of an auxin reporter gene *DR5::GUS*, indicating either there may be redundancy among the *Arabidopsis* DCN1 genes or the DCN1/AAR3 is not playing a predominant role as an neddylation E3 in plants (Biswas et al., 2007).

The CRL activity requires cullin neddylation. *In vitro* experiments have shown that NEDD8 conjugation stimulates the CRL-mediated ubiquitination of IκBα and p27 (Kip1) (Podust et al., 2000; Read et al., 2000; Wu et al., 2000). Treatment of cells with the NEDD8-activating enzyme (NAE) inhibitor, MLN4924, completely inhibits detectable NAE pathway function and disrupts the turnover of CRL substrates (Soucy et al., 2009). When applied to plant seedlings, MLN4924 also blocks neddylation effectively, interferes with the degradation of CRL-regulated proteolysis and thus causes defects in their downstream responses (Hakenjos et al., 2011). *Arabidopsis* mutants of the neddylation pathway, including *axr1*, *ecr1*, and *rce1*, show a reduction in the level of

RUB-modified (neddylated) CUL1, reduced proteolysis of SCF^{TIR1} substrate Aux/IAA proteins and pleiotropic growth defects, including diminished auxin responses (del Pozo et al., 2002; Dharmasiri et al., 2003; Dharmasiri et al., 2007).

Neddylation is a highly dynamic process. Cleavage of NEDD8/RUB from cullins (deneddylation) is promoted by the COP9 signalosome (CSN) (**Figure 4**). The CSN complex purified from porcine spleen deneddylates Cul1 *in vitro* (Lyapina et al., 2001; Yang et al., 2002). Consistently, studies in various organisms have shown that neddylated cullin proteins accumulate in *csn* mutants (Lyapina et al., 2001; Mundt et al., 2002; Gusmaroli et al., 2007; Menon et al., 2007). More details about deneddylation will be discussed in section V.

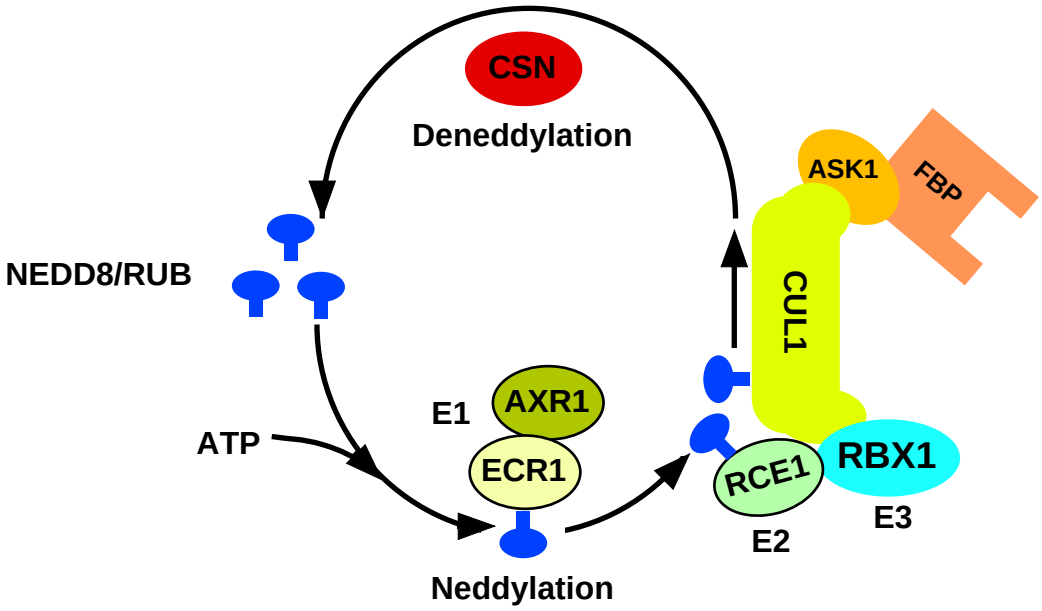

Figure 4. Scheme of neddylation/deneddylation in Arabidopsis. NEDD8/RUB, a ubiquitin related peptide, can be covalently attached to the CUL1 subunit of the SCF E3 ligase (neddylation). Like ubiquitination, neddylation also requires an E1 activating enzyme (AXR1-ECR1 heterodimer), an E2 conjugating enzyme (RCE1) and the E3 ligase (RBX1). The NEDD8/RUB can be cleaved by the CSN protein complex, the process of which is called deneddylation.

The mechanism of neddylation-mediated activation of CRLs is revealed by crystallographic and enzymological analyses. The crystal structure and modeling of the human SCF^{SKP2} ubiquitin ligase suggest that there is a gap of ~50Å between the substrate binding LRR domain of SKP2 and the active-site cysteine of the E2 (Zheng et al., 2002b). SCF catalyzes ubiquitination probably through increasing the effective concentration of the substrate lysine at the E2 active site (Zheng et al., 2002b; Wu et al., 2003). Crystallization of neddylated $Cul5^{ctd}$-Rbx1 complex and the small-angle X-ray scattering analysis of neddylated $Cul1^{ctd}$-Rbx1 to its non-neddylated counterparts indicates that neddylated CRLs are in a more flexible open conformation that prefers adaptor-bound substrates (Duda et al., 2008). Mutations that hinder the orientational flexibility of cullin-Rbx1 complexes will decrease the CRL activity (Duda et al., 2008). Saha et al. employed detailed enzymatic analysis of neddylated SCF and found that neddylation improves Ub E2 recruitment, enhances Ub chain initiation and Ub chain elongation on substrates by bridging the substrate-E2 gap (Saha and Deshaies, 2008).

Besides neddylation, CRL dimerization is another mechanism for positive regulation. Dimerized CRLs acquire conformational variability to accommodate various substrates (Merlet et al., 2009). A number of CRLs have been found forming dimers through the cullin protein, such as CUL1 and CUL3 of their cognate CRL complexes (Chew et al., 2007; Wimuttisuk and Singer, 2007). Besides cullins, F-box proteins can also form a dimer through conserved D-domains and thus are able to connect two SCF ligases, as seen in the case of yeast SCF^{Cdc4} and human $SCF^{\beta\text{-}TrCP}$ E3 ligases (Tang et al., 2007). The dimeric SCF complexes possess different substrate-to-catalytic site

separation distances, allowing them to target different sized substrates and to accommodate various acceptor sites and chain geometries (Tang et al., 2007). Enzymatic studies on substrate ubiquitination further show that CRL dimerization is crucial for the optimal Ub chain initiation and elongation (Tang et al., 2007). However, TIR1 and AFB proteins are lacking the D-domain and so far no dimerization of SCF has been shown in Arabidopsis. Taken together, neddylation of cullins and dimerization of CRLs have been shown to be essential for the activation of CRL ligase activity.

CAND1 inhibits the assembly of CRLs by sequestering cullins

CAND1 (for cullin-associated and neddylation-dissociated 1) is another component involved in regulating CRLs. It selectively binds to unneddylated cullin proteins and disrupts the binding of adaptor proteins (e.g. Skp1 in SCF complex) to the cullin-RBX1 catalytic core, thereby inhibiting CRL assembly (Liu et al., 2002; Zheng et al., 2002a; Min et al., 2003). The crystal structure of the human Cand1-Cul1-Rbx1 complex indicates that CAND1 wraps around the cullin protein in a head-to-tail manner: the CAND1 C-terminus partially occupies the Skp1 binding site at the cullin N-terminus, while the CAND1 N-terminus binds the cullin C-terminal region and prevents the access of NEDD8 to the conserved Lys residue of the cullin (Goldenberg et al., 2004). Therefore, the CAND1-CUL1 interaction and cullin neddylation are mutually exclusive since both happen within the CUL1 C-terminus (Duda et al., 2008). Indeed, CAND1 protein purified from insect cells inhibits Cul1 neddylation *in vitro* (Goldenberg et al.,

2004). Taken together, both biochemical and structural data suggest a negative role of CAND1 in regulating CRL activity.

However, genetic evidence in plants indicates a positive role of CAND1 in SCF-regulated pathways. Loss-of-function mutants of Arabidopsis *CAND1* exhibit various defects in auxin responses and other SCF-regulated processes. Both the *eta2-1/cand1* mutant and *cand1* T-DNA insertion mutants confer reduced SCF^{TIR1}-mediated degradation of Aux/IAAs and more stabilized SCF^{SLY1} substrates (DELLA proteins) (Chuang et al., 2004; Feng et al., 2004). In human cells, CAND1 is also required for the proper SCF^{SKP2} function (Zheng et al., 2002a). In addition, both ectopic overexpression and siRNA-mediated knockdown of CAND1 in human cells decreased the ability of $Cul3^{Keap1}$ to target Nrf2 for ubiquitin-dependent degradation (Lo and Hannink, 2006).

To summarize, CAND1 is not simply a negative regulator, although the *in vitro* data suggest so. Paradoxically, CAND1 acts positively *in vivo* and is required for proper SCF function. It also seems that the CAND1-CUL1 interaction does not affect the *in vivo* CUL1 neddylation status, as in *cand1* loss-of function mutants or siRNA lines no neddylation defects of Cul1 are observed (Zheng et al., 2002a; Chuang et al., 2004; Feng et al., 2004; Zhang et al., 2008).

A cycling model of the dynamic CRL (SCF) assembly-disassembly may explain the aforementioned CAND1 paradox (**Figure 5**). The CAND1-CUL1 interaction causes the disassembly of SCF. However, CAND1 doesn't sequester CUL1 permanently and dissociates from the CAND1-CUL1-RBX1 complex. Subsequently the CUL1-RBX starts to recruit new adaptor-substrate modules to form the SCF complex (Lo and Hannink,

2006). Neddylation on CUL1 then occurs to activate the SCF for substrate ubiquitination. Since CAND1 preferentially binds to deneddylated cullin, the cullin neddylation and the CSN-mediated deneddylation may also assist in the CRL assembly/disassembly cycle (Schmidt et al., 2009).

Gel-filtration chromatography studies on the SCF^{TIR1} assembly in *Arabidopsis* show that the reduced CAND1-CUL1 interaction in the *eta2-1/cand1* mutant results in increased assembly of the SCF^{TIR1} complex, while the stabilized CAND1-CUL1 association caused by the *axr6-2/cul1* mutation leads to the disassembly of ASK1-TIR1 from the CUL1-RBX1 scaffold (Zhang et al., 2008). Interestingly, in both *eta2-1/cand1* and *axr6-2/cul1* mutants the function of SCF^{TIR1} E3 ligase is impaired, strongly supporting the hypothesis that the CAND1-mediated cycling of SCF assembly/disassembly is required for the optimal SCF^{TIR1} activity *in vivo* (Hellmann et al., 2003; Chuang et al., 2004; Zhang et al., 2008). However, a most recent report using the absolute quantification (AQUA) technology to study the architecture of CRL network indicates an alternative model of CRL dynamicity where the abundance of adaptor modules, rather than neddylation/deneddylation or CAND1 binding, drives CRL organization (Bennett et al., 2010). Consistently, the availability of the F-box protein Skp2 and/or its substrate p27, triggers assembly of the SCF^{Skp2} ubiquitin ligase by promoting the Cul1 neddylation and the dissociation of Cul1 from CAND1 *in vitro* (Bornstein et al., 2006). Therefore, whether the CAND1 sequestration of cullin is the only driving force or the first step in the CRL assembly/disassembly cycle remains unclear.

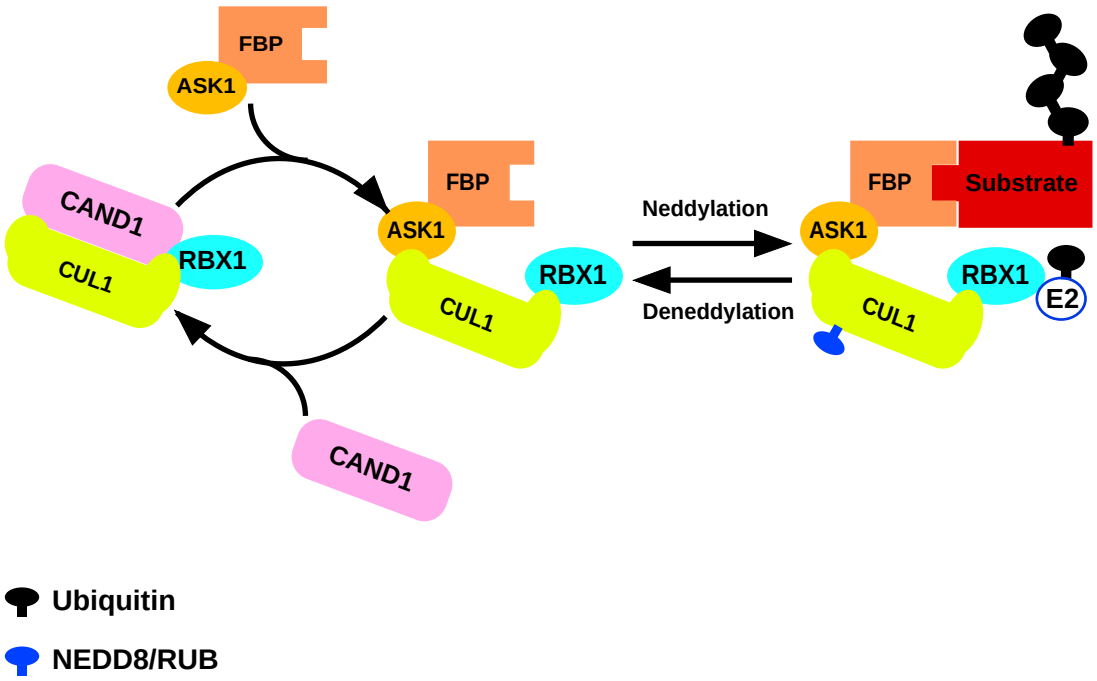

Figure 5. Cycling of SCF assembly/disassembly.
Neddylation on CUL1 activates the SCF for substrate ubiquitination. Once the ubiquitinated substrate is consumed, CSN-mediated deneddylation toggles SCF to the CAND1-mediated disassembly. The transient association of CAND1-CUL1-RBX1 is interrupted by a new set of adaptor-FBP, resulting in the re-assembly of SCF.

V. Deneddylation conducted by the COP9 signalosome

As mentioned earlier, neddylation can be reversed (deneddylation) by an eight-subunit protein complex called the COP9 signalosome (CSN) (Chamovitz et al., 1996; Wei et al., 1998) and **Figure 4**). The CSN complex can be found in most eukaryotes from the fission yeast *Saccharomyces pombe* to human, with the exception of *Saccharomyces cerevisiae*, which only contains one CSN subunit CSN5 (Wei et al., 1998; Mundt et al., 1999; Schwechheimer and Deng, 2001; Serino and Deng, 2003). Genes encoding several CSN subunits were originally identified in *Arabidopsis* through genetic screens for mutants exhibiting the *co*nstitutive *p*hotomorphogenic/*det*iolated/*fus*ca *(cop/det/fus)* phenotype, featured by their photomorphogenic growth in dark, constitutive expression of light-inducible genes and the accumulation of anthocyanin pigment (Wei and Deng, 1996). The recessive nature of those *cop/det/fus* mutants, among which several CSN subunits were identified (Schwechheimer and Deng, 2001; Serino and Deng, 2003), indicates they are negative regulators of photomorphogenesis.

The Structure of CSN

The CSN modular complex has been biochemically purified from both plant and animal protein extracts (Chamovitz et al., 1996; Menon et al., 2005). Sequence alignments indicate that all CSN subunits are homologous with subunits of the 26S proteasome lid subcomplex and the eukaryotic translation initiation factor 3 (eIF3) (Glickman et al., 1998; Kim et al., 2001). It is noteworthy that subunits of CSN exhibit a remarkable one-to-one similarity to those of the 26S proteasome lid (Glickman et al.,

1998). Experiments using electron microscopy and single particle analysis also indicate a conserved architecture among the structure of CSN, the proteasome lid and eIF3 (Enchev et al., 2010).

The CSN protein complex is composed of 8 subunits, including six PCI (for Proteasome, COP9, eIF3) domain-containing subunits (CSN1~ 4, 7, and 8) and two MPN (for Mpr1p, Pad1p N-terminal) domain-containing subunits (CSN5 and CSN6) (Wei et al., 1994). In *Arabidopsis*, two MPN subunits CSN5 and CSN6 are each encoded by two paralogous genes (*AtCSN5A* and *5B*, *AtCSN6A* and *6B*) (Kwok et al., 1998; Peng et al., 2001b). Both CSN6A and 6B contribute redundantly to the CSN-regulated plant development, while CSN5A is predominant over its paralog (Gusmaroli et al., 2007). All of the CSN subunits readily assemble into the holocomplex, while CSN5 can also be detected in a monomer form (Kwok et al., 1998). The integrity of the CSN holocomplex is required for its proper function. In the *Arabidopsis* loss-of-function mutants of any CSN subunit, the CSN holocomplex assembly is completely impaired, causing an identical *cop/det/fus* phenotype and seedling lethality (Peng et al., 2001a; Peng et al., 2001b; Gusmaroli et al., 2007; Dohmann et al., 2008a). Loss of one CSN subunit (such as CSN3, CSN5 or CSN6) may also result in the destabilization of other CSN components and thus impairs the holocomplex assembly (Peng et al., 2001a; Gusmaroli et al., 2007). Yeast two hybrid assays studying the internal-interactions among *Arabidopsis* CSN subunits have revealed a model of CSN topology (Serino et al., 2003). More recently, by analyzing the subcomplex formation of *in vitro* reconstituted (and biochemically active) CSN complex in a mass spectrometry-based approach, Sharon et al. (2009) proposed the

human CSN contains two symmetrical modules (CSN1/2/3/8 and CSN4/5/6/7) and the CSN1-CSN6 interaction connects these two subcomplexes together (Sharon et al., 2009) and **Figure 6**). However, the interaction of CSN subunits reported in the *Arabidopsis* CSN7 structural study, which is the only reported CSN crystallographic data so far, indicated a different interaction map among CSN subunits (Dessau et al., 2008). Therefore the true organization of the CSN complex and how it is assembled are not well understood.

Functions of the CSN complex

The primary biochemical function of the CSN is to cleave the NEDD8/RUB protein from the cullin subunit of a CRL (Lyapina et al., 2001; Cope et al., 2002). Increased cullin neddylation and the *in vitro* SCF ubiquitin ligase activity were observed in the *csn1 (*Δ*caa1*) mutant of fission yeast (Lyapina et al., 2001). The removal of NEDD8 (deneddylation) is catalyzed by the Jab1/MPN domain metalloenzyme (JAMM) motif within the CSN5 subunit (Cope et al., 2002; Cope and Deshaies, 2006) and **Figure 6**). The recombinant CSN5 protein per se has no deneddylation activity (Cope et al., 2002). CSN5 can only fulfill this isopeptidase activity after incorporation into the CSN holocomplex, as deneddylation activity is defective in all previously characterized CSN subunit mutants, in which the CSN5 resides mainly in its monomer form (Dohmann et al., 2005; Gusmaroli et al., 2007; Dohmann et al., 2008a).

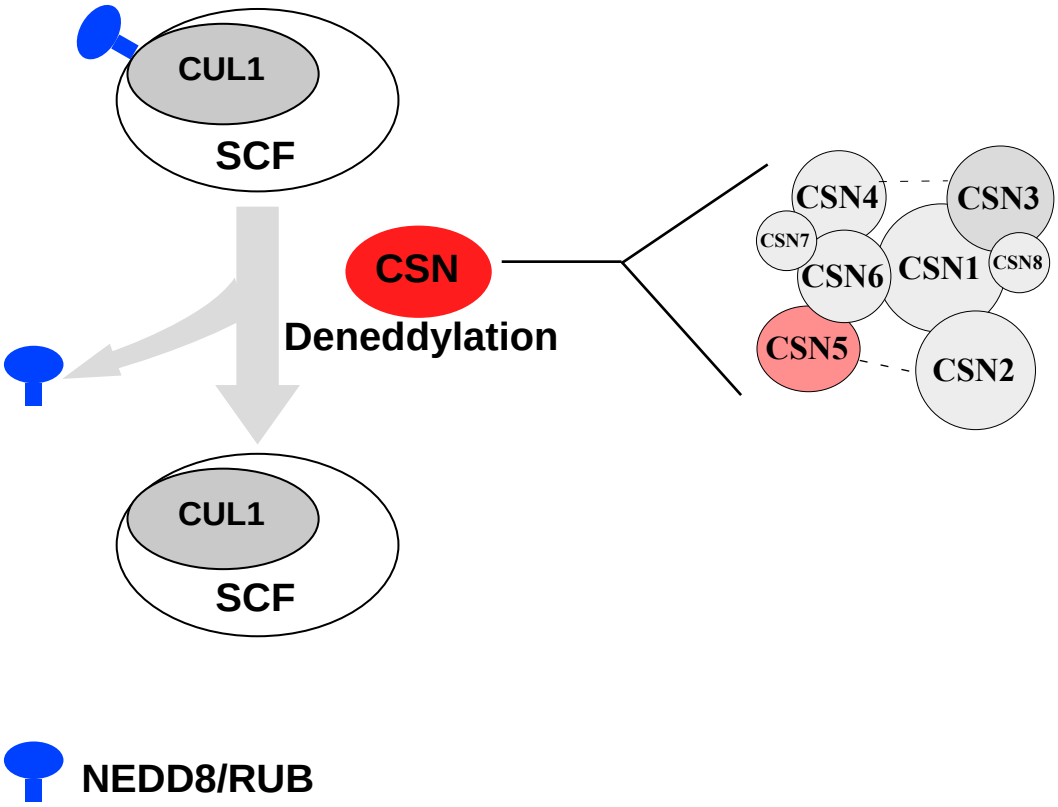

Figure 6. The COP9 signalosome (CSN) deneddylates the CUL1.
The 8-subunit protein complex CSN is proposed to have a symmetrical structure. Among CSN subunits, CSN5 has the deneddylation isopeptidase activity. By assembled into the CSN holocomplex, CSN5 cleaves NEDD8/RUB protein from the CUL1 subunit within a SCF complex.

Like neddylation, deneddylation also represents an important mechanism in regulating CRL activity. By interacting and deneddylating the CUL1 subunit of the SCF ligase, CSN regulates SCF activity and controls various SCF ligases in a plethora of pathways (Schwechheimer and Deng, 2001). In *Arabidopsis* CSN5 antisense and cosuppression lines, plants accumulate neddylated CUL1, resulting in more stabilized Aux/IAA proteins and defects in auxin signaling (Schwechheimer et al., 2001). Besides CUL1, the CSN also deneddylates other cullin proteins, including CUL2, CUL3 and CUL4 (Yang et al., 2002; Chen et al., 2006; Gusmaroli et al., 2007; Olma et al., 2009). Therefore, it is not surprising that the CSN is involved in various biological processes that are controlled by different CRLs. The CSN is required for the CUL3-based-E3 mediated degradation of its substrate MEI-1/Katanin and involved in the meiosis-to-mitosis transition in *C. elegans* (Pintard et al., 2003). Mutation within the Drosophila Csn5 JAMM domain results in arrested development at the larvae stage and abnormalities in photoreceptor differentiation (Cope et al., 2002). Besides auxin signaling in plants, a variety of CRL-regulated processes require proper CSN function, including other hormone responses (such as the jasmonate and the gibberellin signaling pathways mentioned earlier), the light control of plant development via CUL4-based E3 ligase and flower development via the SCF^{UFO} ligase (Feng et al., 2003; Wang et al., 2003; Chen et al., 2006; Dohmann et al., 2010).

Since neddylation activates the CRL activity at multiple levels (Saha and Deshaies, 2008), deneddylation is proposed to inhibit CRL function. The CSN protein complex purified from porcine spleen successfully deneddylated Cul1 and Cul2 from

human Hela cell extract and *in vitro* inhibited the degradation of p27, a substrate of SCF^{SKP2} ubiquitin ligase (Yang et al., 2002). Purified human CSN also inhibited the fission yeast Pcu1p/CUL1 ubiquitin ligase activity in an *in vitro* ubiquitination assay (Zhou et al., 2003). In contrast with the biochemical studies showing the CSN's negative role in regulating CRL ubiquitin ligase activity, genetic evidence suggested that deneddylation is not a pure inhibitory mechanism of regulating CRLs. CSN loss-of-function mutants accumulate substrates of CRLs and phenocopy or exacerbate mutants of CRL components (Schwechheimer et al., 2001; Doronkin et al., 2003; Lykke-Andersen et al., 2003; Stuttmann et al., 2009). Targeted disruption of Csn2 in mice resulted in a drastic increase in cyclin E and elevated level of tumor suppressor p53, the targets of the SCF^{Skp2}, indicating a cooperative role of the CSN in regulating SCF-mediated proteolysis (Lykke-Andersen et al., 2003). In *Arabidopsis*, mutations in the CSN caused defects in $SCF^{TIR1/AFB}$ and SCF^{SLY1} mediated protein degradation, resulting in the accumulation of Aux/IAA proteins and the DELLA proteins, respectively (Schwechheimer et al., 2001; Zhang et al., 2008; Dohmann et al., 2010). These *in vivo* data suggest a positive role played by the CSN in regulating the SCF-mediated proteolysis and demonstrate that cullin neddylation and deneddylation are two transition states required for maintaining the optimal functions of CRLs *in vivo* (Cope and Deshaies, 2003; Wu et al., 2006; Bosu and Kipreos, 2008).

At least in some organisms, the neddylation/deneddylation status of cullins also affects their stability. In *Drosophila csn5* mutants, the steady-state level and half-lives of CUL1 and CUL3 were reduced, which could be rescued by introducing the wild-type

CSN5 protein (Wu et al., 2005). Moreover, introducing a specific CSN5^{D148N} mutant that abolished deneddylating activity but did not affect CSN complex assembly failed to restore CUL1 or CUL3 levels in the *csn5* mutant background (Wu et al., 2005). Furthermore, CUL1 and CUL3 variants with their neddylated lysine residues mutated into arginines were found to be more stable than the wild-type proteins, indicating neddylation promoted the instability of cullins (Wu et al., 2005; Wu et al., 2006). Similarly, in Arabidopsis null mutants of any CSN subunit, the CUL3 proteins were only found in their neddylated form, with greatly reduced protein abundance (Gusmaroli et al., 2007). The instability of Cul1 has also been reported in the *Neurospora csn2* mutant (He et al., 2005). In summary, CSN stabilizes cullins through deneddylation. This may also to some extent explain why the CSN is a positive regulator of CRL-controlled pathways *in vivo*. However, contrasting results were also found in *csn* mutants, showing no reduction in the neddylated cullin abundance. For instance, in human cells, silencing of CSN5 only affected the deneddylation status of cullins but not their abundance (Cope and Deshaies, 2006). In Arabidopsis *csn* null mutants of any CSN subunit, all the CUL1 and CUL4 proteins were in their neddylated form but remained stable (Gusmaroli et al., 2007). Therefore, the question as to if CSN is always a protector of cullin remains uncertain.

The CSN is also required for maintaining the stability of other CRL components, such as the substrate-recognition subunit (SRS). In some cases, the SRS of a CRL is unstable due to the autoubiquitination by their associated CRL (Zhou and Howley, 1998; Galan and Peter, 1999; Geyer et al., 2003). The auto-destruction of the SRS is probably important for terminating the E3 ligase activity and for allowing the cullin-RBX1 core to

recruit a different SRS. *Neurospora* FBPs, such as FWD-1 and SCON-2, were dramatically destabilized in a *csn2* mutant (He et al., 2005). In fission yeast, the half-life of the F-box protein Pop1p as in the SCF^{Pop1p} ubiquitin ligase was decreased in the *csn* mutant, in which deneddylation was deficient (Wee et al., 2005). Several other yeast F-box proteins were also destabilized in the *csn5* mutant, indicating that the CSN may protect them from autocatalytic destruction (Schmidt et al., 2009). However, F-box proteins lacking a critical proline residue were not sensitive to this CSN-mediated protection in fission yeast (Schmidt et al., 2009). Besides, it is unclear if the CSN-mediated protection of FBPs is conserved in other organisms, such as in Arabidopsis.

This CSN-mediated protection of the SRS may also be controlled by proteins that are associated with the CSN. Affinity-purified Csn1p/CSN1 complexes from fission yeast, which probably contain both the CSN and its interacting proteins, inhibited the Pcu3p/CUL3-based ubiquitin ligase activity without deneddylating Pcu3p/CUL3, indicating other mechanisms of CSN-mediated CRL regulation may exist (Zhou et al., 2003). This inhibition was then shown to be due to a CSN-associated deubiquitinating enzyme (DUB) Ubp12 (Zhou et al., 2003). Btb3p, the adaptor protein of the Cul3p/CUL3 ligase, is considerably unstable in either the Δ*csn5* or Δ*ubp12* mutant of the fission yeast (Wee et al., 2005). Studies also have shown that cotransfection of the Ubp12 human ortholog USP15 and the CRL component RBX1 led to the stabilization of RBX1 in human HeLa cells (Hetfeld et al., 2005).

Therefore the association of a deubiquitination enzyme with the CSN may explain why SRSs are less resistant to the autocatalytic destruction in the *csn* mutant. However,

Ubp12 only maintains the stability of Btb3p but not F-box proteins, suggesting CSN-mediated deneddylation is more predominant and Ubp12 may be dispensable for the stability of the FBPs examined so far (Schmidt et al., 2009). Further studies are needed to test the possibility that the deneddylation by CSN and deubiquitination by the CSN-associated DUBs act synergistically to maintain the stabilities of CRL components.

As reviewed above, the CSN plays a negative role in *in vitro* experiments but acts positively *in vivo*. Until now several mechanisms have been proposed in an attempt to resolve this CSN paradox and to explain the *in vivo* CSN-mediated activation of CRL. Firstly, the deneddylation conducted by the CSN appears to be required for CAND1-mediated cycling of CRL assembly/disassembly (Petroski and Deshaies, 2005; Lo and Hannink, 2006; Schmidt et al., 2009). Secondly, the CSN facilitates CRL activities by either maintaining the stability of labile SRSs or by recycling unstable, neddylated cullins into the stable deneddylated isoforms, during which the CSN-associated deubiquitinating enzyme Ubp12/USP15 may act cooperatively (Zhou et al., 2003; He et al., 2005; Hetfeld et al., 2005; Wee et al., 2005; Wu et al., 2005). Additionally, it has been shown that CSN induced the dissociation of ubiquitinated substrates from the substrate recognition subunit of the VBC-Cul2 ubiquitin ligase in an *in vitro* ubiquitination assay using human cells (Miyauchi et al., 2008).

It has also been proposed that the CSN participates in the transcriptional regulation of gene expression. Tsuge et al. (2001) showed that the N-terminal portion of human CSN1 can inhibit gene expression from the *c-fos* promoter, which contains a variety of regulatory elements and can respond to various stimuli (Tsuge et al., 2001).

Studies in human cells also suggest that the CSN may function as a transcriptional regulator since it associates with chromatin through interacting with CUL4-DDB2 and CUL4-CSA ubiquitin ligases (Groisman et al., 2003). The CSN-mediated inhibition of CUL4-DDB2 is independent of deneddylation and can be rapidly relieved when CUL4-DDB2 is recruited to the damaged chromatin upon UV irradiation (Groisman et al., 2003; Fischer et al., 2011). In *Drosophila*, chromatin immunoprecipitation (ChIP) experiments have shown that CSN4 associated with the promoter region of Rbf target genes (Ullah et al., 2007). However, the precise roles the CSN might play in transcriptional regulation are also unclear.

Previous work on *csn* mutants in Arabidopsis

Arabidopsis *null* mutants of any CSN subunit are phenotypically indistinguishable and exhibit the pleiotropic *cop/det/fus* phenotype, which is characterized by short hypocotyl and open cotyledons of dark-grown seedlings, accumulation of anthocyanin and seedling lethality (Wei et al., 1994; Serino et al., 1999; Serino et al., 2003; Gusmaroli et al., 2007). The seedling lethality thus hampers the analyses of CSN functions in later stages of plant development. Recently however, a few weak, viable Arabidopsis *csn* mutants have been described. These include *CSN5* antisense lines (Schwechheimer et al., 2001), mutants lacking one of the two copies of *CSN5* and *CSN6* genes (Peng et al., 2001b); (Gusmaroli et al., 2007), as well as hypomorphic missense alleles of *CSN1* and *CSN2* (Zhang et al., 2008; Stuttmann et al., 2009). Importantly however, these viable *csn* mutants still exhibit diminished deneddylation activity, resulting in the accumulation of

neddylated CUL1 and the stabilization of the SCF substrates (Schwechheimer et al., 2001; Dohmann et al., 2005; Gusmaroli et al., 2007; Dohmann et al., 2008a; Zhang et al., 2008; Stuttmann et al., 2009).

In a previously described genetic screen for enhancers of *tir1-1* (Gray et al., 2003; Chuang et al., 2004; Quint et al., 2005; Ito and Gray, 2006; Quint et al., 2009), we identified two weak *csn* subunit mutants, designated *eta6/csn1-10* (Zhang et al., 2008) and *eta7/csn3-3*. In this dissertation, the phenotypic characterization of these *csn* mutants, together with studies on expression of auxin reporters, demonstrate that both *csn1-10* and *csn3-3* are defective in auxin signaling. However, unlike *csn1-10*, which is a typical *csn* mutant with defects in CSN-mediated deneddylation and Aux/IAA protein degradation (Zhang et al., 2008), neither of these defects was observed in the *csn3-3* mutant. Furthermore, genetic interactions between these *csn* mutants and additional auxin signaling mutants also distinguish *csn3-3* from other *csn* mutants. Data presented in this dissertation suggest that *csn3-3* is a unique *csn* mutant that defines a novel functional activity for the CSN3 subunit of the COP9 signalosome in the regulation of auxin signaling.

Chapter Two: Characterizations of *eta6/csn1-10* and *eta7/csn3-3*

Introduction

We have previously reported the identification of several auxin response mutants isolated from a genetic screen for enhancers of the *tir1-1* auxin response defect (designated as *eta* mutants), including *eta1/axr6-3* (Quint et al., 2005), *eta2-1/cand1* (Chuang et al., 2004), *eta3/sgt1b* (Gray et al., 2003), *eta4/pdr9-2* (Ito and Gray, 2006), and *eta5/iar4* (Quint et al., 2009). Two additional mutants *eta6* and *eta7* were also found in this screen. Map-based cloning analyses suggested that *eta6* is an allele of the *CSN1* gene (*At3g61140*), while *eta7* is an allele of the *CSN3* gene (*At5g14250*) (Quint and Gray, unpublished). We therefore designated *eta6* and *eta7* as *csn1-10* and *csn3-3*, respectively. In this chapter, I applied a series of physiological, genetic and biochemical experiments to confirm that *csn1-10* and *csn3-3* are CSN mutants, investigate the nature of the mutations and the defects caused by them, mainly focusing on the characterizations of *csn3-3*.

Methods

Plant Materials and Growth Conditions

All Arabidopsis lines used in this study are in the Col-0 ecotype, with the exception of *fus11*, which is in Landsberg *erecta* (Ler). Seeds were sterilized by 30% bleach (final concentration of 1.6% sodium hypochlorite)+0.1% Triton-X for 10min and were stratified at 4°C for 1~4 days. Seedlings were grown under sterile conditions on vertically oriented ATS nutrient plates containing 5% sucrose and 0.5% Agargel™ (Sigma) (Lincoln et al., 1990) under long-day conditions. After 7~10 days, seedlings were then transferred to soil (Fafard®) and grown under long-day conditions at 20°C.

The *tir1-1, csn1-10* and *csn3-2* (SALK_106465) mutants have been described previously (Ruegger et al., 1998; Dohmann et al., 2008a; Zhang et al., 2008). The *BA3:GUS* (Oono et al., 1998), *DR5:GUS* (Ulmasov et al., 1997), *HS:AXR3NT-GUS* (Strader et al., 2008) transgenes were introduced into the *csn3-3* and *csn1-10* backgrounds by crossing. The F2 seedlings were screened using the selective condition for the transgene (e.g. resistant to Kanamycin) plus screened by transferring seedlings to 0.05μM 2,4-dichlorophenoxyacetic acid (2,4-D) plates, to identify *csn3-3* and *csn1-10* homozygotes (resistant to 2,4-D induced root growth inhibition). The homozygosity of transgene was then tested on F3 generation.

For the double mutant construction, *axr1-12* (Lincoln et al., 1990), *axr1-3* (Gray et al., 2001), *eta1/axr6-3* (Quint et al., 2005), *eta2-1/cand1* (Chuang et al., 2004), *eta3* (Gray et al., 2003), and *csn5a-2* (Gusmaroli et al., 2007) were described previously and were crossed with *csn1-10* or *csn3-3*. One loss-of-function allele of *AtIBR5* gene (Strader

et al., 2008) that was isolated by our lab (unpublished data) was also crossed with *csn1-10* and *csn3-3*. F2 putative candidates that showed enhanced growth defects (e.g. more severe dwarfism in *csn5a-2 csn1-10/csn3-3* double mutants or embryogenesis defects in *axr1-12/axr1-3 csn3-3* double mutants) or enhanced resistance to the 2,4-D induced root growth inhibition were genotyped for *csn3-3* or *csn1-10*. Further sequencing analyses were used to confirm the homozygosity of the other mutant genotype as referenced in previously.

Genotyping *csn1-10, csn3-3* and *csn3-2*

For *csn1-10*, the DNA fragment over the point mutation was cloned by using primers within exon 3 (CSN1-Ex3-F: 5'-CCTCTGATCCGCGTGTCTTGC-3') and exon 6 (CSN1-Ex6-R: 5'-GCCACCTATGGTGGACTCTG-3') and then sent for sequencing using the CSN1-Ex3-F primer.

For *csn3-3*, a pair of CAPs primers spanning exon 7 and exon 8 was used for the genotyping (CSN3-exon7-F: 5'-CAACGACGGGAAGATTGGTG-3' and CSN3-Ex8-R: 5'-GCCTCCTTAGCATTACCAAG-3'). The wild type version of the amplified fragment has one cutting site for the restriction endonuclease Sty I. The digestion product contained two pieces of the DNA sequence (163bp and 126bp). On the other hand, the G to A mutation in *csn3-3* disrupted the Sty I cutting site (CCTTGG in Col, CCTTGA in *csn3-3*), so that the PCR production remained intact (289bp). For *csn3-2*, a primer near the T-DNA insertion site (CSN3-Ex2R: 5'-CAAACGAATCTGCCCAGCATCAC-3')

and a modified version of T-DNA border primer (LBb1mod: 5'-CAAACCAGCGTGGA CCGCTTGCTG C-3') were used to confirm the T-DNA insertion.

Root growth assay and lateral root initiation assay

For root growth assays, 5-day-old (d.o.) seedlings were transferred to ATS medium supplemented with various concentrations of 2,4-D, and the after-transfer root growth (primary root length) was measured after an additional 4 days.

For measuring IAA-induced root growth inhibition, 6-d.o. seedlings were transferred to freshly made IAA plates and were grown under long-day illumination through yellow long-pass filters to slow indolic compound breakdown (Stasinopoulos and Hangarter, 1990). Measurements of the root growth were taken after 1-day IAA treatment. All the data were normalized to the untreated root growth/length as the percentage of inhibition.

For the lateral root initiation assay, seedlings were grown on unsupplemented ATS plates vertically for 10 days. Lateral root primordia of each seedling was counted and normalized to the root length. Data were presented as the average lateral root number/root length of seedlings ($n \geq 15$).

RNA extraction and RT-PCR

Total RNA from Col and *csn1-10* seedlings was isolated using an RNeasy Plant Mini Kit (QIAGEN) as per the manufacturer's instructions. For reverse transcription (RT) -PCR analysis, first-strand cDNA synthesis was performed using 1 μg RNA and M-

MLV-RTase (Promega, Madison,WI, USA) following the manufacturer's instructions. cDNA samples were then diluted 20-fold and stored at -80°C in aliquots for future use. First-strand cDNAs of Col and *csn1-10* were then amplified using the CSN1-Ex3-F and CSN1-Ex6-R primer pair (94°C for 30s, 51°C for 90s and 72°C for 90s, 28 cycles and 32 cycles) (TECHNE thermal cycler TC-412). The expression of actin was included as the quantitative control using gene specific primers (Act2-F: 5'-GAGAAGATGACTCAGA TC-3' and Act2-R: 5'-ATCCTTCCTGATATC GAC-3'). The *csn1-10* RT-PCR product was sent for sequencing using the CSN1-Ex3-F primer.

Complementation assay using genomic *CSN3* DNA

The *CSN3* genomic DNA construct was composed of the *CSN3* coding region together with a 1.3 kb fragment upstream of the start codon plus a 600bp fragment downstream of the stop codon. The whole sequence was amplified from BAC clone F18022 (gCSN3-attB1: 5'-GGGACAAGTTTGTACAAAAAAGCAGGCTCCTTTG ATGGCGCCATGGTGG-3' and gCSN3-attB2-2: 5'-GGGACCACTTTGTACAAG AAAGCTGGGTCGTATGGAAACATGTGATAACC-3'). The DNA fragment was first gateway cloned into a donor vector pDNOR™207 using Gateway® BP clonase Enzyme Mix (Invitrogen) and then was gateway cloned into the vector pEarleyGate301 (Earley et al., 2006) using Gateway® LR clonase Enzyme Mix (Invitrogen). The construct was then transformed into *csn3-3[BA3:GUS]* plants using *Agrobacterium tumefaciens* strain GV3101 by the floral dip method (Clough and Bent, 1998). Two independent T3

homozygous lines (L2 and L4) were used for the root growth and GUS assays to assess complementation.

GUS Histochemical Staining

BA3:GUS and *DR5:GUS* assays were conducted as described previously with slight modifications (Chuang et al., 2004). 6-d.o. seedlings grown vertically on ATS plates were transferred into liquid ATS medium supplemented with 0.5 μM 2,4-D for 12hrs (*BA3:GUS*) and 4hrs (*DR5:GUS*) before GUS staining.

For *HS:AXR3NT-GUS* assays, 6-d.o. Col, *csn1-10* and *csn3-3* seedlings homozygous for the reporter construct were heat shocked for 2 hrs at 37 °C to induce expression of the transgene. Seedlings then were transferred to 20°C medium with 1μM 2,4-D for 20 min before GUS detection. Quantitative measurements of β-glucuronidase activity were conducted as described previously (Gray et al., 2001) with modifications: after heat shock for 2 hrs at 37°C, seedlings were transferred to 20°C liquid ATS medium for 15 min. Seedlings were then moved into medium supplemented with 1μM 2,4-D, sampled at 0, 20, 40 and 60 min thereafter and stored in liquid nitrogen until protein extraction. Frozen seedlings were homogenized using a laboratory vibration mill (Mixer-Mill; Qiagen, cat. no. MM300) in extraction buffer (50 mM KPO_4 pH 7, 0.1% triton X-100, 10 mM β-mercaptoethanol, 10 mM EDTA). To be specific, one tungsten-carbide bead was added to each tube containing 15~20 seedlings. The samples were then placed on the vibration mill for homogenization using a shaking frequency of 25Hz for 5min. Samples were then centrifuged 10min at 10,000g to remove debris and the protein level

of each sample was measured using Coomassie Plus-The Better Bradford Assay™ Reagent (Thermo Scientific®). Protein extracts were mixed with an equal volume of extraction buffer plus 4 mM 4-methylumbelliferyl-B-D-glucoronide (MUG) and incubated at 37°C overnight. The fluorometric signals were measured using a BioTek FL600 Fluorescence Microplate Reader (Winooski, VT) as per manufacturer's instructions (excitation at 360nm, emission at 460nm). Activity was calculated as fluorometric units per μg protein and was normalized as the percentage of the starting point (0 min).

IAA28-myc degradation assay

Experiments were done as described previously (Strader et al., 2008) with modifications. 6-d.o. light-grown seedlings of Col, *csn1-10* and *csn3-3* carrying the IAA28-myc construct were removed from ATS plates and floated in liquid ATS supplemented with 0.5 μM IAA. At the indicated time points, roots were excised and homogenized for protein extraction.

Antibodies and Immunoblot Analysis

The CUL1 antibody has been described previously (Gray et al., 1999) and the CUL4 antibody was obtained from Dr. Xing Wang Deng (Yale U.).

Antibodies against the CSN1, CSN3, and CSN8 subunits were raised by immunizing New Zealand white rabbits (Cocalico Biological, Reamstown, PA) with recombinant 6xHis-CSNx proteins. The recombinant proteins were purified from IPTG

induced *E. coli* cells expressing CSNx-pET28a constructs. To be specific, 25ml saturated bacteria was transfer to 500ml fresh LB (Lysogeny broth) liquid culture and incubated at 30 °C for 1hr. IPTG (Isopropyl β-D-1-thiogalactopyranoside) was then added to a final concentration of 1mM. Bacteria were then grown for an additional 4hrs at 30 °C. *E. coli* cells were collected by centrifugation at 5000rpm for 5min and resuspended in 10ml lysis buffer (50mM NaH_2PO_4, 300mM NaCl, 10mM Immidazole, adjust pH to 8.0 using NaOH). Resuspended cells were broken using French Press (FRENCH® PRESSURE CELL PRESS, SIM AMINCO®) as per manufacture's instruction. Cell lysates were then centrifuged at 10,000g for 10min to further remove debris. His tagged CSNs in the supernatant were then affinity purified using Ni-NTA Agarose beads (QIAGEN) as referred in the literature (Gray et al., 1999).

Constructs expressing recombinant CSN1 and CSN3 were made by Dr. William Gray. To make the construct expressing CSN8, the CSN8 cDNA was amplified using primers CSN8-EcoRI-F (5'-TTGAATTC ATGGATCTTTCGCCTGT-3') and CSN8-XhoI-R (5'-TTCTCGAGTTAA TGTTCAAG GTGGAA-3'). The Eco RI and Xho I sites (underlined) were used for subcloning CSN8 cDNA into the pET28a vector. Crude sera were subsequently affinity purified against nitrocellulose-bound antigens (Pringle et al., 1989). The CSN4, CSN5 and Rpt5 antibodies were purchased from BIOMOL Int'l, L.P./Enzo Life Sciences. Monoclonal α-myc 9E10 antibody was purchased from Covance and used as recommended.

For IAA28-myc, cullins and CSN subunit immunoblotting, protein extracts were prepared from 7-d.o. seedlings (or seedling roots for IAA28-myc assay) in protein

extraction buffer (50 mM Tris-HCl pH 7.5, 150 mM NaCl, 0.5% NP40, 1 mM DTT, 1 mM phenylmethylsulfonyl fluoride (PMSF), and 1X Protease Inhibitor Cocktail Kit (Thermo Scientific®, Lot# NB1499881)). 50 µg of protein were loaded in each lane and separated by 10% SDS-PAGE (cullins and CSN subunits) or 4~12% NuPAGE® Bis-Tris Gel (Invitrogen). For gel-filtration, protein extractions were made from 7 - 10-d.o. seedlings in liquid ATS medium on a shaker at 20°C. Proteins of each gel-filtration fraction were concentrated with StrataClean™ Resin (Stratagene) and separated on 4~12% NuPAGE® Bis-Tris Gel (Invitrogen), blotted (Nitrocellulose Membranes, 0.2µm, BIO-RAD) and used for western detection.

Gel Filtration Chromatography

These experiments were conducted as described previously (Zhang et al., 2008). In brief, 7-d.o. seedlings grown in liquid ATS medium were homogenized in extraction buffer (50 mM Tris-HCl, pH 7.5, 150 mM NaCl, 1 mM EDTA, 10% glycerol, 10 mM $MgCl_2$, 0.5 mM NaN_3, 1 mM DTT, 1 mM PMSF, and 1X Protease Inhibitor Cocktail Kit (Thermo Scientific®, Lot# NB1499881)). Homogenates were centrifuged twice at 10,000g for 10 min at 4°C to remove debris. Supernatants were then filtered though a 0.45 µm HT Tuffryn® Membrane (Pall Acrodisc®). 600 µg of total protein was fractionated through a Superdex 200 10/300 GL column (Amersham/GE Healthcare). After loading the sample, proteins were eluted in filtered and degassed extraction buffer at a flow rate of 0.2 mL/min. 0.5 mL fractions were collected after the 6 mL void volume was reached. All procedures were carried out at 4°C.

Results

Comparable auxin response defects are found in *csn3-3* and *csn1-10*

It has been well established that the CSN plays an important role in plant auxin signaling (Schwechheimer et al., 2001). Mutants in any CSN subunit exhibit auxin-related phenotypes, such as resistance to auxin-mediated root growth inhibition and lateral root formation (Schwechheimer et al., 2001; Dohmann et al., 2005; Zhang et al., 2008). In a dose-response assay measuring the auxin inhibition of root elongation on plates supplemented with the synthetic auxin 2,4-D, I tested if the *csn1-10* and *csn3-3* were resistant to the exogenous auxin (**Figure 7A**). The root growth of wild type (Col) seedlings was nearly completely inhibited at 0.05μM of 2,4-D. However, like the *tir1-1* seedlings, *csn3-3* seedlings were partically resistant to this inhibition, displaying only ~50% inhibition of root growth, indicating *csn3-3* resulted in mild auxin response defects. A similar extent of auxin resistance was also seen in the *csn1-10* genetic background. Additionally, both *csn1-10* and *csn3-3* enhanced the weak auxin resistance phenotype of *tir1-1*, and *csn3-3 tir1-1* and *csn1-10 tir1-1* double mutants exhibited comparable dose-response profiles in root growth inhibition assays (**Figure 7A**).

I also tested if the *csn1-10 csn3-3* double mutant exhibited enhanced root growth resistance, by a similar root growth assay comparing *csn1-10*, *csn3-3* and the double mutant. As seen in **Figure 7B**, the *csn1-10 csn3-3* double mutant had a similar root growth inhibition curve as either single mutant did. For comparison, I also crossed *csn1-10* and *csn3-3* with another viable *csn* mutant, *csn5a-2*, which is a loss of function allele of one of the *CSN5* paralogs, *CSN5A* (Gusmaroli et al., 2007). As seen in **Figure 7C**,

csn1-10 and *csn3-3* were more resistant to the root growth inhibition than *csn5a-2* at 0.03μM and 0.04μM 2,4-D treatments. Again, *csn5a-2* could not enhance the auxin resistance in either the *csn1-10* or *csn3-3* mutant background.

To rule out the possibility that *csn1-10* or *csn3-3* were specifically resistant to the synthetic auxin 2,4-D, I tested the mutants on plates containing the natural auxin, IAA. Since IAA is not stable under the light, the measurements were taken after 1-day treatment. The *csn3-3* seedlings clearly showed the comparable auxin response defects as the *tir1-1* control in root elongation and exacerbate the *tir1-1* phenotype in the double mutant (**Figure 8A**). In the *csn1-10* case, the mutation also caused very slight defects in response to the IAA treatment and enhanced the *tir1-1* IAA-resistance (**Figure 8B**). Together with my 2,4-D root growth results (**Figure 7**), I concluded that both *csn1-10* and *csn3-3* share quantitatively similar auxin resistance and that both enhance the *tir1-1* phenotype in root elongation.

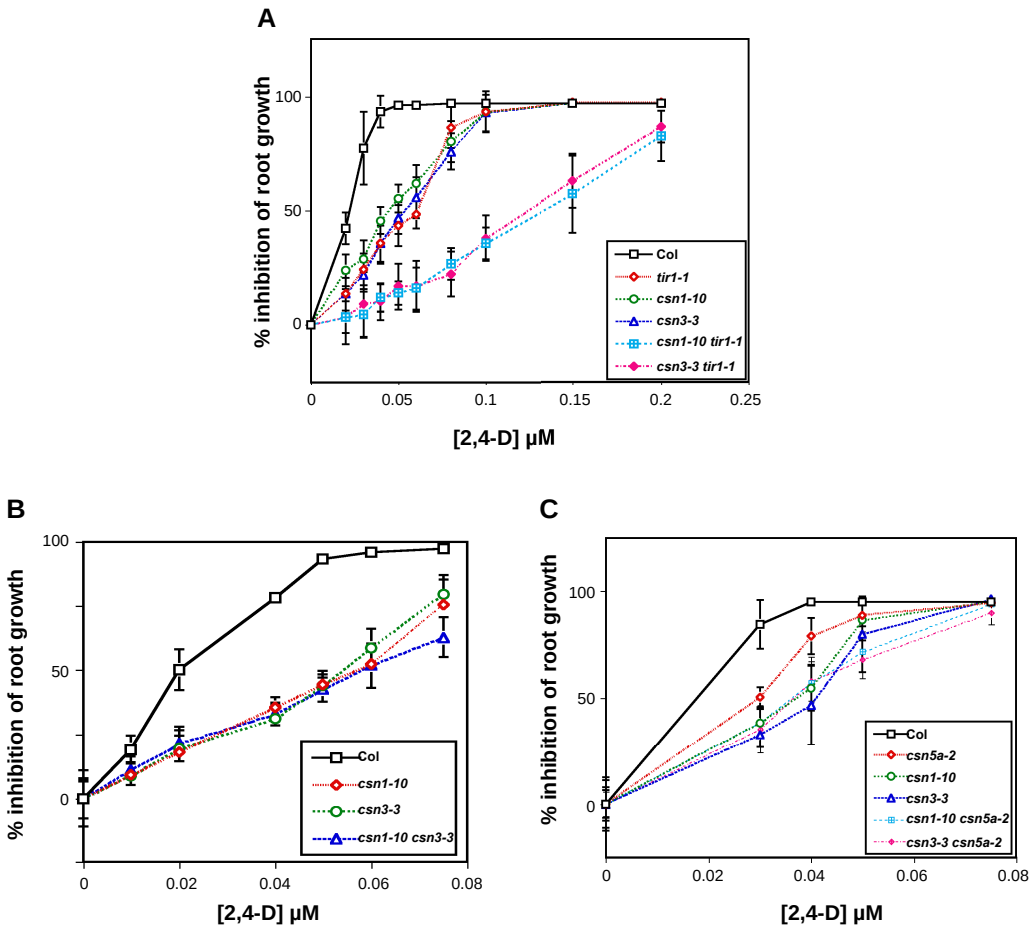

Figure 7. Defects of *csn1-10* and *csn3-3* on 2,4-D induced root growth inhibition.

Inhibition of root elongation by increasing concentrations of the synthetic auxin 2,4-D was measured using 5-day-old (d.o.) seedlings of different genetic backgrounds (A~C). Seedlings (n≥15) grown on ATS medium were transferred to medium containing 2,4-D and grown for another four days. Data are presented as percent inhibition of root growth compared to growth on unsupplemented ATS. Error bars = SD.

(A) Col, *tir1-1*, *csn1-10*, *csn3-3*, *csn1-10 tir1-1* and *csn3-3 tir1-1*.
(B) Col, *csn1-10, csn3-3* and *csn1-10 csn3-3*.
(C) Col, *csn5a-2, csn1-10, csn3-3, csn1-10 csn5a-2* and *csn3-3 csn5a-2*.

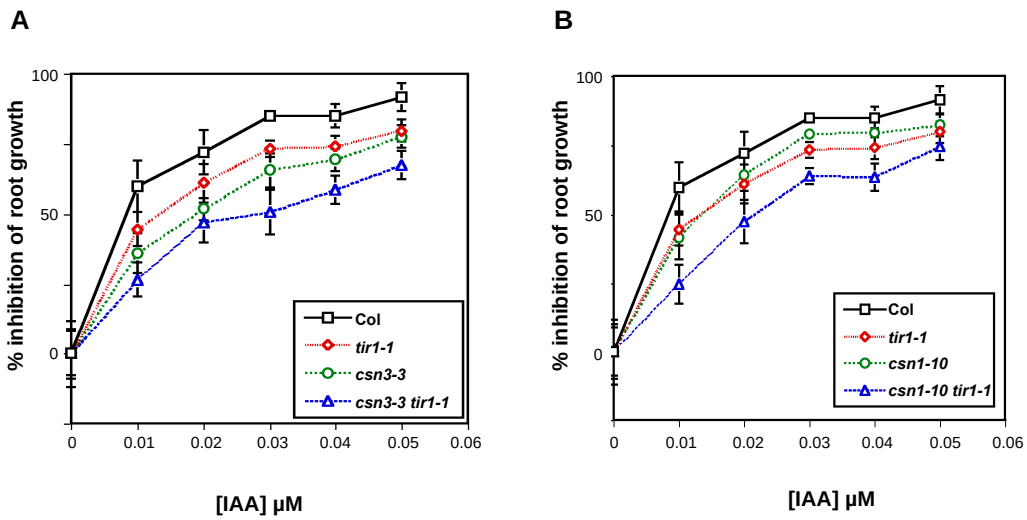

Figure 8. *csn1-10* and *csn3-3* confer slight resistance to IAA induced root growth inhibition.

6-d.o. seedlings of different genetic backgrounds (n≥15) grown on ATS medium were transferred to medium containing IAA and grown for 1 day . Data are presented as percent inhibition of root growth compared to growth on unsupplemented ATS. Error bars = SD.

(A) Col, *tir1-1, csn3-3* and *csn3-3 tir1-1.*

(B) Col, *tir1-1, csn1-10* and *csn1-10 tir1-1*.

45 of 191 F2 seedlings from a *csn3-3* x Col backcross exhibited auxin-resistant root growth on media supplemented with 0.05μM 2,4-D, suggesting the *csn3-3* is a recessive mutation of a single locus (3:1, χ^2=0.211<3.84 at p=0.05). However, when transferred to 0.03 μM 2,4-D media, greater than 50% of the *csn3-3* F2 population exhibited resistance (**Figure 9**). In order to investigate whether this was due to a dominant negative effect of the *csn3-3* mutation or haploinsufficiency, I included *CSN3/csn3-2* heterozygotes as a control. *csn3-2* is a null allele of *CSN3* caused by a T-DNA insertion (SALK_106465), and was seedling lethal when homozygous (Dohmann et al., 2008a). As expected, among the non-*csn3-2* homozygotes (*CSN3/csn3-2* or *CSN3/CSN3*) obtained from the *csn3-2* segregating population, nearly all exhibited the Col-like sensitivity to the treatment of 0.03μM 2,4-D, suggesting *CSN3/csn3-2* seedlings are behaving like the wild type control and loss of one copy of *CSN3* does not result in the auxin resistance at low 2,4-D concentrations. However, in the *csn3-3* x Col F2 segregating population, more than one fourth of the seedlings exhibited resistance to 2.4-D (**Figure 9**). Genotyping the mild resistant seedlings of the *csn3-3* x Col F2s confirmed they are *CSN3/csn3-3*. These findings suggest that the *csn3-3* mutation displayed a weak dominant behavior at a lower concentration of exogenous auxin.

Previous reports have shown that plants expressing a CSN5 antisense construct develop fewer lateral roots and reduced root hair elongation compared to wild-type controls (Schwechheimer et al., 2001). Although *csn3-3* or *csn1-10* alone did not confer such defects when compared to Col, the *csn3-3* and the *csn1-10* mutations enhanced the weak lateral root defect of *tir1-1* seedlings, with both double mutants developing fewer

than 50% of the number of lateral roots observed in *tir1-1* seedlings (**Figure 10**). Furthermore, *csn1-10 csn3-3* double mutants developed significantly fewer lateral roots, suggesting that auxin response was more severely impaired in the double mutant background (**Figure 10**).

To summarize, both *csn3-3* and *csn1-10* are weak auxin mutants, exhibiting a quantitatively similar defect in the auxin-induced root growth inhibition. In addition, both *csn3-3* and *csn1-10* can enhance the root growth phenotype as well as the lateral root initiation defect of the *tir1-1* mutant.

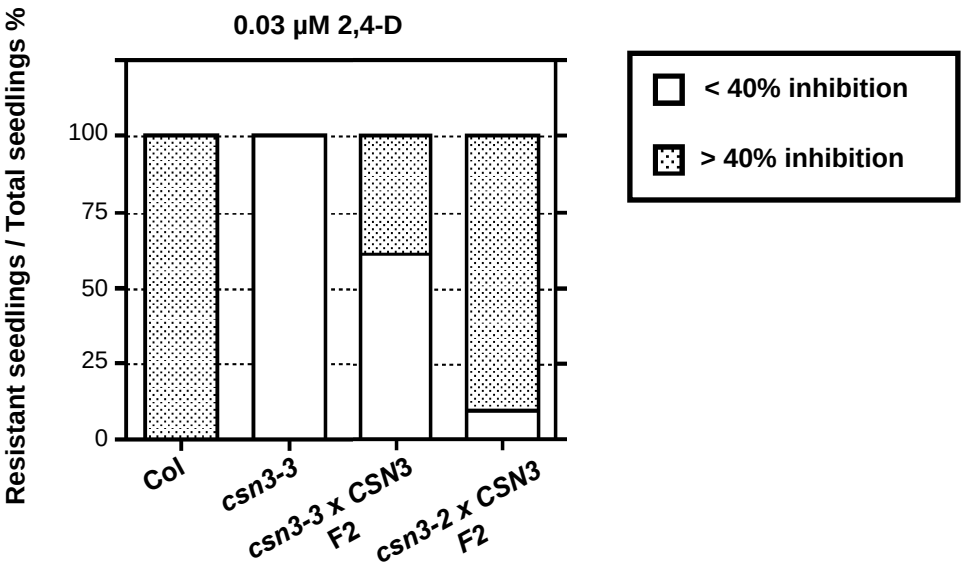

Figure 9. *csn3-3* exhibits semi-dominance on low concentration of 2,4-D.
csn3-3 x Col F2 seedlings (n = 60) were tested in a root growth assay similar to as described in **Figure 7**, but on ATS medium containing 0.03 µM 2,4-D. Data are presented as proportion of seedlings displaying greater than or less than 40% inhibition of root growth. Col, *csn3-3* and viable (non *csn3-2/csn3-2*) progeny from *CSN3/csn3-2* parental plants were used as controls.

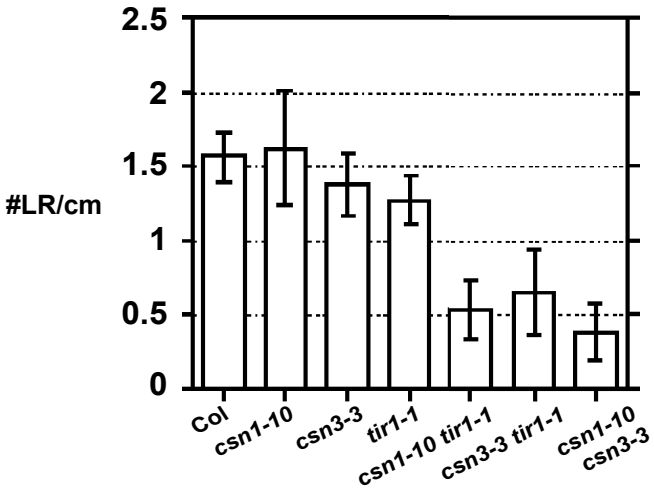

Figure 10. *csn1-10* and *csn3-3* enhance the lateral root initiation phenotype of *tir1-1*.
Lateral root (LR) initiation was measured in 11-d.o. seedlings grown on unsupplemented ATS medium. Data were presented as number of the lateral root initiations (#LR) per cm root length. Error bars = SD (n≥15).

Similar defects in the expression of auxin responsive reporters are found in *csn3-3* and *csn1-10*

To further investigate the auxin response defects of *csn3-3* and *csn1-10* mutants, I introduced the *BA3:GUS* auxin responsive reporter (Oono et al., 1998; Chuang et al., 2004) into the mutants. Treatment of Col [*BA3:GUS*] control seedlings with 1μM 2,4-D triggered a strong GUS signal in the root elongation zone. In contrast, only a slight induction of BA3-GUS activity was observed in *csn3-3* seedlings carrying the *BA3:GUS* construct (**Figure 11A**, upper). Auxin-inducible gene expression was also examined by using the *DR5:GUS* auxin reporter (Ulmasov et al., 1997), the expression of which is stronger than the *BA:GUS* reporter upon auxin treatments (**Figure 11A**). Again, the comparison between 2,4-D treated *csn3-3* [*DR5:GUS*] and Col [*DR5:GUS*] seedlings showed that the expression of DR5-GUS was reduced in the mutant background (**Figure 11A**, lower). I also examined *csn1-10* seedlings carrying the BA3- or DR5-GUS reporters for comparison with *csn3-3*. Similarly, *csn1-10* seedlings displayed defects that are were virtually identical to those of *csn3-3* in expression of both auxin responsive reporters (**Figure 11A**).

When treated with IAA, *csn3-3* and *csn1-10* mutants carrying either the *BA:GUS* or the *DR5:GUS* reporter also showed similar defects in reporter expression, with reduced GUS signal detected in both mutant backgrounds compared to the wild type control at indicated conditions (**Figure 11A**, right). However, the DR:GUS signal triggered by the endogenous auxin (Mock treatment) in *csn1-10* appeared stronger than

either wild type or the *csn3-3* seedlings (**Figure 11B**). In addition, the GUS signal was detected in a broader region within the root tip of *csn1-10*.

Together, my results on auxin responsive reporter expression also suggested that both *csn3-3* and *csn1-10* share similar auxin response defects. The different response to the endogenous IAA may distinguish *csn1-10* from *csn3-3*.

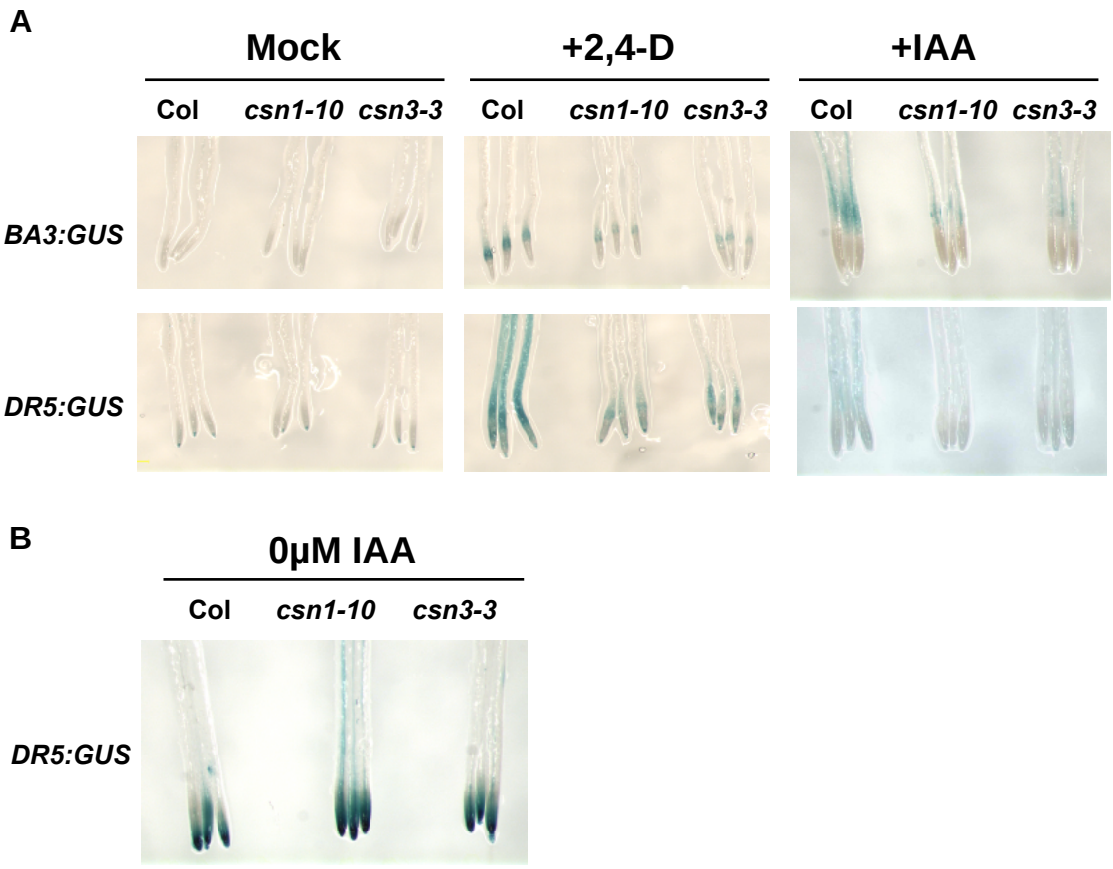

Figure 11. Auxin induced reporter expression is reduced by the *csn1-10* and *csn3-3* mutations to a similar extent.

(A) Transgenic Col, *csn1-10* and *csn3-3* carrying either the *BA3:GUS* or *DR5:GUS* reporters. For 2,4-D treatment (middle), 6-d.o. seedlings were treated with 0.5μM 2,4-D for 12 hrs (BA3:GUS) or 4 hrs (DR5:GUS) before histochemical staining.
For IAA treatment (right), BA3-GUS seedlings were incubated with 1uM IAA for 3 hrs before histochemical staining, while DR5-GUS seedlings were incubated with 0.5μM IAA overnight and were stained for less than 10 min.

(B) Endogenous auxin induced DR5:GUS expression in transgenic Col, *csn1-10* and *csn3-3* carrying *DR5:GUS*. Seedlings were treated with unsupplemented ATS media (0μM IAA) for 3 hrs before GUS staining.

csn3-3 is a weak missense allele of *CSN3* with normal skotomorphogenesis

Sequencing of the *CSN3* locus revealed that *csn3-3* is a G to A point mutation located in the exon 8 of *AtCSN3*, resulting in a G293E substitution within the PCI domain (**Figure 12A**). The PCI domain is important for subunit interaction and complex assembly (Tsuge et al., 2001). It can be further divided into the N-terminal helix bundle (HB) subdomain and the C-terminal winged-helix (WH) subdomain based on the crystal structure of AtCSN7 PCI domain (Dessau et al., 2008). Using an online secondary structure prediction tool (Kelley and Sternberg, 2009), I found that the Gly 293 is located within the WH subdomain. Primary sequence alignment among PCI domains of several CSN3 orthologs revealed that Gly 293 is extremely highly conserved throughout eukaryotes (**Figure 12B**).

In order to demonstrate that the auxin defects I observed were caused by the *csn3-3* mutation, I conducted complementation tests with the *fus11 allele of CSN3* (Peng et al., 2001a). Heterozygous *CSN3/fus11* plants in the Ler ecotype were crossed with *csn3-3* homozygotes. F1 seedlings tested on 0.05μM 2,4-D plates showed a 1:1 segregation for auxin-resistant root growth (sensitive vs. resistant seedlings =57: 70, χ^2=1.33), indicating that *csn3-3* and *fus11* are indeed allelic. To rule out potential complications resulting from ecotype differences, I also conducted complementation tests by transforming a genomic *CSN3* construct into the *csn3-3* [*BA3:GUS*] background. In testing two independent complementation lines (L2 and L4), I found that the *CSN3* genomic DNA was able to rescue both the auxin inhibition of root growth and reduced BA3-GUS phenotypes of *csn3-3* plants (**Figure 12C and 12D**). Both L2 and L4 lines have a wild-

type-like root growth inhibition curve and BA:GUS signal in response to the 2,4-D treatment. These findings confirmed that the auxin related phenotypes of this mutant were indeed caused by mutation of *CSN3*.

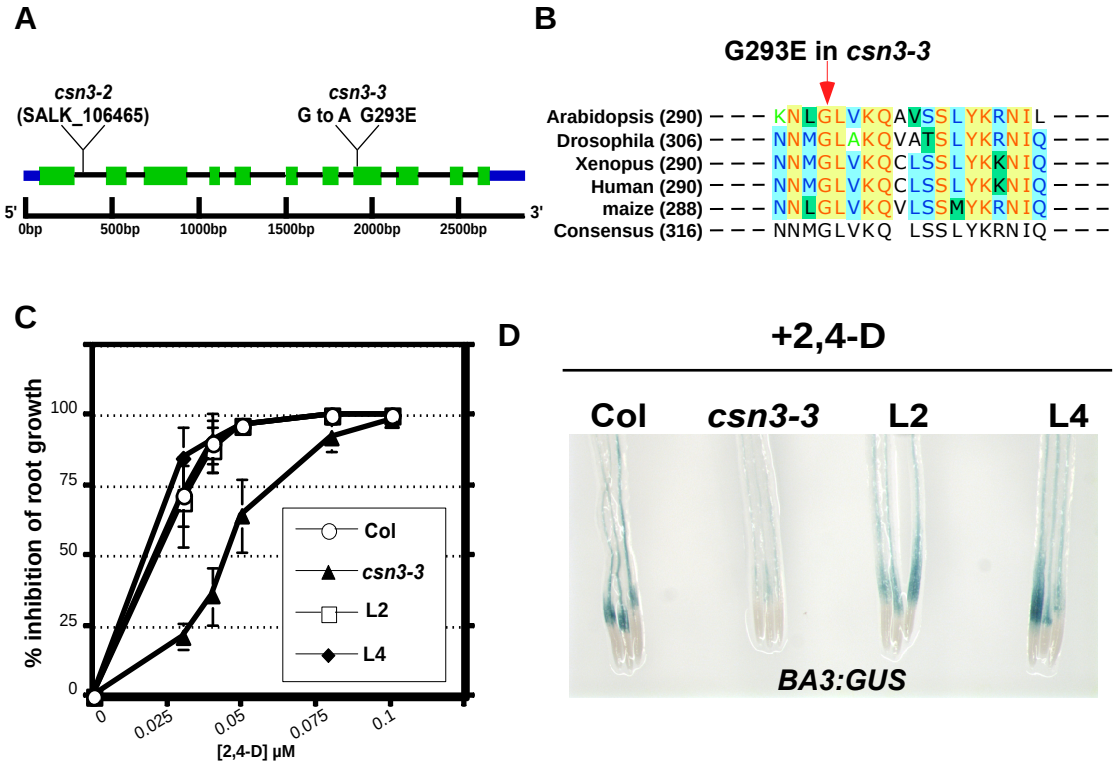

Figure 12. Auxin response defects in *csn3-3* is caused by a missense mutation within the *AtCSN3* gene.

(A) Schematic representation of the Arabidopsis *CSN3* gene. Exons are shown as green boxes and introns and upstream sequences as lines. 5‘ and 3’ untranslated regions are shown as blue boxes. Positions of the T-DNA insertion of *csn3-2* (SALK_106465) and the point mutation in *csn3-3* are indicated.

(B) Sequence alignment around the *csn3-3* mutation among the *CSN3* homologs from *Arabidopsis thaliana, Drosophila melanogaster, Xenopus laevis, Homo sapiens* (Human) and *Zea mays* (maize). The arrow indicates the *csn3-3* G293E missense mutation.

(C-D) Complementation of the *csn3-3* auxin resistance (C) and reduced BA3:GUS expression (D) phenotypes by introduction of a genomic *CSN3* transgene. L2 and L4 are two independent *csn3-3* [*gCSN3*] transformants.

In Arabidopsis, loss of any of the eight CSN subunits results in an identical suite of phenotypes, including constitutive photomorphogenesis, anthocyanin accumulation, and seedling lethality (Gusmaroli et al., 2004; Gusmaroli et al., 2007; Dohmann et al., 2008a). Previously described viable *csn* mutants include single mutants of the two MPN domain subunits, which are each encoded by two highly homologous genes (*CSN5A/CSN5B* (Kwok et al., 1998) and *CSN6A/CSN6B* (Peng et al., 2001b)), *csn1-10* (Zhang et al., 2008) and *csn2-5* (Stuttmann et al., 2009) missense mutants. Unlike previously described *csn3* alleles (Peng et al., 2001a; Gusmaroli et al., 2007; Dohmann et al., 2008b), *csn3-3* is viable throughout development compared to the seedling lethal phenotype of *csn3-2* (**Figure 13A**). The *csn3-3* adult plants grow to a similar height as wild type plants do (**Figure 13A**) and the *csn3-3* seedlings do not exhibit a *co*nstitutive *p*hotomorphogenic (*cop*) phenotype when grown in the dark (**Figure 13C**).

Similarly, the adult plants of *csn1-10* are also viable throughout the entire life cycle, although the mutant adult exhibits mild dwarfism when compared with the Col control (**Figure 13A**). When combined with *csn3-3*, the dwarf growth phenotype of *csn1-10* is enhanced (**Figure 13B**). Both the *csn1-10* and *csn1-10 csn3-3* are viable and distinguished from prior *csn1* alleles (Staub et al., 1996; Gusmaroli et al., 2007), which are arrested at the seedling stage. Different from *csn3-3* dark grown seedlings, the etiolated *csn1-10* seedlings exhibit subtle *cop/fus/det* phenotype with their cotyledons slightly open (**Figure 13C**) and shorter hypocotyls (**Figure 13C and 13D**). The *csn1-10 csn3-3* double mutants also have shorter hypocotyls and more opened cotyledons when grown in dark (**Figure 13C and 13D**).

Together, my results show that both *csn3-3* and *csn1-10* are viable *csn* mutants and provide useful genetic tools to study the CSN functions throughout the entire plant life cycle.

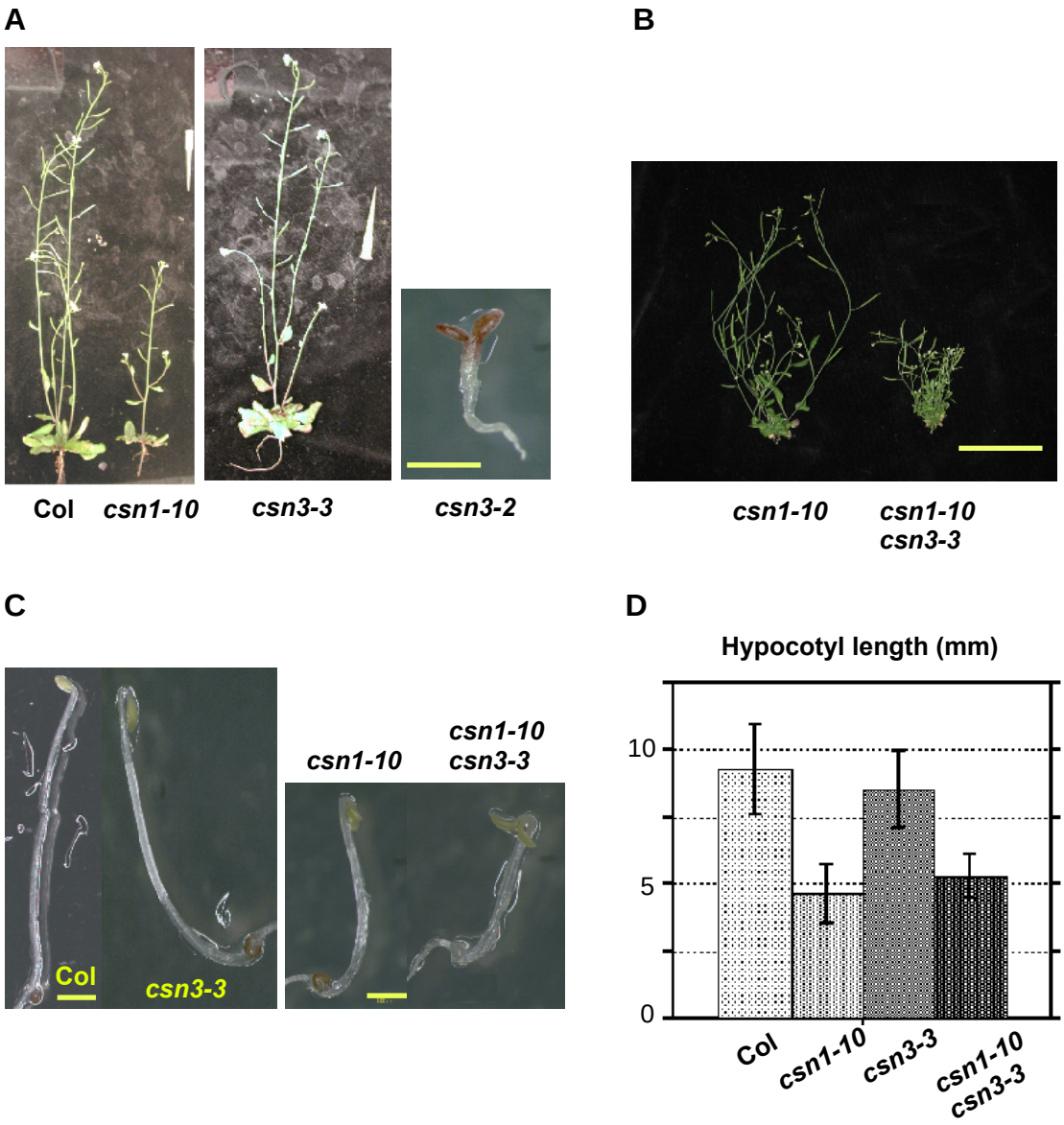

Figure 13. Both *csn1-10* and *csn3-3* are viable *csn* mutants.

(A) Phenotypes of Col, *csn1-10* and *csn3-3* adult (30-d.o.) plants (left two panel), in comparison with the seedling-lethal *cop/det/fus* phenotype of *csn3-2* null mutant (right). Scale bar=1mm.

(B) 45-d.o. adult plants of *csn1-10* and *csn1-10 csn3-3*, showing the enhanced dwarfism in the double mutant. Scale bar=4cm.

(C) 4-d.o. Col, *csn1-10*, *csn3-3* and *csn1-10 csn3-3* etiolated seedlings. Scale bar=1mm

(D) Hypocotyl length of etiolated 4-d.o. Col, *csn1-10, csn3-3* and *csn1-10 csn3-3* seedlings (n≥15).

The *csn1-10* mutation results in an alternative RNA splicing and reduces the abundance of CSN1.

37 of 160 F2 seedlings from *csn1-10* x Col backcross exhibited auxin-resistant root growth on media supplemented with 0.05μM 2,4-D, suggesting the *csn1-10* is a recessive mutation of a single locus (3:1, χ^2=0.3<3.84 at p=0.05). Fine mapping and the sequencing results of the *CSN1* locus in *csn1-10* revealed that there is a G to A point mutation within the last base of the *AtCSN1* exon 4 and results in a S305N substitution of the amino acid. (**Figure 14A**). Alignment of the CSN1 sequence among various organisms revealed that the Ser305 is also located in the PCI domain and highly conserved throughout eukaryotes (**Figure 14B**).

As revealed by the RT-PCR analysis, the CSN1 mRNA level was reduced in the *csn1-10* mutant (**Figure 14C)**. Sequencing results of the amplified product also revealed that the point mutation in *csn1-10* caused an alternative splicing event and generated a premature stop codon (Zhang et al., 2008 and **Figure 39**). The CSN1 protein abundance was dramatically reduced in *csn1-10* (**Figure 14D**). However, no truncated form of CSN1 protein was detected in the western blotting, which possibly means that the CSN1 alternative mRNA product cannot be translated into the protein or that the truncated CSN1 is not stable and rapidly degraded. The decrease of the CSN1 abundance may explain the more severe (dwarf) growth phenotype of the *csn1-10* mutant than *csn3-3* (**Figure 13A**), since the *csn3-3* mutation had no effects on the CSN3 protein level (**Figure 18E**). Furthermore, the ectopic expression of either the *CSN1* wild type cDNA or its *csn1-10* mutated form in *csn1-10* background could rescue the mutant root growth

phenotype on 2,4-D plates (**Figure 14E**), indicating that the *csn1-10* auxin phenotype is not due to the missense mutation but reduction of the protein abundance.

To summarize, defects caused by the *csn1-10* mutation are complicated. The mutation reduces mRNA level, causes an alternative splicing event and decreases the protein production. However, the reduction of CSN1 protein, rather than the missense mutation, is the main cause for the auxin phenotype observed in *csn1-10*.

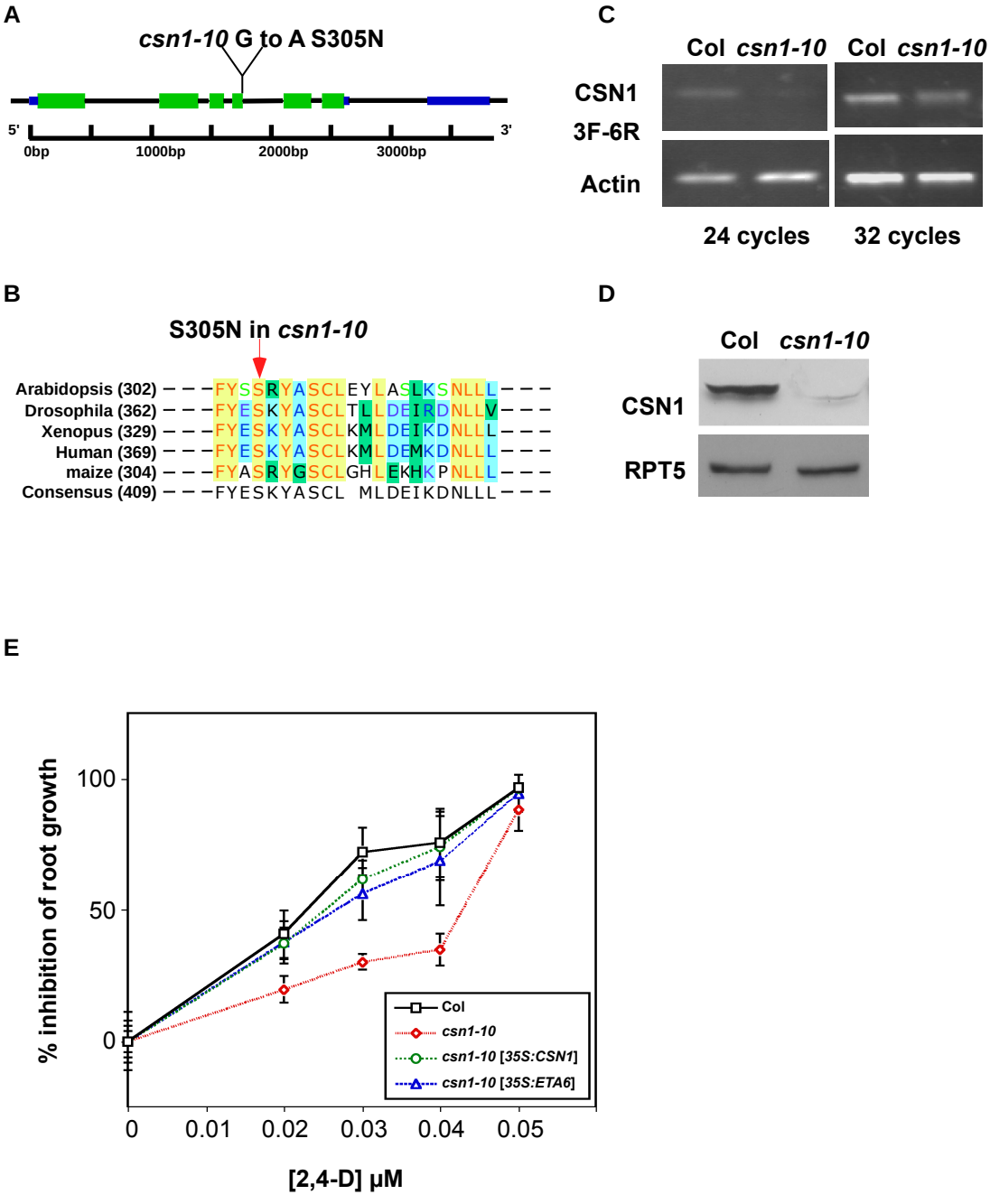
A
csn1-10 G to A S305N
5'
3'
0bp
1000bp
2000bp
3000bp
C
Col csn1-10 Col csn1-10
CSN1
3F-6R
Actin
24 cycles
32 cycles
B
S305N in csn1-10
Arabidopsis (302)
Drosophila (362)
Xenopus (329)
Human (369)
maize (304)
Consensus (409)
D
Col csn1-10
CSN1
RPT5
E
% inhibition of root growth
100
50
0
0
0.01
0.02
0.03
0.04
0.05
[2,4-D] µM
Col
csn1-10
csn1-10 [35S:CSN1]
csn1-10 [35S:ETA6]

Figure 14. The *csn1-10* mutation causes reduction of the CSN1 protein abundance.

(A) Schematic representation of the Arabidopsis *CSN1* gene. Exons are shown as green boxes and introns and upstream sequences as lines. 5‘ and 3’ untranslated regions are shown as blue boxes. The point mutation in *csn1-10* is indicated.

(B) Sequence alignment around the *csn1-10* mutation among the CSN1 homologs from *Arabidopsis thaliana, Drosophila melanogaster, Xenopus laevis, Homo sapiens* (Human) and *Zea mays* (maize). The arrow indicates the *csn1-10* S305N missense mutation.

(C) RT PCR analysis of Col and *csn1-10*. Gene specific primers spanning the *AtCSN1* exon 3 and exon 6 were used to amplify the transcript. The expression level of actin was used to normalize the data. Numbers of RT-PCR amplification cycles are labeled at the bottom.

(D) CSN1 protein level is affected by the *csn1-10* mutation. Western detection of CSN1 using seedling protein extracts. RPT5 is used as a loading control.

(E) The 2,4-D induced inhibition on root elongation of Col, *csn1-10*, *csn1-10* [*35S:CSN3*] and *csn1-10* [*35S:ETA6*] seedlings. The root growth assay was done as prior mentioned to test the 2,4-D sensitivity of transgenic plants (n≥15). Data are presented as percent inhibition of root growth compared to growth on unsupplemented ATS. Error bars = SD.

CUL1 deneddylation and Aux/IAA stability in *csn1-10* and *csn3-3*

The CSN cleaves the NEDD8/RUB peptide from the CUL1 subunit of the SCF ubiquitin ligases (deneddylation). All previously reported *csn* mutants, such as *csn3-2* (Dohmann et al., 2008a), *csn5a-2* (Gusmaroli et al., 2007), and the weaker *csn2-5* mutant (Stuttmann et al., 2009), result in an increase in the CUL1-RUB to unmodified CUL1 ratio. Therefore I examined if the *csn3-3* or *csn1-10* mutation affected the CUL1 deneddylation.

The immunoblot detection of CUL1 in wild type control could clearly identify both neddylated or deneddylated forms of CUL1 (CUL1-RUB or CUL1). CUL1 was almost exclusively in its neddylated form (CUL1-RUB) in the *csn3-2* null mutant (**Figure 15A**). Consistent with prior reports (Dohmann et al., 2008a), this result suggested the null mutation completely abolished the CSN-mediated CUL1 deneddylation. A clear increase in the CUL1-RUB:CUL1 ratio was seen in extracts prepared from *csn1-10* mutant seedlings, as well as in extracts made from the previously reported *csn5a-2* seedlings (Gusmaroli et al., 2007) and **Figure 15A**), suggesting both mutation affect the CSN-mediated deneddylation to a similar extent. However, no such defect was detected in *csn3-3*. The CUL1-RUB/CUL1 distribution in *csn3-3* resembled that in the wild type control (**Figure 15A**). It is possible that the *csn3-3* mutation caused subtle defects on deneddylation, which was difficult to detect in the single mutant background. To test this possibility, I constructed double mutants with *csn1-10* to examine if *csn3-3* might enhance the weak deneddylation defect seen in *csn1-10*. Once again however, the *csn1-*

10 csn3-3 double mutant had the same extent of deneddylation defect when compared to that of the *csn1-10* single mutant (**Figure 15A**).

Since the CSN also regulates other cullin-based E3 ubiquitin-ligases by deneddylating their cullin subunit, I applied a similar immunoblotting assay to examine CUL4 modification in *csn3-3* seedlings. Similar to our findings with CUL1, I observed no accumulation of the CUL4-RUB isoform in *csn3-3* extracts and in Col, whereas CUL4-RUB was readily detected in *csn1-10* and *csn5a-2* extracts (**Figure 15B)**. Again, the *csn1-10 csn3-3* double mutant didn't enhance the *csn1-10* CUL4 deneddylation defects (**Figure 15B)**. Together, my analyses of CUL1 and CUL4 immunoblots suggest that unlike *csn1-10* or previously characterized *csn* mutant, the *csn3-3* mutation did not affect the deneddylation activity of the CSN.

The reduced deneddylation activity of several previously characterized *csn* mutants has been found to result in diminished $SCF^{TIR1/AFB}$ activity, making the Aux/IAA proteins more stable (Schwechheimer et al., 2001; Stuttmann et al., 2009). Since our finding that *csn3-3* plants exhibited no change in cullin deneddylation was quite surprising, I examined $SCF^{TIR1/AFB}$ activity by monitoring Aux/IAA stability using the previously described HS:AXR3NT-GUS reporter protein (Gray et al., 2001). Again, *csn1-10* seedlings were included for comparison. 6-d.o. Col, *csn1-10* and *csn3-3* seedlings, all of which were homologous for the *HS:AXR3NT-GUS* transgene, were heat shocked to induce reporter expression, followed by return to ambient temperature and treatment with auxin. AXR3NT-GUS activity was examined both qualitatively and quantitatively at 20 min intervals during the treatment to monitor the remaining levels of

AXR3NT-GUS fusion protein (**Figure 15C and 15D)**. Following the 2h heat-shock induction, similar AXR3NT-GUS levels were observed in wild type, *csn1-10* and *csn3-3* seedlings (**Figure 15C**). During the auxin treatment, AXR3NT-GUS activity in *csn3-3* and wild type seedlings diminished with comparable kinetics (**Figure 15D)**, suggesting that $SCF^{TIR1/AFB}$ activity was unaffected in *csn3-3* plants. In contrast, *csn1-10* seedlings exhibited significantly slower AXR3NT-GUS degradation (Zhang et al., 2008) and **Figure 15C and 15D**. These results indicate that the $SCF^{TIR1/AFB}$-mediated proteolysis was affected by *csn1-10* but not *csn3-3*.

To further confirm that *csn3-3* had no effect on $SCF^{TIR1/AFB}$-mediated proteolysis, I examined the *in vivo* degradation of another Aux/IAA reporter, IAA28-myc (Strader et al., 2008). The IAA28-myc construct was crossed into *csn3-3* and *csn1-10* backgrounds. Abundance of IAA28-myc in IAA-treated seedlings was detected by western blots using root protein extracts. As previously reported (Strader et al., 2008), IAA28-myc was rapidly degraded in wild type seedlings and was nearly undetectable after a 10-minute IAA treatment (**Figure 15E**). While IAA28-myc was clearly more stable in *csn1-10* seedlings, it was rapidly degraded in the *csn3-3* background (**Figure 15E**). At the 10' time point, the remaining level of IAA28-myc fusion protein in *csn3-3* looks similar as that of Col. Combined with our HS:AXR3NT-GUS degradation data, this strongly suggests that $SCF^{TIR1/AFB}$ activity was unaltered by the *csn3-3* mutation.

To summarize, unlike *csn1-10* or other previously reported *csn* mutants (Gusmaroli et al., 2007; Stuttmann et al., 2009), both the cullin modification and the Aux/IAA degradation was not affected by the *csn3-3* mutation.

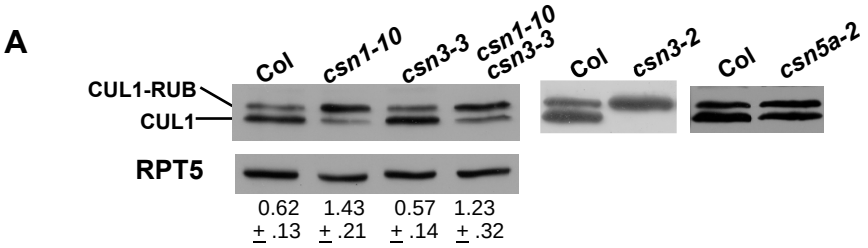
A
Col
csn1-10
csn3-3
csn1-10 csn3-3
Col
csn3-2
Col
csn5a-2
CUL1-RUB
CUL1
RPT5
0.62 ± .13
1.43 ± .21
0.57 ± .14
1.23 ± .32

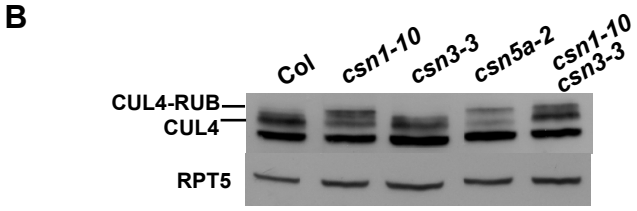
B
Col
csn1-10
csn3-3
csn5a-2
csn1-10 csn3-3
CUL4-RUB
CUL4
RPT5

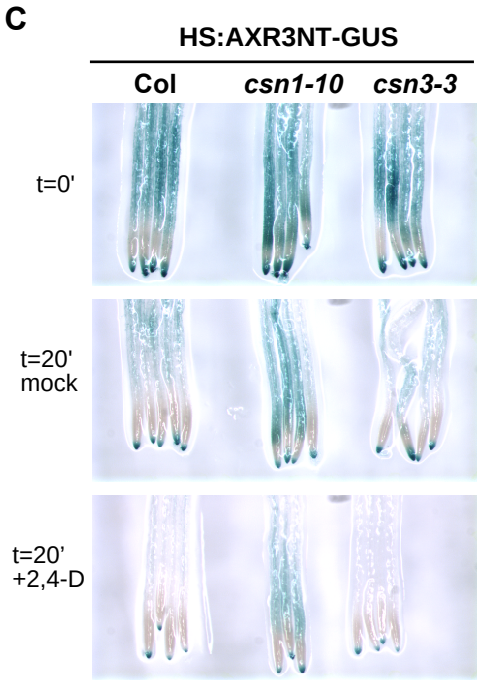
C
HS:AXR3NT-GUS
Col
csn1-10
csn3-3
t=0'
t=20' mock
t=20' +2,4-D

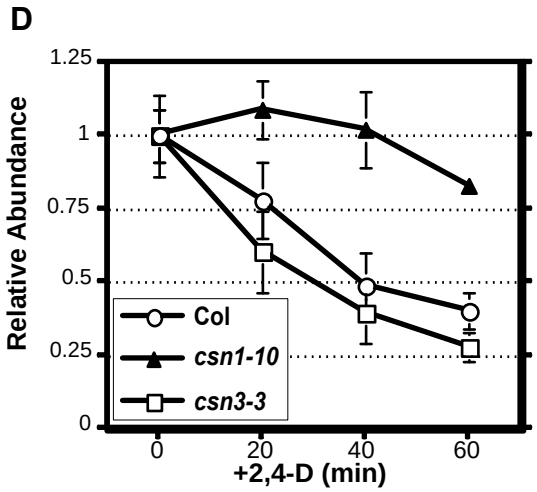
D
Relative Abundance
1.25
1
0.75
0.5
0.25
0
0
20
40
60
+2,4-D (min)
Col
csn1-10
csn3-3

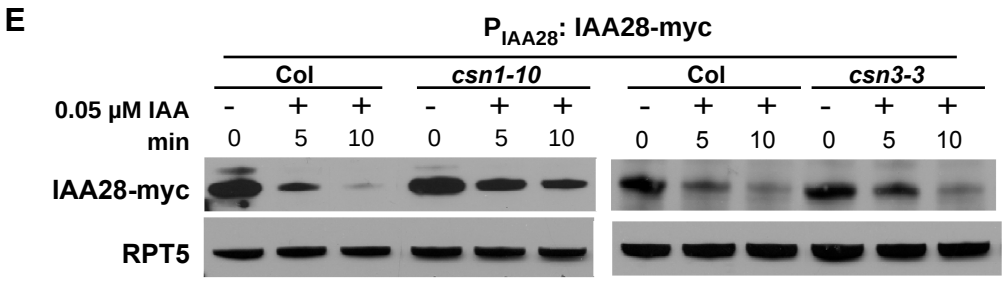
E
P IAA28: IAA28-myc
Col
csn1-10
Col
csn3-3
0.05 µM IAA
min
IAA28-myc
RPT5

Figure 15. *csn3-3* affects auxin response by an $SCF^{TIR1/AFB}$- independent mechanism.

(A) CUL1 western blot analysis of protein extracts prepared from Col and *csn* mutant seedlings. The upper band indicates the RUB-modified (neddylated) CUL1. RPT5 is shown as a loading control. Numbers at the bottom show the ratio of CUL1-RUB:CUL1 plus ±SD from three experiments.

(B) Western blot analysis of CUL4 neddylation status in Col and *csn* mutant seedling extracts.

(C) Col, *csn1-10* and *csn3-3* carrying *HS:AXR3NT-GUS* transgene were heat shocked for 2hrs and stained immediately or following incubation with 1 μM 2,4-D for 20 min.

(D) Quantitative measurement of the GUS signal of the *HS:AXR3NT-GUS* reporter in Col, *csn1-10*, and *csn3-3* seedlings. Seedlings were heat-shocked for 2hrs, and then returned to room temperature and treated with 1 μM 2,4-D for 20, 40, or 60 min. GUS signal is presented as the percentage remaining compared to the 0 min time point. Values shown depict the mean±SD of 3 assays.

(E) myc western detection of the IAA28-myc fusion protein. The P_{IAA28}*:IAA28-myc* reporter was introduced into the *csn1-10* and *csn3-3* backgrounds by crossing. Protein extracts were made from 7-d.o. seedling roots treated with IAA or solvent control. RPT5 was used as a loading control.

Genetic interactions distinguish *csn3-3* and *csn1-10*

The CSN regulates auxin signaling by deneddylating CUL1 to modulate the $SCF^{TIR1/AFB}$ activity (Lyapina et al., 2001; Schwechheimer et al., 2001). My findings with the *csn1-10* mutant were consistent with this model. The *csn3-3* mutation on the other hand, affected neither CUL1 deneddylation nor $SCF^{TIR1/AFB}$-mediated Aux/IAA degradation, yet conferred auxin response defects virtually identical in severity to *csn1-10*. These findings strongly suggest that the CSN, or at least the CSN3 subunit, plays a second role in the regulation of auxin signaling in addition to deneddylating CUL1. If so, *csn3-3* and *csn1-10* may exhibit distinct genetic interactions when combined with other mutations affecting auxin signaling.

I therefore crossed *axr1-12* plants with *csn1-10* and *csn3-3* to generate double mutants. The *axr1-12* mutation affects a subunit of the NEDD8 activating enzyme (E1, **Figure 4**). This mutation confers a reduction in CUL1 neddylation and strong auxin response defects (Lincoln et al., 1990; del Pozo and Estelle, 1999; del Pozo et al., 2002). The interaction between *axr1-12* and *csn1-10* appeared additive, as double mutants exhibited a moderately more severe dwarf phenotype than the single mutant parents (**Figure 16A**). In sharp contrast, *csn3-3 axr1-12* doubles displayed a seedling-lethal phenotype (**Figure 16B**), indicating that *axr1-12* and *csn3-3* interact synergistically. Double mutant seedlings exhibited cotyledon morphogenic defects and lacked a basal pole similar to loss-of-function mutants of the *monopteros* (*mp*) auxin response factor and the dominant negative *axr6-1* and *axr6-2* alleles of *CUL1* (Hardtke and Berleth, 1998; Hobbie et al., 2000). Furthermore, a slightly less severe phenotype was observed in

CSN3/csn3-3 axr1-12/axr1-12 seedlings (**Figure 16B**). Similar results were found when I crossed *axr1-3*, a relatively weak allele of *AXR1*, with these *csn* mutants: *axr1-3 csn1-10* plants are dwarf viable (data not shown), while *csn3-3 axr1-3* caused seedling lethality (**Figure 16C**). Again, in the dead seedlings of the F2 population, I found some of them are *CSN3/csn3-3*, showing less severe phenotype.

Another set of genetic interactions was tested when *csn1-10* and *csn3-3* were combined with *axr6-3*. *axr6-3* is a temperature-sensitive allele of *CUL1* that exhibits reduced CUL1 neddylation and severe auxin response defects (Quint et al., 2005). Similar results to the *axr1* double mutants were found in this combination. While *csn1-10 axr6-3* plants were viable, flowered, and produced a few seeds, *csn3-3 axr6-3* plants exhibited arrested development, with virtually no root growth occurring even after 45 of growth (**Figure 16D and 16E**).

In contrast to the double mutants with *axr1-12* and *axr6-3*, the phenotypic severity was reversed when *csn1-10* and *csn3-3* were combined with the *eta2-1* mutation. *eta2-1* is a missense mutation in CAND1, a cullin binding protein that mediates cycles of SCF complex assembly and disassembly (Chuang et al., 2004; Zhang et al., 2008) and **Figure 5**). While the *eta2-1* mutation abolished CUL1 binding activity and thus disrupted SCF cycling, it had no detectable effect on CUL1 neddylation. Whereas *csn1-10 eta2-1* double mutants failed to progress past the seedling stage (Zhang et al., 2008) and **Figure 16F**), *csn3-3* only slightly enhanced the developmental defects of *eta2-1* (**Figure 16G**).

The last auxin mutant I used for crossing was *ibr5*. The Arabidopsis *IBR5* gene encodes a putative dual-specificity protein phosphatase. A previously described loss-of-

function allele of *IBR5* has been shown to cause diminished auxin response without disturbing $SCF^{TIR1/AFB}$-mediated control of Aux/IAA stability (Strader et al., 2008). Our lab has found another loss-of-function *ibr5* mutant, which was then used to make the *csn1-10 ibr5*, *csn3-3 ibr5* double mutants. In my effort to test the root growth phenotype of *csn1-10 ibr5* and *csn3-3 ibr5*, I surprisingly found that *ibr5* is epistatic to *csn1-10*, suggesting that the *IBR5*-mediated regulation in auxin signaling may be at the downstream of $SCF^{TIR1/AFB}$ (**Figure 16H**). In contrast, *csn3-3* enhanced the *ibr5* root growth resistance. Together, the genetic interactions with *ibr5* also indicated *csn1-10* and *csn3-3* caused distinctive defects in auxin signaling.

To summarize, the highly differential genetic interactions conferred by the *csn1-10* and *csn3-3* mutations in combination with *axr1-12*, *axr6-3*, *eta2-1* and *ibr5* clearly indicated that these two mutations in CSN subunits affect distinct aspects of auxin signaling. This notion is consistent with our finding that only *csn1-10* exhibited defects in cullin deneddylation and $SCF^{TIR1/AFB}$-mediated regulation of Aux/IAA protein stability.


A
csn1-10
axr1-12
csn1-10
axr1-12

B

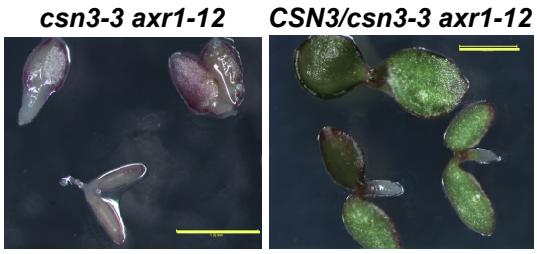
csn3-3 axr1-12
CSN3/csn3-3 axr1-12

C

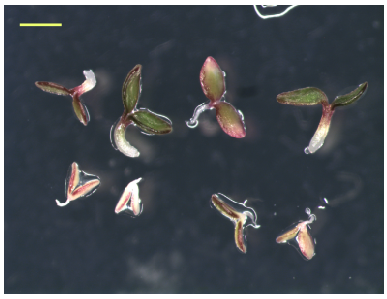
axr1-3xcsn3-3 F2
CSN3/csn3-3 axr1-3
csn3-3 axr1-3

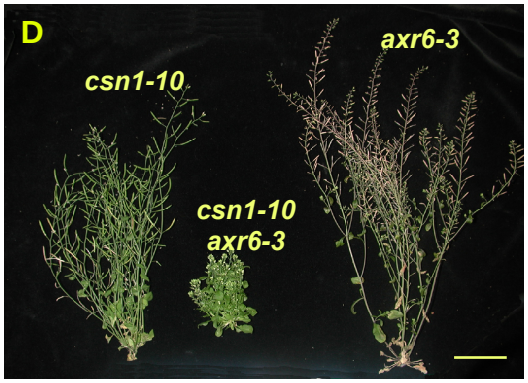
D
csn1-10
axr6-3
csn1-10
axr6-3

E

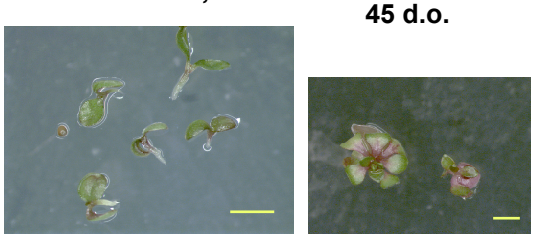
csn3-3 axr6-3; 7 d.o.
csn3-3 axr6-3;
45 d.o.

F

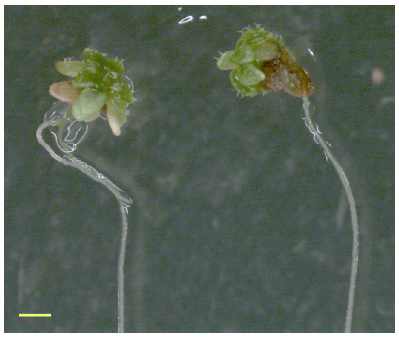
csn1-10 eta2-1

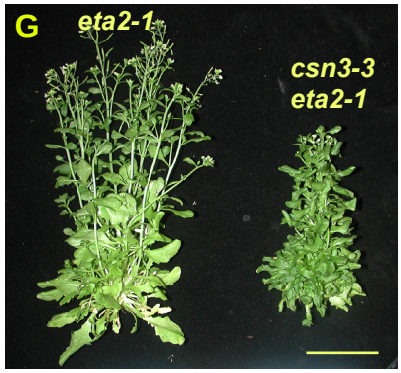
G
eta2-1
csn3-3
eta2-1

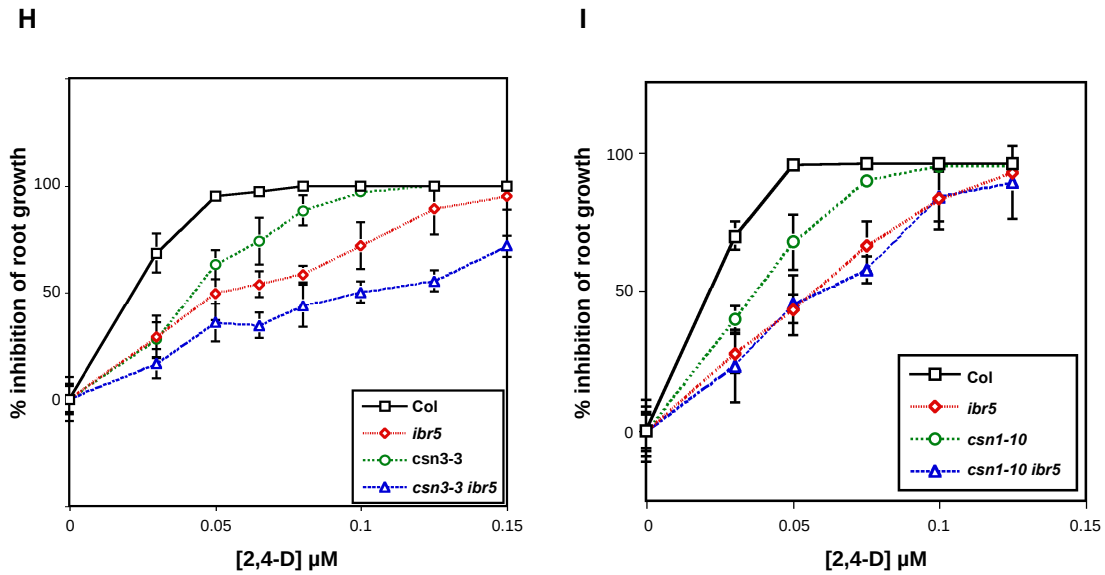

Figure 16. *csn3-3* and *csn1-10* exhibit distinct double mutant interactions.

(A) Adult *csn1-10 axr1-12* double mutant exhibit a slightly more severe dwarf phenotype than either of the single mutants. Size bar = 4 cm.

(B) *csn3-3* interacts with *axr1-12* synergistically, resulting in the seedling lethality. Right panel shows the seedling-lethal phenotype of heterozygous *csn3-3/CSN3* in the *axr1-12* background. Size bar = 1 mm.

(C) Dead seedlings from the *axr1-3*x*csn3-3 F2* population.
Less severe dead seedlings were genotyped as *CSN3/csn3-3 (upper),* while the more severe ones are *csn3-3* homozygous.

(D-E) While *csn1-10 axr6-3* plants are viable and complete the life cycle, *csn3-3* interacts with *axr6-3* synergistically, with double mutants exhibiting developmental arrest at the seedling stage. Size bars = 4 cm (D) and 1 mm (E), respectively.

(F-G) *csn1-10* exhibits a stronger interaction with *eta2-1* than does *csn3-3*. As previously reported (Zhang et al., 2008), *csn1-10 eta2-1* seedlings fail to develop past the early seedling stage. Size bars = 1 mm (F) and 4c m (G), respectively.

(H-I) Root growth assays of Col, *ibr5*, *csn1-10*, *csn3-3*, *csn1-10 ibr5* and *csn3-3 ibr5*. Seedlings (n≥15) grown on ATS medium were transferred to medium containing 2,4-D and grown for another three days. Data are presented as percent inhibition of root growth compared to growth on unsupplemented ATS. Error bars = SD.
(H) Col, *ibr5, csn3-3* and *csn3-3 ibr5*
(I) Col, *ibr5*, *csn1-10* and *csn1-10 ibr5*

Gel-filtration analysis reveals a novel CSN3-containing complex

The CSN deneddylase activity is catalyzed by the CSN5 subunit, in which the JAMM motif is the catalytic center required for the isopeptidase activity to remove NEDD8/RUB from the cullin proteins (Cope et al., 2002; Cope and Deshaies, 2003). However, the proper assembly of the holocomplex is required for deneddylating cullins: a previously reported *csn3* null mutant (*csn3-1*) resulted in the loss of the CSN holocomplex, the redistribution of all the CSN5 into its monomer form and severely damaged the CSN-mediated deneddylation on CUL1, CUL3 and CUL4 (Dohmann et al., 2008a). Since both *csn1-10* and *csn3-3* are weak *csn* mutants, I wanted to know to what extent the assembly of CSN holocomplex was affected by the mutations. Therefore I conducted a series of gel filtration analyses, followed by immunoblottings with antibodies against several CSN subunits, to analyze the integrity of CSN complex assembly in wild type, *csn1-10* and *csn3-3* backgrounds.

The gel-filtration profiles using Col protein extracts followed by probing with several CSN antibodies indicated that CSN subunits cofractionated into high molecular mass fractions corresponding to 440 kDa (**Figure 17 and 18,** fractions 6 to 9), consistent with the previously observed molecular mass of the CSN holocomplex (Gusmaroli et al., 2004; Gusmaroli et al., 2007). In wild type, the PCI domain CSN subunit CSN1, CSN4 and CSN8 were detected primarily in fractions corresponding to the CSN holocomplex (**Figure 17A,** fractions 6~9). The MPN subunit CSN5 can be readily detected not only in the high molecular mass fractions of the CSN holocomplex (**Figure 17B**, fraction 6~9), but also in its monomer form of a lower molecular mass (**Figure 17B,** fraction 15~18).

In the gel-filtration profiles of *csn1-10*, however, the majority of CSN5 proteins were no longer assembled into the holocomplex but mostly in the monomer form (**Figure 17B**). This finding was consistent with my aforementioned results that *csn1-10* displayed deficient deneddylation of CUL1 phenotype and exhibit reduced SCF mediated proteolysis (**Figure 15**), since CSN5 alone cannot function properly as a deneddylating isopeptidase. However, the *csn1-10* mutation didn't prevent other subunits from being assembled into the holocomplex, as was revealed by CSN3 and CSN4 immunoblot detection of the gel-filtration fractions (**Figure 18C and Figure 32)**. Although the *csn1-10* mutation dramatically reduced the CSN1 protein level (**Figure 14D**), the remaining mutated *csn1-10* protein could still be detected in the CSN holocomplex fractions using a more sensitive ECL detection (**Figure 17A and Appendix**). This result further supported the idea that it was the reduction of CSN1 protein levels rather than the missense mutation that caused the mutant phenotype.

To our surprise, the above gel filtration findings with CSN1, CSN4, CSN5, and CSN8 indicate that CSN holocomplex assembly was unaffected by *csn3-3* (**Figure 17**). Consistent with this conclusion, I found that the abundance of the *csn3-3* mutant protein (ETA7) was similar to wild-type (**Figure 18E**), and most of the *csn3-3* mutant protein also was incorporated into the CSN holocomplex, suggesting the integrity of CSN holocomplex was probably intact (**Figure 18A**). Since CSN5 can be properly assembled into the CSN holocomplex, it well explained the fact that no deneddylation defects were seen in *csn3-3*.

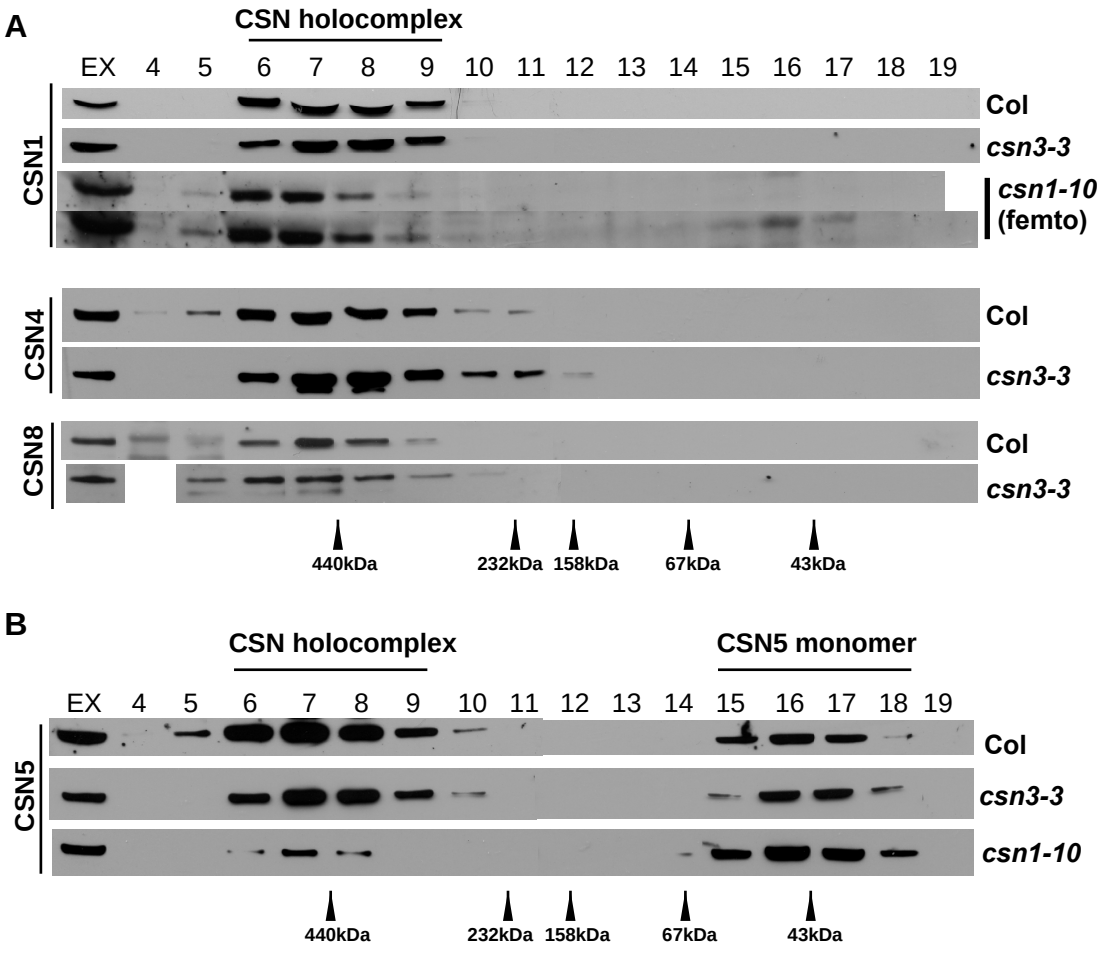

Figure 17. The assembly of CSN holocomplex is not affected by the *csn3-3* mutation.

Protein extracts from 7-d.o. Col, *csn1-10* and *csn3-3* seedlings were fractionated on a Superdex-200 gel-filtration column and fractions (4 to 19) were collected and blotted with CSN1, CSN4, and CSN8 (A) and CSN5 (B) antibodies. In (A), the CSN1 detection of *csn1-10* GF fractions were using the femto ECL detection with both the light (upper) and dark (lower) exposure.

The gel-filtration fractions 6 to 8 correspond to the size of CSN holocomplex, while CSN5 can also be found in lower molecular mass fractions (15 to 18) that represent its monomer form. Molecular mass standards are shown at the bottom of each panel. EX indicates the protein crude extract before gel filtration.

However, during my gel filtration studies with CSN3, I noticed an additional CSN3 elution peak centered around 130 kD in wild-type extracts (**Figure 18A**, fractions 12 to 14). Interestingly, this small CSN3-containing complex (sCSN3c) was absent in *csn3-3* seedlings, indicating that the *csn3-3* missense mutation disrupts the formation of this complex. In *csn3-3* gel-filtration experiments, the CSN3 signal was detected in two elution peaks: the majority of mutated CSN3 was found in the CSN holocomplex fractions, while the remaining CSN3 signal was detected within fraction 14 to 16 (**Figure 18A**), probably corresponding to the CSN3 monomer. A closer comparison of the fractions 12 ~ 17 derived from Col and *csn3-3* gel-filtration samples was taken and samples made from the *csn3-2* null allele was included as an additional control. Again, different fractionation patterns of CSN3 were seen between Col and *csn3-3* (**Figure 18B**). Additionally, in the *csn3-2* null mutant, the absence of CSN3 signals in fractions corresponding to that CSN3-containing small complex confirmed that the signal I detected was CSN3 rather than some unspecific cross-reacting protein. In a comparison of CSN3 distribution between *csn1-10* and *csn1-10 csn3-3* samples, I also detected the existence of that CSN3-contatining small complex in the *csn1-10* sample (fractions 12 to 14), while the CSN3 signal migrated into a lower molecular mass region (fractions 13 to 16) in the *csn1-10 csn3-3* double mutant background (**Figure 18C**). Therefore I reasoned that in addition to the CSN holocomplex, CSN3 was also assembled into a small CSN3-containing complex (sCSN3c), which was affected by the *csn3-3* mutation.

Since the gel-filtration was performed using size-exclusion columns, the shift of this CSN3 small complex into lower mass fractions indicated that the *csn3-3* mutation

probably caused the loss of one or more components that were originally present. Therefore, I hypothesize that the defective assembly of the sCSN3c may correlate with the auxin response defects in the mutant. To test this hypothesis, I analyzed the CSN3 gel-filtration profile in one of our complementary lines (L4) that has been shown having restored auxin responses (**Figure 12C and 12D**). As seen in **Figure 18A**, the complementary line which expressed the genomic CSN3 in the *csn3-3* background also restored the CSN3 fractionation pattern: similar to the wild type, the majority of CSN3 small complex was found in the fractions 12~13, while slight CSN3 signals observed in the lower mass fractions (fraction 14~16) was presumably the endogenous mutated CSN3 (ETA7).

I also tested the possibility that CSN3 small complex may be due to partial disassembly of the CSN that occurred during our *in vitro* fractionations. Fractions containing the CSN holocomplex were isolated and subjected to a second round of gel filtration and subsequently immunoblotted with α-CSN3 antibody (**Figure 18D**). However, no CSN3 protein was detected in the low molecular mass fractions corresponding to sCSN3c, demonstrating that the CSN was stable under our conditions.

To summarize, the only biochemical defects I found so far in *csn3-3* was the defective assembly of a small CSN3-containing protein complex (sCSN3c). My results also suggested that it was likely the loss of sCSN3c in *csn3-3* correlates with the auxin defects of the mutant.

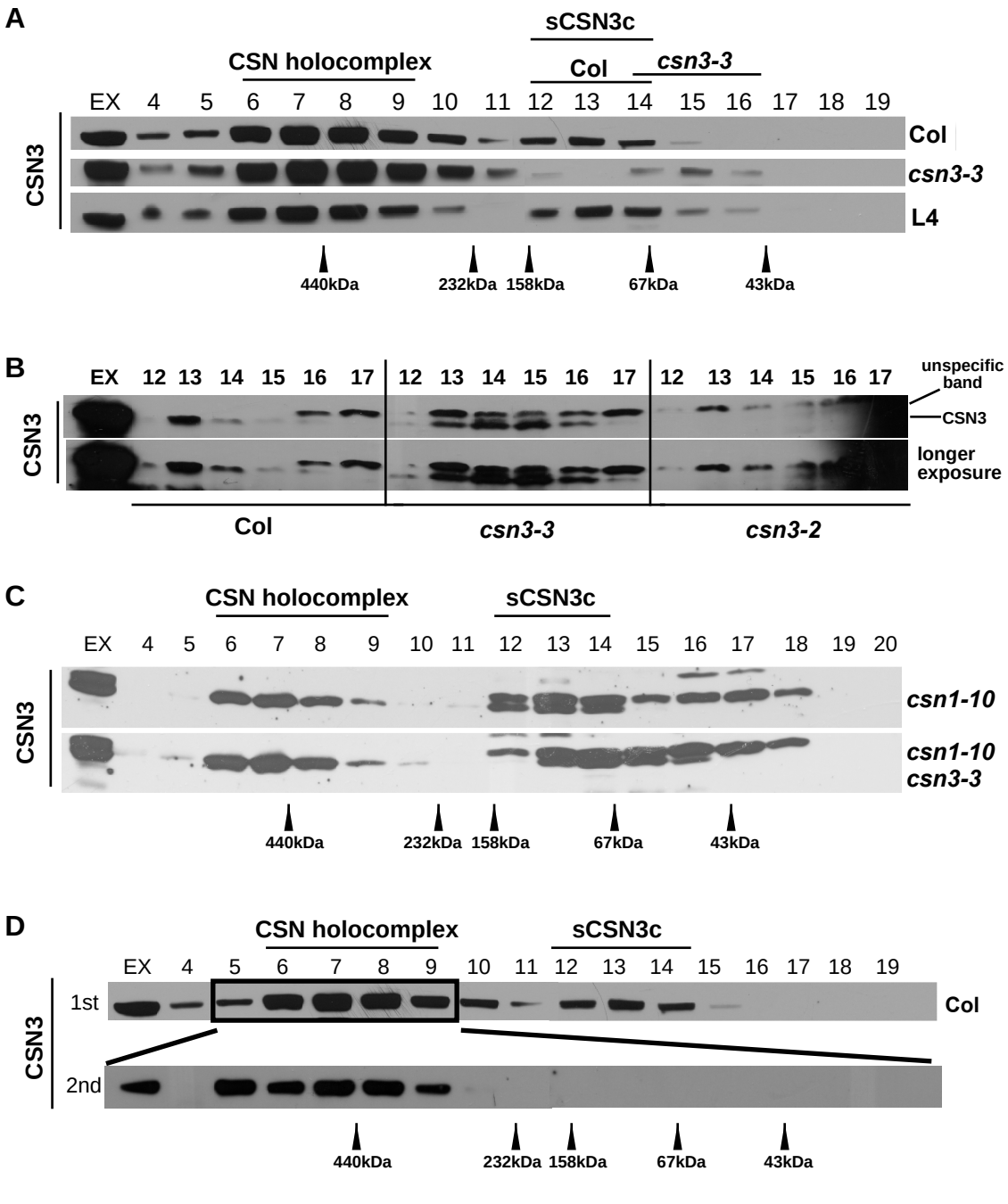
A
sCSN3c
CSN holocomplex
Col
csn3-3
EX 4 5 6 7 8 9 10 11 12 13 14 15 16 17 18 19
CSN3
Col
csn3-3
L4
440kDa
232kDa
158kDa
67kDa
43kDa
B
EX 12 13 14 15 16 17 12 13 14 15 16 17 12 13 14 15 16 17
unspecific band
CSN3
longer exposure
Col
csn3-3
csn3-2
C
CSN holocomplex
sCSN3c
EX 4 5 6 7 8 9 10 11 12 13 14 15 16 17 18 19 20
csn1-10
csn1-10 csn3-3
440kDa
232kDa
158kDa
67kDa
43kDa
D
CSN holocomplex
sCSN3c
EX 4 5 6 7 8 9 10 11 12 13 14 15 16 17 18 19
1st
2nd
Col
440kDa
232kDa
158kDa
67kDa
43kDa
E
Col
csn3-3
CSN3
RPT5

Figure 18. A novel small CSN3-containing complex (sCSN3c) is affected by the *csn3-3* mutation.

(A) CSN3 detection of gel-filtration fractions of Col, *csn3-3* and a *csn3-3* complementation line (L4). In Col gel-filtration profiling, the assembly of a small CSN3-containing protein complex (sCSN3c) was observed in fractions 12-14. This complex was absent in *csn3-3* extracts, but was restored by introduction of a genomic CSN3 transgene (L4 complementation line). Molecular mass standards are shown at the bottom of each panel. EX indicates the protein crude extract before gel filtration.

(B) Protein extracts from 7-d.o. Col, *csn3-3* and *csn3-2* seedlings were fractionated on a gel-filtration column. Fractions 12 to 17 from each genetic background were collected and separated on a same SDS gel with the CSN3 western detection.

(C) Comparison of CSN3 gel-filtration patterns in *csn1-10* and *csn1-10 csn3-3* double mutants. The upper band is a unspecific cross-linked protein.

(D) sCSNc is not a breakdown product of the CSN holocomplex during the in vitro fractionation. Fractions (5~9) of the 1st gel-filtration using Col seedling protein extracts were isolated and injected into the column to run another round of gel-filtration. CSN3 western detection was conducted using fractions from the 2nd gel-filtration. No CSN3 was detected in the sCSN3c fractions.

(E) CSN3 protein level is unaffected by the *csn3-3* mutation. RPT5 is used as a loading control.

Discussion

csn1-10 is a typical *csn* mutant.

In plants, animals, and fungi, the CSN has a well-established role as a cullin deneddylase that regulates CRL ubiquitin-ligase activity (Cope and Deshaies, 2003). Prior reports in Arabidopsis have demonstrated that reduced deneddylase activity in various *csn* mutants affects $SCF^{TIR1/AFB}$ ubiquitin-ligase activity and consequently results in impaired auxin signaling (Schwechheimer et al., 2001; Stuttmann et al., 2009). Consistent with the existing model, my analyses of *csn1-10* indicated that the mutation causes defects in the CSN-mediated deneddylation and affects the Aux/IAA degradation by $SCF^{TIR1/AFB}$ (**Figure 15**), which consequently result in auxin response defects (**Figure 7, 8** and **11**).

The G to A point mutation in *csn1-10* caused a missense mutation of a conserved serine residue within the PCI domain, reduced the *CSN1* mRNA transcript and most importantly greatly decreased the CSN1 protein level (**Figure 14**). My data also suggest that the resulting reduction in CSN1 protein levels was responsible for the *csn1-10* mutant defect rather than the substitution of the serine residue, which was supported by the fact that ectopic expression of either the wild type CSN1 or the mutated *csn1-10* cDNA could rescue the root growth phenotype in *csn1-10* (**Figure 14E**). Additional evidence came from the gel-filtration analysis that showed the remaining mutated *csn1-10* protein can still be assembled into the CSN holocomplex (**Figure 17A**), which indicated the missense mutation didn't affect the interaction between CSN1 and other

CSN subunits. However, the reduction in *csn1-10* protein levels disrupted CSN5 assembly (**Figure 17B**), affecting the deneddylase activity of the CSN holocomplex.

csn3-3 may define a novel function of the CSN

The comparison of auxin related phenotypes in *csn1-10* and *csn3-3* revealed several similarities. Both mutants exhibited auxin resistant root growth, and display 50% growth inhibition at ~ 0.05μM 2,4-D (**Figure 7A**). Likewise, both mutants enhanced the *tir1-1* auxin resistant root growth and reduced lateral root development phenotypes to a similar extent (**Figure 7, 8 and 10**). Furthermore, both *csn3-3* and *csn1-10* conferred comparable reductions in auxin-mediated expression of the *BA3*- and *DR5-GUS* reporters. However, whereas *csn1-10* exhibited clear increases in cullin neddylation and Aux/IAA stability, *csn3-3* displayed neither of these molecular phenotypes. Prior studies had clearly demonstrated that the CSN3 subunit was required for CSN deneddylase activity (Gusmaroli et al., 2007; Dohmann et al., 2008a), which I have confirmed with the *csn3-2* null allele. The *csn3-3* missense mutation however, conferred a reduction in auxin response without affecting cullin deneddylation, suggesting that CSN3 played a second role in auxin signaling in addition to its role in regulating the $SCF^{TIR1/AFB}$ ubiquitin ligase (**Figure 19**).

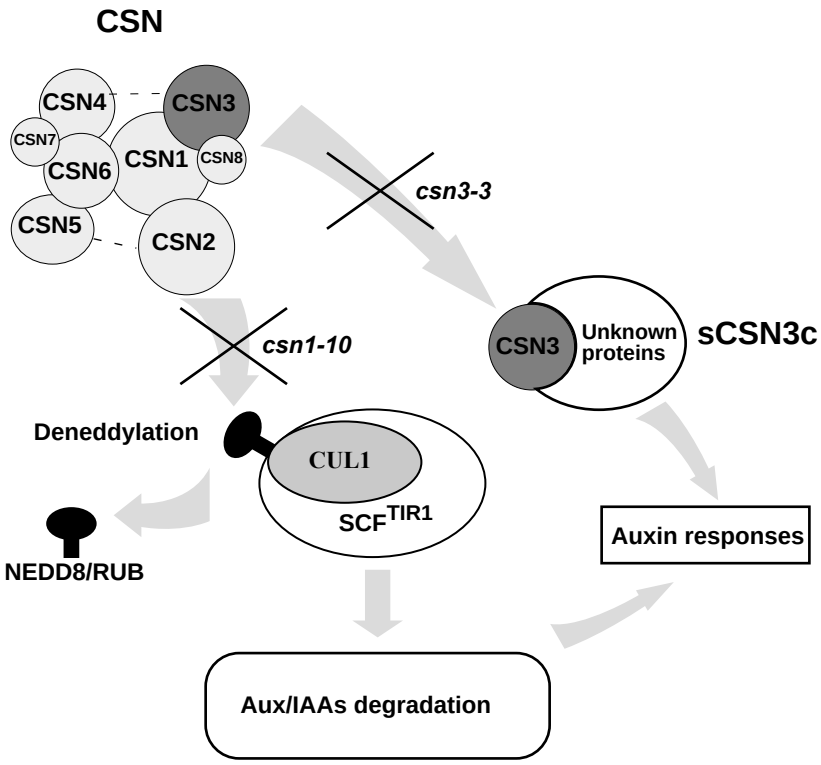

Figure 19. The CSN3 subunit plays multiple roles in auxin signaling.
We hypothesize that in addition to its role in the CSN as a cullin deneddylase, the CSN3 subunit also regulates auxin signaling independently of the $SCFT^{IR1/AFB}$ ubiquitin-ligase. This second regulatory mechanism may involve the small CSN3-containing complex (sCSN3c) whose assembly is disrupted by the *csn3-3* point mutation.

Genetic interaction analyses further distinguish *csn3-3* from *csn1-10*.

The dramatically different double mutant phenotypes exhibited when the *csn1-10* and *csn3-3* mutations were combined with *axr6-3*, *axr1-12*, *eta2-1* or *ibr5* also strongly suggested that *csn1-10* and *csn3-3* affected distinct aspects of auxin signaling. While *csn3-3* conferred seedling lethality when combined with *axr6-3* or *axr1-12*, the *csn1-10* mutation did not. Rather, *csn1-10* conferred a dramatic seedling arrest phenotype in the *eta2-1* background. Although it was difficult to predict what these differential genetic interactions might mean mechanistically, it was interesting to note that both *axr6-3* and *axr1-12* resulted in a reduction in active CUL1 (del Pozo et al., 2002; Quint et al., 2005; Dharmasiri et al., 2007; Saha and Deshaies, 2008). The *eta2-1* mutation on the other hand abolished the CUL1 binding activity of the CAND1 protein, resulting in more CUL1 associating with TIR1 in an SCF complex (Zhang et al., 2008). However, given that $SCF^{TIR1/AFB}$ activity appeared unaffected in *csn3-3* plants, it seemd unlikely that the lethality of *csn3-3 axr1-12* and *csn3-3 axr6-3* seedlings was due to a further reduction in $SCF^{TIR1/AFB}$ activity. Instead, I speculated that *csn3-3* specifically affected auxin signaling downstream or perhaps independently of the $SCF^{TIR1/AFB}$ (**Figure 19**), such that the combination of *csn3-3* with *axr6-3* or *axr1-12* caused auxin sensitivity to fall below the threshold required for early seedling development.

Possible explanation for the *csn1-10 eta2-1* severe phenotype

It has been proposed that the CSN-mediated deneddylation toggles the CUL1 displacement from the SCF complex by virtue of CAND1, which transiently sequesters

unneddylated CUL1 and together with the substrate-driven (the availability of substrate and adaptor) CUL1 neddylation, promotes a continuous cycle of SCF assembly/disassembly (Schmidt et al., 2009). In other words, the neddylation-deneddylation cycle and the CAND1 cycle are integrated to maintain the proper function of SCF (**Figure 5**).

The *eta2-1* mutation abolishes the CUL1-CAND1 interaction, resulting in more CUL1 staying with TIR1 in an SCF complex (Zhang et al., 2008), while *csn1-10* damages the deneddylation pathway. Therefore the severe phenotype between *csn1-10* and *eta2-1* was probably due to defects in both the deneddylation and the CAND1-CUL1 interaction and presumably affect all the SCF ubiquitin ligases. It is noteworthy that although the *csn1-10 eta2-1* double mutant was arrested at the seedling stage, no defects were found in embryogenesis and root development at the early stages of seedling growths. This was different from the seedling lethal phenotypes seen in *csn3-3 axr1-12/axr1-3/eta1* mutant, which had similar defects in developing a basal pole like the *monopteros* (*mp*) loss-of function mutant or the dominant negative *axr6-1* and *axr6-2* alleles of *CUL1* do (Hardtke and Berleth, 1998; Hobbie et al., 2000). Therefore, I reason that the reduction in auxin signaling caused by *csn1-10 eta2-1* was not as severe as in the *csn3-3 axr1/eta1* mutants.

Other $SCF^{TIR1/AFB}$ independent pathway

My results on *csn3-3* suggest an $SCF^{TIR1/AFB}$-independent pathway may exist to regulate auxin signaling. Consistent with this notion, the previously described *ibr5*

mutants of Arabidopsis also exhibited diminished auxin response without disturbing $SCF^{TIR1/AFB}$-mediated control of Aux/IAA stability (Strader et al., 2008). Although Aux/IAA proteins were highly unstable in both *csn3-3* and *ibr5*, *ibr5* mutants exhibited reduced steady-state levels of the AXR3NT-GUS and IAA28-myc reporter proteins. In our analysis of *csn3-3* mutants, however, both of these reporter proteins were present at levels comparable to wild-type controls. Furthermore, unlike *csn3-3*, *ibr5* did not interact with *axr1* in a synergistic manner (Strader et al., 2008). Together, these findings suggest that it is unlikely that *csn3-3* and *ibr5* share a common auxin-signaling defect.

Potential novel function of the CSN or the sCSN3c

While deneddylation is the only known biochemical activity of the CSN itself, additional activities including deubiquitinylating and protein kinase activities have been reported to be associated with the CSN (Cope and Deshaies, 2003; Uhle et al., 2003; Zhou et al., 2003). One interesting question to ask is if CSN can bypass the SCF and directly regulate the expression of certain auxin-responsive genes. Indeed, studies in animal systems suggested CSN might have a role in transcriptional regulation. Tsuge et al. (2001) showed that the N-terminal portion of human CSN1 inhibited gene expression from the *c-fos* promoter, which contains a variety of regulatory elements and can respond to various stimuli (Tsuge et al., 2001). Studies in human cells also suggested that the CSN might function as a transcriptional regulator based on its ability to associate with chromatin through interacting with CSA and DDB2- containing E3 ubiquitin ligases (Groisman et al., 2003). In Drosophila, a ChIP experiment showed that CSN4 was able to

interact with the promoter region of Rbf target genes (Ullah et al., 2007). However, whether in plants the CSN also functions at the transcriptional level remains unknown and the *csn3-3* mutant may be a good candidate for answering this question.

Also, whether or not all CSN subunits function solely within the CSN holocomplex is unclear. On one hand, null mutations in any of the eight Arabidopsis subunits conferred identical seedling-lethal phenotypes (Gusmaroli et al., 2007) and transcription profiles (Dohmann et al., 2008a), suggesting that each subunit only functions within the CSN. However, it is possible that CSN subcomplexes or individual subunits have additional functions that are masked by the early seedling lethality of these null mutants. Consistent with this possibility, fission yeast *csn1* and *csn2* mutations conferred DNA replication defects whereas other subunit mutations did not (Mundt et al., 2002). Similarly, while both Drosophila $csn4^{null}$ and $csn5^{null}$ mutants were embryo-lethal, these two mutants exhibited distinct developmental arrest phenotypes (Oron et al., 2002; Harari-Steinberg et al., 2007) and differentially affected gene expression (Oron et al., 2007). Such findings clearly raise the possibility of subunit functional specialization. While our work couldn't definitively distinguish whether *csn3-3* defines a novel function of the CSN holocomplex or the CSN3 subunit specifically, I identified a previously undescribed ~ 130 kD small CSN3-containing complex (sCSN3c). This complex did not appear to contain other CSN subunits, and unlike the CSN holocomplex, was disrupted by the *csn3-3* mutation. Expression of a P_{CSN3}*:CSN3* transgene in *csn3-3* mutant plants not only rescued the auxin response defects (**Figures 12, C and D**) but also restored the

assembly of sCSN3c (**Figures 18A**). Thus, I hypothesize that a defective sCSN3c may be the basis of the auxin signaling defects displayed by *csn3-3* mutant plants.

csn3-3 provides a unique genetic tool for CSN functional study

The fact that *csn3-3* displayed auxin responsive defects without any dramatic defects in cullin deneddylation or in SCF activity established its unique existence among all the other *csn* mutants in Arabidopsis. Our results suggested that the deneddylation might not be the only biochemical function of CSN3 in regulating auxin signaling. Identification of the other components of the sCSN3c complex may provide functional insight into what role this complex might play in auxin signaling. Furthermore, since the residue affected by the *csn3-3* missense mutation is extremely highly conserved across eukaryotes, it seems likely that sCSN3c function may be similarly conserved.

Chapter Three: Purification of the small CSN3-containing complex (sCSN3c)

Introduction

In Chapter Two, I discussed a novel 130kDa CSN3-containing complex (sCSN3c). This complex did not appear to contain other CSN subunits, and unlike the CSN holocomplex, was disrupted by the *csn3-3* mutation. The loss of sCSN3c is the only biochemical defect observed in the *csn3-3* mutant so far and correlated with the auxin phenotype of the *csn3-3* mutant as revealed by the gel filtration chromatography (GF) and complementation assays using *csn3-3 [gCSN3]* (**Figure 18A and 12C-D**). Therefore, the composition of the sCSN3c is of great interest. In this chapter, I will describe my first attempts to isolate and enrich the sCSN3c by combining different chromatographic purification steps.

Methods

Plant Materials and Growth Conditions

Cauliflower heads and Arabidopsis seedlings were used for protein extractions. Fresh cauliflower heads were bought at a local supermarket, the inflorescence tissues of which were used for the protein extraction. All the Arabidopsis seedlings were grown in liquid ATS for 7~10 days under 24 hr light unless otherwise indicated. The root growth assay was carried as mentioned in the methods section of Chapter Two.

Plasmid and transgenic plants construction

The CSN3 wild type cDNA (from *CSN3-pDONR207* construct (pGB 520)) and the *eta7/csn3-3* cDNA (from *ETA7- pDNOR207* construct (pGB 521)) were gateway cloned into pEarley Gate vector (pEG) by an LR reaction to generate the N-terminal fusion myc-CSN3/ETA7 (*35S:myc-CSN3* and *35S:myc-ETA7*). Constructs were then transformed into *csn3-3* for making *csn3-3* [*35S:myc-CSN3*] or [*35S:myc-ETA7*] lines. The myc construct was also introduced into the *csn3-2* background by crossing homozygous *csn3-3* transgenic lines with *csn3-2/csn3-3* plants. F3 homozygous or F2 segregating plants of *csn3-2* [*35S:myc-CSN3/ETA7*] were used for assays.

A gateway destination vector expressing the HPB tag (*35S:HPB*) was obtained from Dr. Katagiri's lab (Qi and Katagiri). The C-terminal *CSN3-HPB* construct was made by gateway cloning *CSN3* from pGB520 into the HPB vector. The *35S:CSN3-HPB* construct was transformed into the *csn3-2* +/- heterozygous plants. The T1 generation of *csn3-2 [35S:CSN3-HPB]* (leaves) was used for making protein extracts.

Antibodies and Immunoblotting

The myc, CSN1, CSN3, CSN5 and CSN8 antibodies were described in the methods section of Chapter Two. Proteins in each FPLC fraction were concentrated with StrataClean™ Resin (Stratagene) and separated on 4~12% NuPAGE® Bis-Tris Gel (Invitrogen), blotted and used for immunoblot detection.

Protein extraction from cauliflower and $(NH_4)_2SO_4$ precipitation

Protein extracts were made from cauliflower as described (Menon et al., 2005) with modifications: 60 grams fresh cauliflower inflorescence tissues were homogenized using a pre-cooled blender in 100ml cold extraction buffer containing 50mM Tris-HCl, pH7.5, 150 mM NaCl, 10 mM $MgCl_2$, 1 mM EDTA, 10% glycerol and 0.1% NP40 (before use, 1 mM phenylmethylsulfonyl fluoride (PMSF) and 1 mM dithiothreitol (DTT) were added). The homogenate was filtered through four layers of cheesecloth (Fisher Scientific) and centrifuged twice at 14,000 rpm for 5min to pellet the debris. All steps were carried out on ice or in a cold room.

For $(NH_4)_2SO_4$ precipitation, freshly made protein extracts from cauliflower were mixed with the appropriate amount of 3.9M saturated (100%, at 10 ^oC) $(NH_4)_2SO_4$ solution or solid $(NH_4)_2SO_4$ to make a desired final concentration of 20%, 30% and 40% (w/v) $(NH_4)_2SO_4$ according to the calculation (Wingfield, P. 2001). Notice the stock solution or solid powders were added slowly to avoid the local concentration from getting too high. The mixture was then stirred for 2hrs in a cold room and centrifuged at 14,000

rpm for 20 min. In a gradient precipitation, both pellets and supernatant were saved at each precipitation/centrifugation. Appropriate amount of $(NH_4)_2SO_4$ stock or powders were mixed with the supernatant in order to reach to the next concentration. At last, pellets were dissolved in 2ml gel-filtration buffer with 2x PMSF and 2x Protease Inhibitor Cocktail Kit (Thermo Scientific®, Lot#NB1499881) and dialyzed in 1L gel-filtration buffer overnight with gentle stirring. Before running through the GF column, NP40 was added to a final concentration of 0.5% to increase the solubility of precipitates. The extracts were filtered through a 0.45 μm HT Tuffryn® Membrane (Pall Acrodisc®) before loading.

Protein extraction from Arabidopsis seedlings and PEG precipitation

Approximately 8 grams (fresh weight) of Arabidopsis seedlings were homogenized by a glass homogenizer/tissue grinder in 10ml extraction buffer containing 50mM Tris-HCl pH 7.0, 1.5mM $MgCl_2$, 10mM KCl, 0.2mM EDTA, 5% glycerol, 2mM PMSF, 2mM DTT and 0.5x Protease Inhibitor Cocktail Kit (Thermo Scientific®, Lot# NB1499881). The protein crude extract was then centrifuged at 14,000 rpm for 10min. The supernatant was collected and centrifuged at 14,000 rpm for another 5 min to further remove the debris.

To proceed to the PEG precipitation, the protein extracts were slowly mixed with 1/3 of its volume with 60% polyethylene glycol (PEG) (dissolved in the extraction buffer) in a droplet-to-droplet manner to make a final concentration of 15% PEG. The sample was then stirred for 1hr in a cold room and then centrifuged at 14,000 rpm for

10min. The pellet/precipitate was collected and dissolved in buffer containing 50mM Bis-Tris pH 6.4, 200mM NaCl, 10% glycerol, 1.5mM $MgCl_2$, 10mM KCl, 0.2mM EDTA, 0.01%NP40, 2mM PMSF, 4mMDTT and 1x Protease Inhibitor Cocktail Kit (Thermo Scientific®, Lot# NB1499881). The dissolved pellet was then placed on a shaker at 4°C for 2 hrs to fully break the pellet and centrifuged at 14,000 rpm for 30min to further remove the debris. After that, the supernatant was collected for further FPLC steps.

Fast Protein Liquid Chromatography (FPLC)

Operations on the AKTA FPLC system were done according to the manual. All the buffers were pre-filtered, degassed and kept at 4 ^{o}C. The FPLC was conducted at 4 ^{o}C. Protein samples were filtered through a 0.45 μm HT Tuffryn® Membrane (Pall Acrodisc®). Before loading to the column, samples (crude protein extracts, 15% PEG precipitates or GF fractions pools) were first buffer exchanged to the desired buffer. The buffer exchange was done by using a PD-10 Desalting Column according to its instructions (GE Healthcare). In brief, 2.5ml sample was loaded to a pre-equilibrated PD-10 column and eluted by gravity with 3ml of desired buffer.

Ion exchange chromatography (IEX)

The ion exchange chromatography (IEX) equilibrations buffers used in this chapter all contained 10% glycerol, 100mM NaCl (unless addressed in particular). The pH of the equilibration buffer is adjusted by 20mM Bis-Tris propane (pH 7) or 20mM

Tris (for pH 7.5 and 8). The elution buffer contained the same composition as that of the equilibration buffer but with 400~ 500mM NaCl.

Strong anion IEX columns, such as Mono Q™ 5/50 GL and HiTrap™ Q FF, were used as recommended by the user instructions with 200ul, 1ml or 2ml samples injected. After the injection, the column was washed with the equilibration buffer at 1 ml/min for 5 column volumes (CV) to collect unbound proteins. The proteins bound to the column were then eluted with a linear gradient of NaCl in the range of 100 to 500mM in the equilibration buffer at a flow rate of 1 ml/min for 12 CV (for Mono Q) or 18 CV (for Hitrap Q FF). 0.75 ml (For Mono Q) or 1ml (for Hitrap Q FF) fractions were collected after the sample injection. At the end of IEX, buffer containing 1M NaCl was used to strip off (flow rate=1ml/min for 5CV) all the remaining proteins bound to the column. In order to find a pH condition at which sCSN3 can be separated from the CSN holocomplex, equilibration/elution buffers of different pH and NaCl concentrations were applied. For detailed information, please refer to the text and legends for each figure.

Another strong anion IEX column HiPrep™ 16/10 Q FF (CV=20ml) was used as recommended by the manufacturer's instructions to separate sCSN3c from the CSN holocomplex at pH 7**,** 100 mM~500mM NaCl. 2 ml crude extracts (~7mg) made from leaves of wild type plants were loaded to the pre-equilibrated column. The column was then washed with the equilibration buffer (20 mM Tris-Bis propane pH 7, 100 mM NaCl and 10% glycerol) at 1ml/min for 2 column volumes (CV) to collect unbound proteins. The proteins bound to the column were then eluted with a linear gradient of NaCl up to 500 mM in the equilibration buffer at a flow rate of 1 ml/min for 5CV. 5 ml fractions

were collected after the sample injection. The unbound fractions corresponding to sCSN3c (fractions 4 and 5) were collected and concentrated through a centrifugal 10kDa cut-off filter (Amicon® Ultra-4 Centrifugal Filter Devices, MILLIPORE) for future purification steps.

Gel-filtration chromatography

The gel-filtration (GF) protocol was as described in the methods section of Chapter Two. For loading a Superdex™ 200 10/300 GL column (CV=24ml, GE Healthcare), 200 µl sample of 500~800 µg proteins was injected into the column and was eluted in filtered and degassed GF buffer at a flow rate of 0.2 ml/min. 0.5 ml fractions were collected after the 6 ml void volume was reached. Fractions were then concentrated and separated on a gel to detect the CSN3 presence.

For loading a HiLoad™ 16/60 Superdex™ 200 prep grade column (CV=125 ml, GE Healthcare), 2 ml sample of 14.5 mg proteins was loaded and eluted at 1 ml/min. 2.5 ml fractions were then collected after the 42 ml void volume was reached. 200 µl of each fraction were concentrated and separated on a gel to detect CSN3.

Optimization of the IEX conditions to enrich the sCSN3c.

The sCSN3c containing GF fractions (fractions 12~14) or the CSN holocomplex fractions (fractions 6~8) from two Col GF assays using a Superdex™ 200 10/300 GL column were pooled and buffer exchanged with the IEX equilibration buffer. 2 ml of the sCSN3c pool was injected into either a pre-equilibrated Mono Q™ 5/50 GL or HiTrap™

Q FF column. The salt strength ranged from 100 mM NaCl to 500 mM NaCl and pH varies from pH 7 to pH 8 (see **Figure 23** for details).

To validate the enrichment of the sCSN3c, the 15% PEG precipitates or the clarified crude protein extracts made from Col seedlings were buffer exchanged to pH 8, 100 mM NaCl (for both PEG precipitates and crude extracts), or pH 7.5, 100 mM NaCl (for crude extracts). 2 mg of total proteins in 1 ml equilibration buffer was loaded to the IEX column HiTrap™ Q FF. The IEX fractions 11 & 12, 13 or 14 of the PEG precipitates were picked for the following GF analysis. The IEX fraction 13 of the crude extracts was picked for the following GF analysis (see **Figure 24** for more details).

Affinity purification and Immunoprecipitation

The immunoprecipitation (IP) procedure was carried out as described in previously literature with modifications (Gray et al., 1999). Arabidopsis protein extracts were prepared from leaves or seedlings of transgenic plants expressing tagged CSN3 (myc-CSN3, myc-ETA7 or CSN3-HPB) using either the IEX equilibration buffer (20 mM Bis-Tris propane pH 7, 100 mM NaCl and 10% glycerol, for *csn3-2* [*35S:myc-CSN3/ETA7*] extracts) or buffer A (50 mM Tris-HCl pH 7.5, 150 mM NaCl, 0.5% NP40, for *csn3-2* [*35S:myc-CSN3*], *csn3-3* [*35S:myc-CSN3/ETA7]* and *csn3-2* [*35S:CSN3-HPB*] extracts) plus 1 mM DTT, 1 mM phenylmethylsulfonyl fluoride (PMSF), and 1X Protease Inhibitor Cocktail Kit (Thermo Scientific®, Lot# NB1499881). Extracts were then clarified by centrifugation at 14,000 rpm for 10 min to remove debris. 1~2 mg of extract was used for IP.

Commercial affinity matrix for myc IP (monoclonal α-myc antibody 9E10, cross-linked to protein A agarose beads) was purchased from COVANCE. For HPB affinity purification, streptavidin coupled magnetic beads (Dynabeads® M-280 streptavidin, Invitrogen) were used. 50 µl of beads was pre-washed with the extraction buffer three times (5 min each) and then incubated with protein extracts on a shaker at 4°C for 3 hrs. For IPs using the α-CSN3 antibody, 5 µl of affinity purified α-CSN3 antibody was added to the protein extract and incubated at 4°C for 3 hrs. Then the CSN3 IP complexes were collected by adding 50 µl protein A-agarose beads and incubated 4°C for another 1 hr. The beads were collected by brief centrifugation (myc beads or protein A beads) or by a magnetic stand (Dynabeads) and washed 4 times with the extraction buffer (5 min each) and resuspended in SDS-PAGE sample buffer.

Results

GF analysis using cauliflower protein extracts.

The CSN holocomplex was originally purified from inflorescence tissues of *Brassica oleracea L.* (cauliflower), a member of the same *Brassica* family as Arabidopsis (Chamovitz et al., 1996). Since the CSN is highly conserved in all higher eukaryotes and it is much easier to get large amount of plant materials from cauliflower than from Arabidopsis, cauliflower may be a good alternative material for purifying the sCSN3c. Therefore I want to test if the sCSN3c is conserved in cauliflower by applying gel filtration (GF).

I first applied a gradient $(NH_4)_2SO_4$ precipitation to the cauliflower protein extracts, in order to concentrate CSN3 and reduce contaminates such as lipids. As seen in **Figure 20A**, limited amount of CSN3 was detected in the 20% $(NH_4)_2SO_4$ precipitates or in the supernatant portion after 40% $(NH_4)_2SO_4$ precipitation, while about 90% of CSN3 was harvested in the 30%~40% $(NH_4)_2SO_4$ precipitates. Therefore I used the 30% and 40% $(NH_4)_2SO_4$ precipitates for the future GF analysis.

After dissolving the pellet in the GF buffer and dialysis, 500~600 μg of total protein was loaded to a Superdex™ 200 10/300 GL column. The α-CSN3 detection of collected fractions indicated that the majority of cauliflower CSN3 were eluted in the CSN holocomplex fractions (4 to 8, **Figure 20B**) as referred in previous literature (Chamovitz et al., 1996). Again, the CSN3 signal was also present in the sCSN3c fractions (12 to 14, **Figure 20B**) in GF using either the 30% or the 40% $(NH_4)_2SO_4$ precipitates. Therefore, the GF analyses suggested that the cauliflower CSN3, as its

homolog in Arabidopsis, was also eluted into two major peaks that might correspond to the CSN holocomplex and sCSN3c. However, due to the fact that GF separates proteins only by size, I could not rule out the possibility that signals in fractions 12 to 14 represented another CSN3-containing protein complex rather than the sCSN3c seen in Arabidopsis.

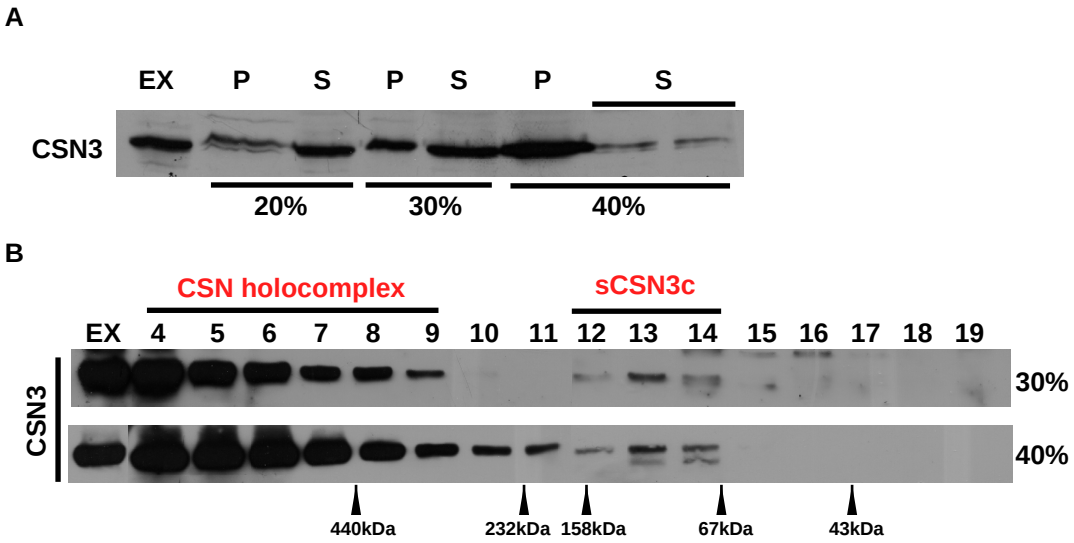

Figure 20. Cauliflower CSN3 is also assembled into a small protein complex besides the CSN holocomplex.

(A) 30% and 40% $(NH_4)_2SO_4$ precipitation can harvest most of the cauliflower CSN3 proteins from crude extracts. Cauliflower protein extracts were mixed with $(NH_4)_2SO_4$ powder to make a gradient precipitation. Both the precipitate and the supernatant at each $(NH_4)_2SO_4$ concentration were collected and loaded on a SDS gel for CSN3 detection. 50μg of total protein from each sample was loaded to each lane, except for the last two lanes (40% supernatant), each of which contains 25μg of total protein. EX stands for crude extracts, P means precipitates, while S indicates the supernatant at each precipitation.

(B) CSN3 detection of GF fractions. 30% (upper) and 40%(lower) $(NH_4)_2SO_4$ precipitates of cauliflower crude protein extracts were resuspended in GF buffer and loaded to a Superdex 200 gel-filtration column. Fractions 4 to 19 were collected for CSN3 western. Molecular mass standards are shown at the bottom of each panel. EX indicates the precipitates before gel filtration.

The Arabidopsis sCSN3c can be readily detected in a scaled GF.

The maximum amount of crude protein extracts loaded to a Superdex™ 200 10/300 GL gel filtration column (**Figure 17 and 18**) cannot exceed 1 mg. Such low quantities are far from enough for the purification purpose of the sCSN3c, not to mention that sCSN3c only contains < 10% of the total CSN3 (**Figure 18A**). Therefore, I tried to scale up the GF assay by applying a bigger size-exclusion column: HiLoad™ 16/60 Superdex™ 200 prep grade, which has a column volume (CV) of 125 ml and is capable to load up to 20 mg sample. However, different GF column may have different resolution to separate proteins. Whether the sCSN3c can still be separated from the CSN holocomplex by the bigger GF column remains uncertain. Therefore, I tested the GF profiles of Col and *csn3-3* seedlings extracts using the HiLoad™ 16/60 Superdex™ 200 prep grade column. Both Col and *csn3-3* crude extracts were loaded to the column for comparison.

As shown in **Figure 21**, α-CSN3 western detections of the Col GF fractions indicated that the sCSN3c could still be separated from the holocomplex when running through a HiLoad™ 16/60 Superdex™ 200 prep grade column. The fractionation pattern was similar as that of using the smaller column (Superdex™ 200 10/300 GL), with the sCSN3c (fractions 11 to 13, upper panel) readily separated from the CSN holocomplex (fractions 4 to 8, upper panel) in Col sample. When comparing the *csn3-3* GF profile with that of Col, the mutation consistently caused CSN3 signal diffused into lower molecular mass fractions (11 to 15, lower panel), indicating the loss/disassembly of

sCNS3c in the mutant background. Therefore, by applying a bigger size-exclusion column, I could still separate sCSN3c from the CSN holocomplex.

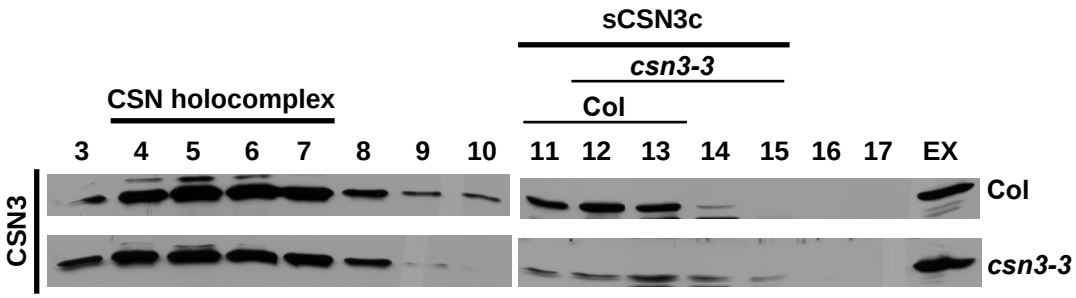

Figure 21. CSN3 detection on GF fractions of a bigger column.

Similar GF experiment and CSN3 detection as mentioned earlier. A column of bigger volume (HiLoad™ 16/60 Superdex™ 200 prep grade column, CV=124ml) was used to separate protein extracts made from Col and *csn3-3* seedlings. EX indicates the crude exacts before gel filtration.

PEG precipitation and IEX enriches CSN3 and co-purifies other CSN subunits.

In order to purify sCSN3c, I planned to apply a three-stage protein purification strategy (CIPP, for Capture, Intermediate Purification and Polishing) (Strategies for Protein Purification, Handbook. GE Healthcare). The objective of the capture step in the CIPP protein purification strategy is to isolate and concentrate the target protein. The ion exchange chromatography (IEX) is one of the commonly used methods to separate biomolecules of interest from impurities, based on the fact that different proteins have different net surface charges at certain buffer condition. The pH and the ion strength in the IEX equilibration buffer must be selected to ensure that target proteins bind to the IEX matrix while the contaminants don't. By increasing the salt strength in the buffer, the column bound proteins will be gradually eluted.

According to the TAIR database, the isoelectric point (pI) of CSN3 is 6.3. In a neutral equilibration buffer, such as pH 7, or in a more basic buffer, the CSN3 is likely negatively charged. Additionally, with the exception of CSN1, the pI values of all the other CSN subunits are below 7. Since all the CSN subunits together contribute to the net surface charge of the CSN holocomplex, it is likely that at pH7 the CSN holocomplex is negatively charged, too. Therefore I applied a strong anion IEX column (Mono Q™ 5/50 GL) to concentrate CSN3 using Arabidopsis seedling protein extracts.

To increase the enrichment of CSN3, I also added a 15% polyethylene glycol (PEG) precipitation step in the sample preparation before loading to an IEX column as previously referred (Menon et al., 2005). The dissolved PEG precipitates were then buffer exchanged to the IEX equilibration buffer of pH 7, 200 mM NaCl and loaded to

the Mono Q column. By increasing the salt concentration up to 400 mM NaCl, proteins bound to the column were eluted and collected.

At pH 7 and an ion strength ranging from 200 mM to 400 mM NaCl, the majority of CSN3 proteins bound the Mono Q column and was eluted mainly in fractions 18 and 19, which corresponds to a salt concentration of 350 mM~360 mM NaCl (**Figure 22A**). Immunoblot detections using α-CSN1 and α-CSN5 indicated that CSN1 and CSN5 also bound the column and had a similar retention time as CSN3, with the signal peak located at fractions 18~19 (**Figure 22A**). Together, these results suggested that the CSN holocomplex was enriched by using the Mono Q anion exchange column at pH 7 and was eluted at a salt strength of 350 mM~360 mM NaCl.

To further confirm that the IEX fraction 18 and 19 contains the CSN holocomplex, these two fractions were pooled and loaded to a GF column (Superdex™ 200 10/300 GL). Compared to my previous GF experiments, the CSN3 immunoblot detection of the GF fractions showed that all the CSN3 coming from IEX fractions 18&19 were in the CSN holocomplex GF fractions (6 to 8, **Figure 22B**). To my surprise, no CSN3 signals were found in GF fractions corresponding to the sCSN3c (12 to 14, **Figure 22B**). To exclude the possibility that sCSN3c was present in other IEX fractions, such as fraction 16~17 and 20~21 (**Figure 22A** and the middle IEX blotting of **Figure 22C)**, I conducted similar GF experiments using proteins from those IEX fractions. Surprisingly, still no CSN3 signal was detected in lower molecular mass fractions (12 to 14) that correspond to sCSN3c and all the CSN3 were found in the holocomplex GF fractions (6 to 8, **Figure 22C**, upper and lower GF blottings) in any of the GF results.

It is likely that the other components within the sCSN3c affect the net surface charge of the sCSN3c. This may result in two possible consequences: the sCSN3c cannot bind the anion column at pH 7, or it strongly interacts with the anion exchanger of the IEX column. Consistently, in either the unbound proteins (in fractions 3) or the strongly bound proteins that were stripped off the column using 1M NaCl (in faction labeled as "strip"), I detected the weak presence of CSN3 in the immunoblot (**Figure 22C,** the middle IEX blotting).

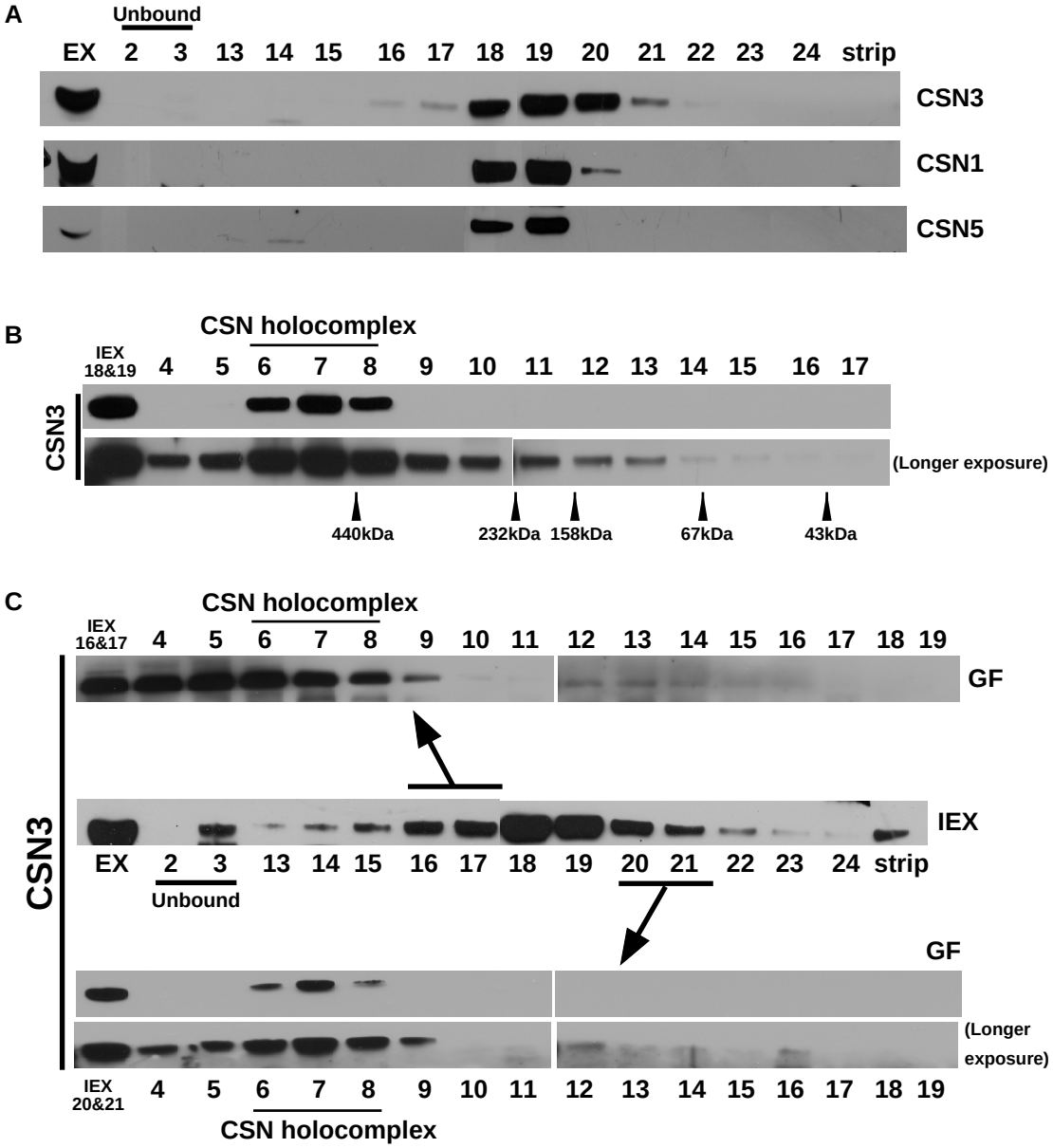
A
Unbound
EX 2 3 13 14 15 16 17 18 19 20 21 22 23 24 strip
CSN3
CSN1
CSN5
B
CSN holocomplex
IEX 18&19 4 5 6 7 8 9 10 11 12 13 14 15 16 17
CSN3
(Longer exposure)
440kDa
232kDa
158kDa
67kDa
43kDa
C
CSN holocomplex
IEX 16&17 4 5 6 7 8 9 10 11 12 13 14 15 16 17 18 19
GF
IEX
EX 2 3 13 14 15 16 17 18 19 20 21 22 23 24 strip
Unbound
CSN3
GF
(Longer exposure)
IEX 20&21 4 5 6 7 8 9 10 11 12 13 14 15 16 17 18 19
CSN holocomplex

Figure 22. PEG precipitation and IEX using the Mono Q anion exchange column enriches the CSN holocomplex.

(A) Col seedlings were homogenized and precipitated with 15% polyethylene glycol (PEG). The dissolved PEG precipitates were loaded to an anion exchange column (Mono Q). The IEX fractions containing the unbound fractions (2 and 3) as well as elutions (13 to 24) were collected for western detection of CSN3, CSN1 and CSN5. EX stands for PEG precipitates before IEX. “strip” indicates the column-bound proteins that are stripped off the column by applying 1M salt solution at the end of the IEX.

(B) IEX fractions 18 and 19 from (A) were pooled and loaded to a GF column (Superdex 200). CSN3 western of the GF fractions was presented. Molecular mass standards are shown at the bottom of each panel. EX indicates the IEX 18&19 pool before gel filtration. Lower panel shows the longer exposure of the CSN3 western result.

(C) In the middle shows a repeating experiment of (A) showing the longer exposure of CSN3 immunoblotting using the IEX fractions, notice the slight CSN3 signal at the unbound fraction 3 and the “strip” fraction. The IEX fractions 16&17, 20&21 were pooled and were injected to a GF column to decide whether CSN3 is in the holocomplex form or sCSN3 form (upper and bottom GF blottings, respectively).

Optimize the IEX condition to separate the sCSN3c from the CSN holocomplex.

As seen in **Figure 18A**, about 90% of the endogenous CSN3 was found in the CSN holocomplex, while the sCSN3c only contained the rest 10%. Therefore, one big challenge for the purification of sCSN3c is to develop a method that can efficiently separate the small complex from the holocomplex. My IEX data demonstrated that I could successfully enrich the CSN holocomplex by using the anion exchange column at pH 7, and suggested that the sCSN3c is probably in the unbound or the stripped off fractions (**Figure 22**). In this section, I will talk about using a reverse approach to find an optimized IEX condition, at which the sCSN3c was readily separated from the holocomplex.

As illustrated in **Figure 23A**, I first did two GF runs using protein extracts made from Arabidopsis wild type seedlings. GF fractions that contained either the CSN holocomplex (fractions 6 to 8) or the sCSN3c (12 to 14) were pooled (holocomplex pool and sCSN3c pool) for future IEX-FPLC analyses. Since both the pH and ion strength of the IEX buffer can affect the net surface charge of target protein/protein complex, I started to use a fixed range of salt concentration (100 mM~400 mM NaCl) and switched to different pH conditions for the IEX elution. The pooled protein sample of either the holocomplex or sCSN3c was buffer exchanged to match the IEX equilibration buffer conditions of different pH and loaded to an IEX column.

I started with a strong anion IEX column (Mono Q™ 5/50 GL) to separate the loaded sample (holocomplex pool and sCSN3c pool in **Figure 23B**) with the equilibration buffer of pH 7, 100 mM NaCl. In the upper panel of **Figure 23B** showing

the α-CSN3 detection of the holocomplex pool IEX fractions, the CSN3 in the holocomplex bound the column and was eluted at fractions 20 to 25. The majority of CSN3 was eluted at fractions 21 and 22, which corresponded to a salt concentration of 360~380 mM NaCl, slightly different from my previous result using 15% PEG precipitated crude protein extracts (**Figure 22A**). Interestingly, the sCSN3c couldn't bind the Mono Q column at pH 7, as the CSN3 signal from the sCSN3c pool IEX fractions was detected only in the flow-through fractions (2 to 4, lower panel of **Figure 23B**). Additionally, when I increased the salt concentration of the start/equilibration buffer (from 100 mM NaCl to 200 mM NaCl), the holocomplex still bound the Mono Q column at pH 7 and was eluted mainly in fractions 18 and 19 (350~36 0mM NaCl, upper panel of **Figure 23 C)**, consistent with the 15% PEG-IEX results (**Figure 22A**), while the sCSN3c was again washed into the unbound flow-through **(**fractions 3 to 5, lower panel of **Figure 23C**). Therefore at pH 7, the sCSN3c was isolated from the holocomplex by using the Mono Q column.

To test if I could still separate the sCSN3c from the holocomplex by IEX at a more basic condition, I compared the IEX fractionation patterns of CSN with that of the sCSN3c at pH 8, while maintaining the salt concentration as in **Figure 23B**. CSN3 was now mainly eluted by a higher concentration of salt (380~400mM NaCl) and collected in later fractions (22 to 25, upper panel of **Figure 23D**), indicating the CSN holocomplex was more negatively charged and its association with the Mono Q column matrix became even stronger. Additionally, when loading the sCSN3c pool to the Mono Q column at pH 8, the increased pH also caused sCSN3c to be negatively charged and to bind the column.

As seen in the lower panel of **Figure 23D**, CSN3 was no longer present in the IEX flow-through fractions but was eluted later by increasing the ion strength (fractions 19 to 21, 320 mM~360 mM NaCl). However, the comparison of CSN3 IEX patterns clearly showed that the holocomplex and sCSN3c bound to the Mono Q column with different strengths at pH 8 and could still be readily separated from each other.

Similar tests on the holocomplex pool and sCSN3c pool were also conducted using another strong anion column HiTrap™ Q FF (CV=1ml) at pH 7.5, 100~500 mM NaCl. As shown in **Figure 23E,** the CSN3 peak of the sCSN3c pool was centered at fractions 13 to 15 (lower panel, corresponding to 275 mM to 325 mM NaCl), while CSN3 of the holocomplex pool was eluted mainly at fractions 15 to 18 (upper panel, corresponding to 325 to 400 mM NaCl). Although the peaks of CSN3 signal from the holocomplex pool and sCSN3c IEX partially overlapped with each other, the sCSN3c still had a weaker binding to the HiTrap Q FF anion exchange column and was eluted earlier. When I increased salt concentration of the start/equilibration buffer to 250 mM NaCl without changing the pH (pH 7.5), the CSN3 from the sCSN3c pool no longer bound the column and was only found in the flow-through fractions (lower panel of **Figure 23F**, fractions 2 to 4). The increased salt concentration also caused the CSN3 of the holocomplex to be eluted earlier (upper panel of **Figure 23F,** fractions 9 to 16), as well as slight CSN signal detected in the flow-through fractions (upper panel of **Figure 23F**, fractions 2 and 3).

To summarize, I used the protein pools from GF fractions that contained either the CSN holocomplex or sCSN3c to run through an IEX anion exchange column at different

pH, followed by the α-CSN3 immunoblot detection of IEX fractions. I found that the sCSN3c was less negatively charged at pH 7~8 compared to the holocomplex and barely or weakly bound the anion IEX columns. For instance, by applying IEX at pH 7 with 100~400 mM NaCl using a Mono Q column, I could easily separate the sCSN3c, which was in the unbound fractions, from the CSN holocomplex that bound the column.

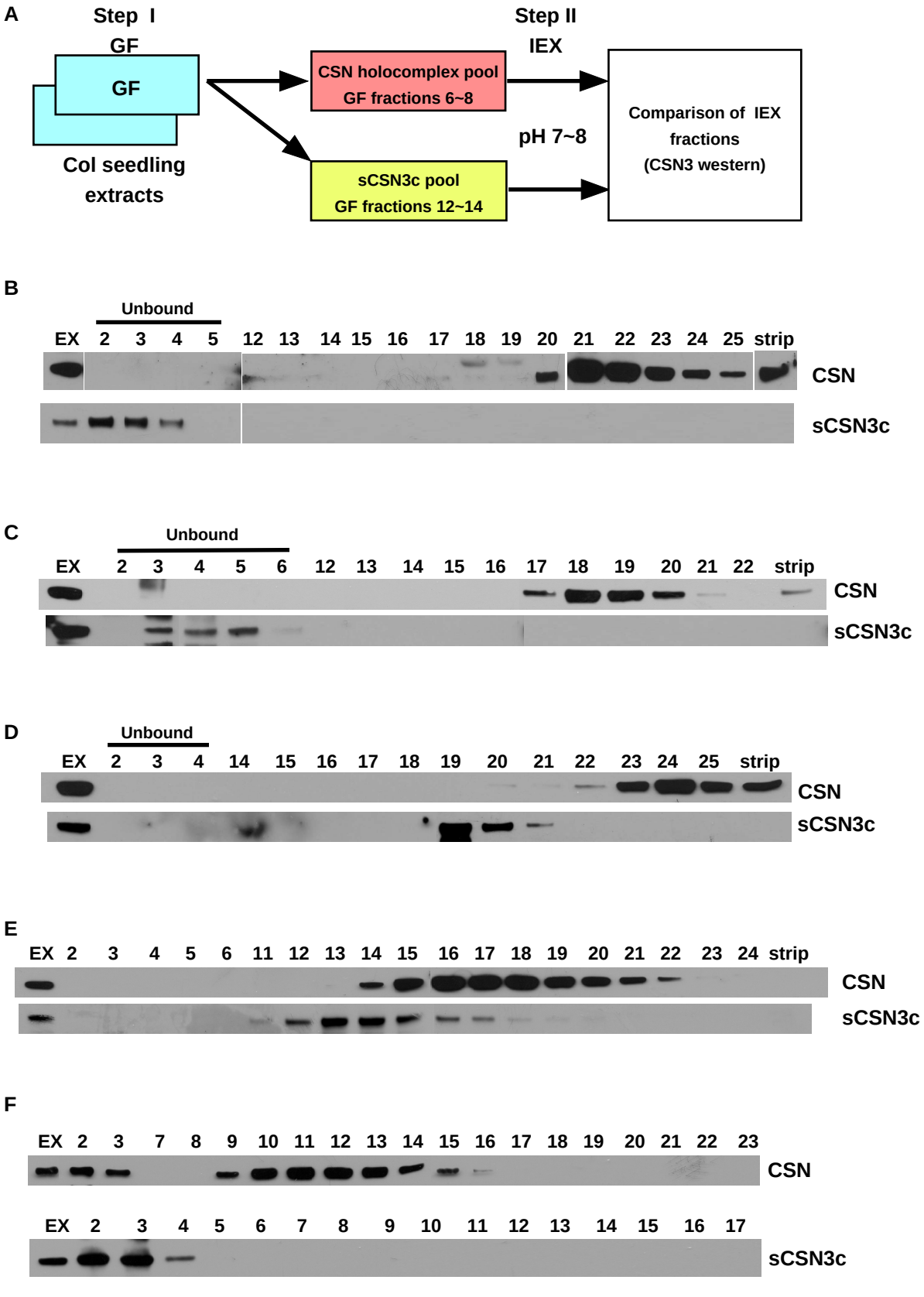
A
Step I
GF
GF
Col seedling extracts
CSN holocomplex pool
GF fractions 6~8
sCSN3c pool
GF fractions 12~14
Step II
IEX
pH 7~8
Comparison of IEX fractions
(CSN3 western)
B
Unbound
EX 2 3 4 5 12 13 14 15 16 17 18 19 20 21 22 23 24 25 strip
CSN
sCSN3c
C
Unbound
EX 2 3 4 5 6 12 13 14 15 16 17 18 19 20 21 22 strip
CSN
sCSN3c
D
Unbound
EX 2 3 4 14 15 16 17 18 19 20 21 22 23 24 25 strip
CSN
sCSN3c
E
EX 2 3 4 5 6 11 12 13 14 15 16 17 18 19 20 21 22 23 24 strip
CSN
sCSN3c
F
EX 2 3 7 8 9 10 11 12 13 14 15 16 17 18 19 20 21 22 23
CSN
EX 2 3 4 5 6 7 8 9 10 11 12 13 14 15 16 17
sCSN3c

Figure 23. Optimization of IEX conditions to separate the sCSN3c from the holocomplex.

(A) shows the work scheme of (B~F). In brief, at Step I, Col protein extracts were used to run two GF experiments. Fractions containing the CSN holocomplex (6~8) or the sCSN3c (12~14) from two GF runs were then pooled. At Step II, the pooled proteins were loaded to anion IEX columns (Mono Q for B~D, Hitrap Q FF fro E~F) at various conditions. Then the IEX fractions of both unbound proteins and elutions were separated on SDS-PAGE for CSN3 western detection.

(B~F) The CSN3 IEX fractionation patterns of the holocomplex pool (CSN) and the sCSN3c pool (sCSN3c) were compared, hoping to find a condition at which the sCSN3c can be separated from the holocomplex by IEX. EX stands for the protein pool before IEX. “strip” indicates the column-bound proteins that are stripped off the column by applying 1M salt solution at the end of the IEX.

(B) IEX using a Mono Q column at pH 7, 100~400mM NaCl for elution.
(C) IEX using a Mono Q column at pH 7, 200~400mM NaCl for elution.
(D) IEX using a Mono Q column at pH 8, 100~400mM NaCl for elution.
(E) IEX using a Hitrap Q FF column at pH 7.5, 100~500mM NaCl for elution.
(F) IEX using a Hitrap Q FF column at pH 7.5, 250~500mM NaCl for elution.

sCSN3c from crude extracts can be enriched by using an IEX anion column

Since the aforementioned experiments were done in a reversed manner (GF to IEX) looking for the optimized IEX conditions, I wanted to validate that the use of IEX at a desired pH could isolate the sCSN3c from the plant protein extracts. As illustrated in **Figure 24A**, crude protein extracts made from wild type Arabidopsis seedlings were first concentrated using 15% PEG precipitation and then loaded to a HiTrap™ Q FF anion exchange column at pH 8, 100 mM~500 mM NaCl.

The α-CSN3 immunoblot of IEX fractions revealed that the majority of CSN3 was found in column-bound fractions (**Figure 24B**, fractions 11 to 21). Based on my previous result shown in **Figure 23E**, at pH 7.5, the sCSN3c weakly interacted with the column matrix and was eluted in earlier fractions compared to the holocomplex. At pH 8, the sCSN3c was expected to be more negatively charged and more likely to bind the column. Therefore the CSN3 signals detected in the unbound fractions were probably due to the overly loaded protein sample (fractions 2 to 3).

Since the sCSN3c could only weakly bind the anion column, I hypothesized that the CSN3 in the early IEX elutions of **Figure 24B** was mainly in its sCSN3c form. To test this hypothesis, I conducted a GF experiment using proteins from the IEX fraction 13 or 14. Surprisingly, as seen in **Figure 24C**, the α-CSN3 immunoblot detection of GF fractions showed that nearly all the CSN3 signal were in GF fractions corresponding to the holocomplex (fractions 7 to 9), indicating CSN3 from either the IEX fraction 13 or 14 were mainly in the CSN holocomplex form. To rule out the possibility that the sCSN3c was eluted in much earlier IEX fractions such as 11 and 12, I pooled proteins from these

two IEX fractions to run through a GF column. However, the GF result repeatedly showed that CSN3 was mainly present in its holocomplex form and the sCSN3c was not enriched (**Figure 24D**).

Another possible explanation is that the 15% PEG precipitation during the sample preparation step may disrupt the interactions between CSN3 and other components within the sCSN3c. To test this possibility, I skipped the 15% PEG precipitation during the sample preparation and loaded the clarified crude protein extracts directly to the IEX column. At the same condition of pH 8, 100 mM~500 mM NaCl, no major changes were found in the CSN3 IEX fractionation pattern between using the crude extracts (**Figure 24E**) and using the PEG precipitate (**Figure 24B**), with both CSN3 peaks centered at fractions 15 to 18. However, in the follow-up GF analysis on proteins of the IEX fraction 13 (**Figure 24E)**, about more than 50% of the total CSN3 from the IEX fraction 13 were found in the sCSN3c form (GF fractions 12 to 14, **Figure 24F**), while the remaining CSN3 were assembled into the holocomplex (fractions 7 to 9, **Figure 24F**). In a analogous experiment, I ran the crude protein extract through HiTrap™ Q FF at pH 7.5, 100~500 mM and also picked the IEX fraction 13 to conduct a GF analysis. Similar results were found in the CSN3 detection of GF fractions (**Figure 24G**), with about 50% of the total CSN3 detected in the sCSN3c fractions. Therefore, by directly applying the crude extracts to the HiTrap Q FF anion exchange column at pH 7.5 and 8, I could enrich the sCSN3c, which was mainly present in the early IEX elutions.

In summary, I found that the 15% PEG precipitation during the protein extract preparation affected the assembly of sCSN3c. I also validated that even at pH 7.5 or pH

8, the sCSN3c could be partially separated from the holocomplex by loading the crude extracts directly to an anion exchange column. Additionally, compared with previous GF result, in which over 90% of CSN3 were found in the holocomplex (**Figure 18A**), adding an IEX step before GF could enrich the sCSN3c (**Figure 24F and 24G**).

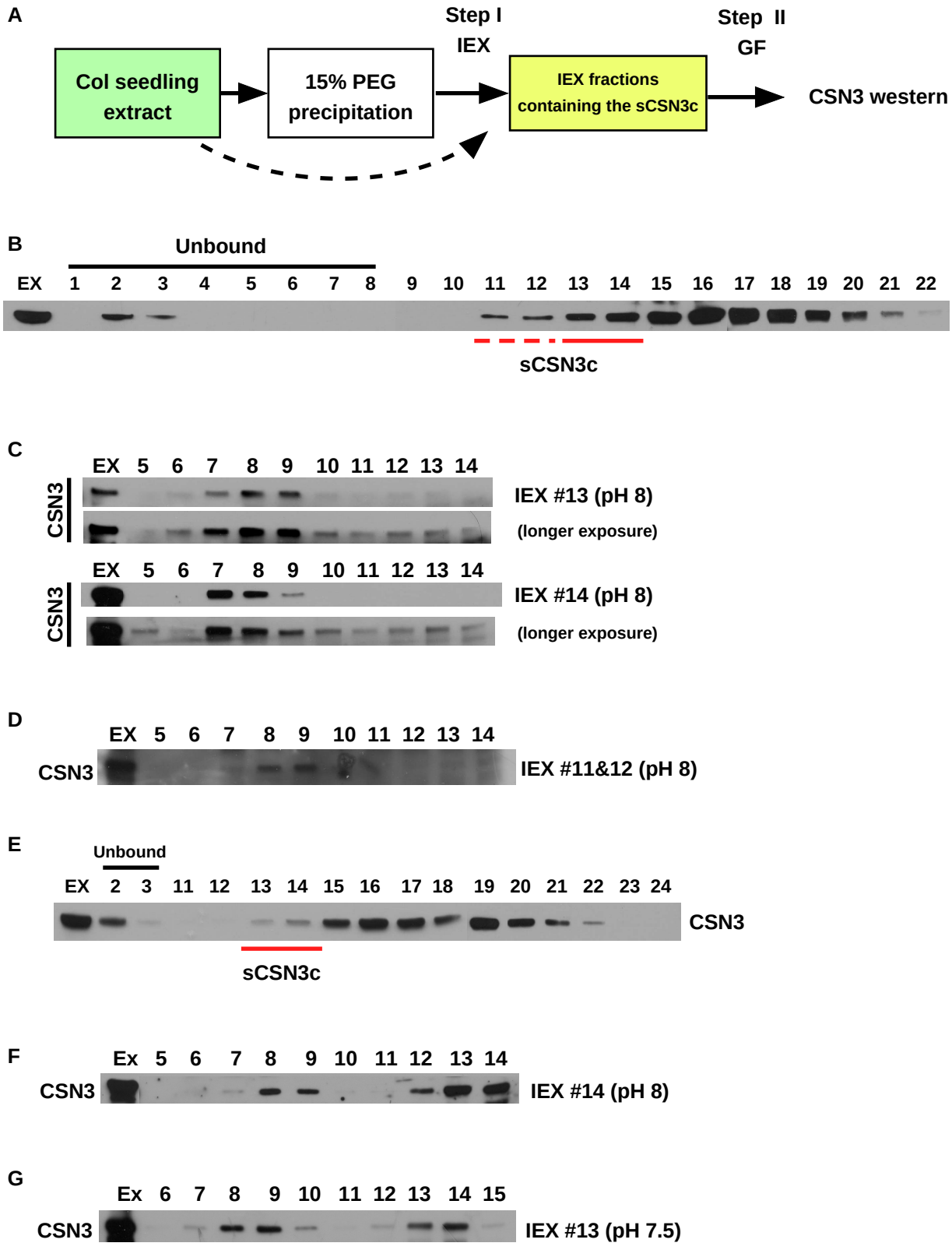
A
Step I
IEX
Step II
GF
Col seedling extract
15% PEG precipitation
IEX fractions containing the sCSN3c
CSN3 western
B
Unbound
EX 1 2 3 4 5 6 7 8 9 10 11 12 13 14 15 16 17 18 19 20 21 22
sCSN3c
C
EX 5 6 7 8 9 10 11 12 13 14
CSN3
IEX #13 (pH 8)
(longer exposure)
EX 5 6 7 8 9 10 11 12 13 14
CSN3
IEX #14 (pH 8)
(longer exposure)
D
EX 5 6 7 8 9 10 11 12 13 14
CSN3
IEX #11&12 (pH 8)
E
Unbound
EX 2 3 11 12 13 14 15 16 17 18 19 20 21 22 23 24
CSN3
sCSN3c
F
Ex 5 6 7 8 9 10 11 12 13 14
CSN3
IEX #14 (pH 8)
G
Ex 6 7 8 9 10 11 12 13 14 15
CSN3
IEX #13 (pH 7.5)

Figure 24. Validate the IEX condition at which the sCSN3c can be separated from the holocomplex.

(A) shows the work scheme of (B~G). In brief, Col protein extracts were PEG precipitated or directly loaded to an anion exchange column (Hitrap Q FF, Step I) at a desired condition. Fractions containing the sCSN3c were pooled and loaded to a GF column (Superdex 200). CSN3 detection of GF fractions was applied to validate that the sCSN3c is enriched by IEX.

(B) shows the CSN3 detection of IEX fractions of Step I, with both the unbound fractions and elutions. 15% PEG precipitates of Col seedling extracts were loaded to a Hitrap Q FF column at pH 8, 100~500mM NaCl. EX stands for the protein pool before IEX. Fractions that may contain the sCSN3c were indicated.

(C~D) The IEX fractions 13, 14 (C) and protein pool of IEX fractions 11&12 (D) were loaded to a GF column. Figures C and D show the CSN3 detection of GF fractions.

(E) The PEG precipitation step was skipped. Col seedling crude extracts were directly loaded to a Hitrap Q FF column at pH 8, 100~500mM NaCl. Figure shows the CSN3 detection of IEX fractions, with both unbound fractions and elutions.

(F) shows the GF analysis and CSN3 detection using the IEX fraction 14 in (E).

(G) Col seedling crude extracts were loaded to a Hitrap Q FF column at pH 7.5, 100~500mM NaCl. IEX fraction 13 was chosen to run a GF analysis. Figure shows the CSN3 detection of GF fractions.

Scale up the IEX to capture sCSN3c

For the protein purification purpose, I need to start with a relatively large amount of protein crude extract and use an efficient method to concentrate the target protein/protein complex. As shown in previous two sections, the IEX using a strong anion exchange column at pH 7 can effectively separate the sCSN3c from the holocomplex, while at pH 7.5 or 8 the IEX fractionation patterns of the holocomplex and the sCSN3c partially overlap with each other (**Figure 23 and 24**). Since the aforementioned Mono Q and HiTrap Q FF columns are small columns that are designed for the polishing step or for optimizing experimental conditions, I switched to a bigger IEX column for the capture step of the CIPP to harvest as much sCSN3c as possible from the crude protein extracts. About 7 mg of total protein was injected to a HiPrep™ 16/10 Q FF (CV=20 ml) anion IEX column and eluted at pH 7, 100~500 mM NaCl. As expected, the CSN3 signal was found in both the flowthrough (fractions 4 and 5, **Figure 25B**) and the elution portion (fractions 13to 19, **Figure 25B**), within two peaks as seen in the IEX chromatograph (**Figure 25A**). Based on my prior analyses, at pH 7 the sCSN3 didn't bind the anion Q column. Consistently, the chromatograph of GF analysis using the IEX flow-through fractions (Pool I in **Figure 25A**, IEX fractions 4 and 5 in **Figure 25B**) showed that all the proteins were present in lower molecular mass fractions (A11 to B11, **Figure 25C**). In contrast, the GF chromatograph of the IEX elutions (Pool II in **Figure 25A**, fractions 13 to 17 in **Figure 25B**) indicated that bigger protein/protein complexes were present (fractions A5 to A9), which probably include the CSN

holocomplex (**Figure 25D**). Together, my results suggested that scaling up the IEX capture step still separated the sCSN3c from the holocomplex.

A

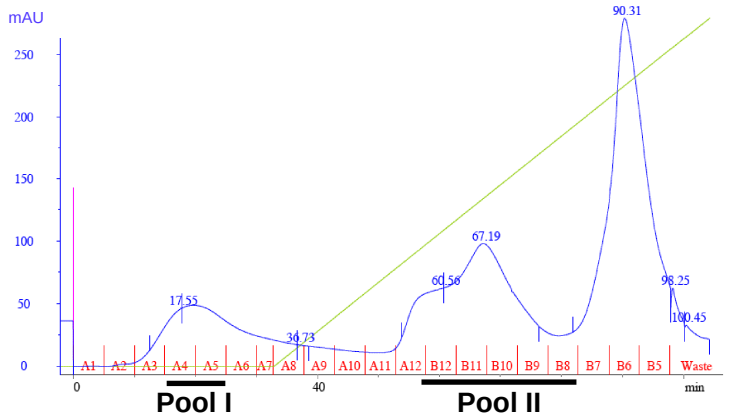
mAU
250
200
150
100
50
0
90.31
67.19
60.58
17.55
36.73
98.25
100.45
A1 A2 A3 A4 A5 A6 A7 A8 A9 A10 A11 A12 B12 B11 B10 B9 B8 B7 B6 B5 Waste
0
40
min
Pool I
Pool II

B

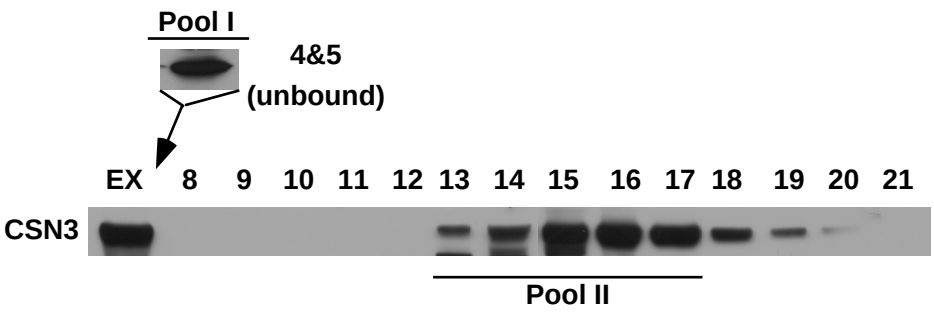
Pool I
4&5
(unbound)
EX 8 9 10 11 12 13 14 15 16 17 18 19 20 21
CSN3
Pool II

C

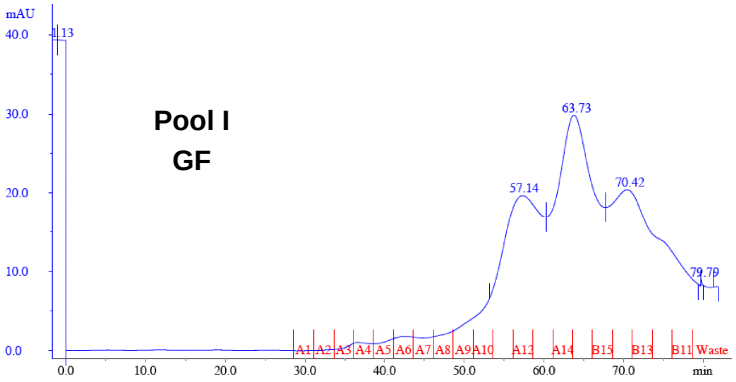
mAU
40.0
30.0
20.0
10.0
0.0
1.13
Pool I
GF
63.73
57.14
70.42
79.79
A1 A2 A3 A4 A5 A6 A7 A8 A9 A10 A12 A14 B15 B13 B11 Waste
0.0 10.0 20.0 30.0 40.0 50.0 60.0 70.0
min

D

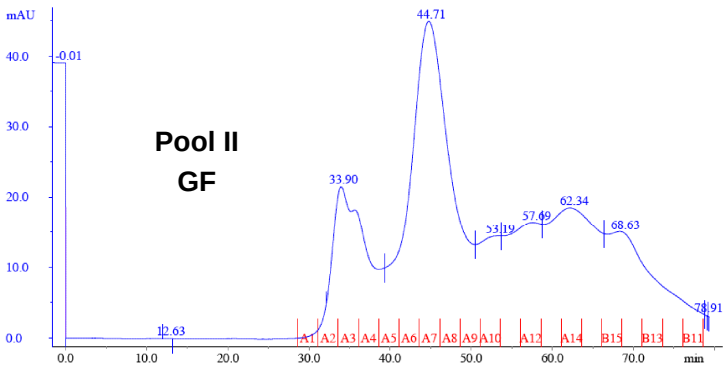
mAU
40.0
30.0
20.0
10.0
0.0
0.01
Pool II
GF
44.71
33.90
53.19
57.69
62.34
68.63
12.63
78.91
A1 A2 A3 A4 A5 A6 A7 A8 A9 A10 A12 A14 B15 B13 B11
0.0 10.0 20.0 30.0 40.0 50.0 60.0 70.0
min

Figure 25. A scale-up IEX experiment can still separate the sCSN3c from the holocomplex at pH 7.

The HiPrep™ 16/10 Q FF (CV=20ml) IEX column was used to enrich the sCSN3c from the Col seedling protein extracts.

(A) The chromatograph of IEX using the HiPrep column at pH 7, 100~500mM NaCl. Fractions were labeled at the bottom, while the Y-axis shows the UV detection of eluted proteins. The first several fractions contain unbound proteins, while the elution starts at fraction 8 (A8). The light green line indicates the increasing concentration of salt. At pH 7, the sCSN3c are most likely present in unbound fractions (Pool I), while the holocomplex are mainly in the early elutions (Pool II) according to prior data.

(B) CSN3 detection of IEX fractions, indicating CSN3 are present in both Pool I and Pool II. Fraction 13~20 represent the B12~B5 in (A). EX indicates the extract before IEX.

(C~D) Chromatographs of GF analyses using proteins of the Pool I (C) or Pool II (D) IEX fractions. Again, GF fraction numbers were labeled at the bottom, with B15~B12 representing fractions 16~19 in prior GF results. Y-axis indicates the UV detection of eluted proteins.

Tagged CSN3 has a similar GF profile as that of endogenous CSN3

Affinity chromatography (AC) is usually included in the CIPP protein purification process, either as a capture step or an intermediate purification step. Therefore, I ectopically expressed the CSN3 protein with an affinity tag and introduced them into either the *csn3-3* or *csn3-2* backgrounds.

The myc tag was fused to the N-terminus of either the wild type or the *csn3-3* mutated form of *CSN3* cDNA under the Cauliflower Mosaic Virus 35S promoter (*35S:myc-CSN3* and *35S:myc-ETA7*). Before using the transgenic lines for protein purification, I first need to confirm that the affinity tagged CSN3 can be assembled into the CSN holocomplex as well as the sCSN3c. GF analyses were conducted to test the myc-CSN3 GF fractionation pattern using protein extracts made from *csn3-3 [35S:myc-CSN3]* homozygous seedlings.

Since the myc construct only has one copy of myc peptide, which is a very small affinity tag (less than 5kDa) compared to the size of CSN3 (Earley et al., 2006), it is less likely the N-terminal myc-fusion will cause a dramatic conformational change of the CSN3 protein. Consistent with this hypothesis, in the immunoblot detection of CSN3, both over-expressed myc tagged CSN3 and the endogenous ETA7 in *csn3-3* were mainly found in the GF fractions corresponding to the CSN holocomplex (fractions 6 to 9, **Figure 26A**). When expressed in the *csn3-2* mutant background, the majority of myc-CSN3 signal was also found in the holocomplex fractions, resembling the fractionation pattern of the endogenous CSN3 in the wild type control (fractions 4 to 8, **Figure 26B**). In addition, in a co-immunoprecipitation assay using both α-myc or α-CSN3 antibodies

to precipitate the myc-CSN3 in the *csn3-2 [35S:myc-CSN3]* background, other CSN subunits such as CSN1 and CSN8 could be readily co-purified, indicating the tagged CSN3 maintained the capability to interact with other CSN subunits (**Figure 26C**) and form the holocomplex. Last but not least, the overexpression of myc-CSN3 also rescued the *csn3-2* seedling lethal phenotype (data not shown), which was caused by the assembly defects within the CSN holocomplex (Dohmann et al., 2008a). Therefore, I concluded that myc-CSN3 was assembled into the CSN holocomplex.

The myc-CSN3 protein was also eluted into GF fractions corresponding to the sCSN3c (12~14, **Figure 26A**), while the endogenous mutated form of CSN3 (ETA7) in *csn3-3 [35S:myc-CSN3]* was detected in lower molecular mass fractions (lower band in **Figure 26A**, fractions 12 to 16). Interestingly, in those lower molecular mass fractions, I noticed that the endogenous ETA7 of the transgenic plants was eluted into broader fractions (fractions 12 to 16, **Figure 26A**) than the ETA7 of the *csn3-3* plants (fractions 14 to 16, **Figure 18A**). This result suggested that the ectopic expression of tagged wild-type CSN3 might affect the endogenous mutated ETA7 GF fractionation. One possibility is that myc-CSN3 may hetero-dimerize with the endogenous ETA7, so that part of the ETA7 signal in fractions 12 and 13 represented the myc-CSN3-ETA7 dimer. Consistently, in a co-IP experiment, myc-CSN3 was shown to interact with endogenous ETA7 (**Figure 27D**). Another interesting finding of the *csn3-3 [35S:myc-CSN3]* GF result was that the small complex containing myc-CSN3 was enriched. As shown in **Figure 26A**, the myc-CSN3 was equally assembled into the holocomplex and the sCSN3c. In comparison, almost 90% of the endogenous CSN3 (ETA7) was assembled

into the holocomplex. This was possibly caused by the ectopic expression of myc-CSN3: myc-CSN3 might compete with endogenous EAT7 for CSN holocomplex assembly and the extra myc-CSN3 couldn't be incorporated into the holocomplex but into the small complex.

To rule out the effects of endogenous CSN3, I introduced the transgene into the csn3-2 null background by crossing. GF analysis of *csn3-2 [35S:myc-CSN3]* homozygous plants also indicated that the myc tagged CSN3 migrated into sCSN3c fractions as the endogenous CSN3 of the Col control did (fractions 12 and 13, **Figure 26B**). In contrast, the myc-ETA7 of *csn3-3 [35S:myc-ETA7]* homozygous plants was detected in fractions corresponding to the CSN3 monomer in addition to the holocomplex fractions, which resembled the GF fractionation pattern of the endogenous mutated CSN3 (ETA7) in *csn3-3* or *csn3-3 [35S:myc-ETA7]* transgenic plants (fractions 13 to 15, **Figure 26E**).

To summarize, GF results suggested that the myc-tagged CSN3 had a similar capability as the endogenous CSN3 to form protein complexes (either the CSN holocomplex or sCSN3c). The comparison between myc-CSN3 and myc-ETA7 also suggested that the *csn3-3* mutation prevented myc-ETA7 from recruiting other protein/proteins to form the sCSN3c.

Another affinity tag I used for AC was the HPB tag (for HA-PreScission-Biotin), which contained the 80 amino acid sequence of the C-terminus of Arabidopsis MCCA protein (3-methylcrotonyl CoA carboxylase, *At1g03090*) for biotinylation and was designed to create C-terminal fusions to the target proteins (Qi and Katagiri). One-step

purification utilizing the biotin-streptavidin interaction could efficiently purify the proteins of interest (Qi and Katagiri). The *35S:CSN3-HPB* construct was transformed into the *csn3-2* +/- background. In a GF analysis using the protein extracts from the T2 segregation population of transgenic plants, the CSN3-HPB signal was also found in two peaks that represent either the CSN holocomplex (fractions 4 to 7) or sCSN3c (fractions 11 to 13), as revealed by the α-CSN3 immunoblot detection in **Figure 26D.** This result suggested that as the N-terminal myc tag, the C-terminal HPB tag did not affect assemblies of the holocomplex and sCSN3c, either.

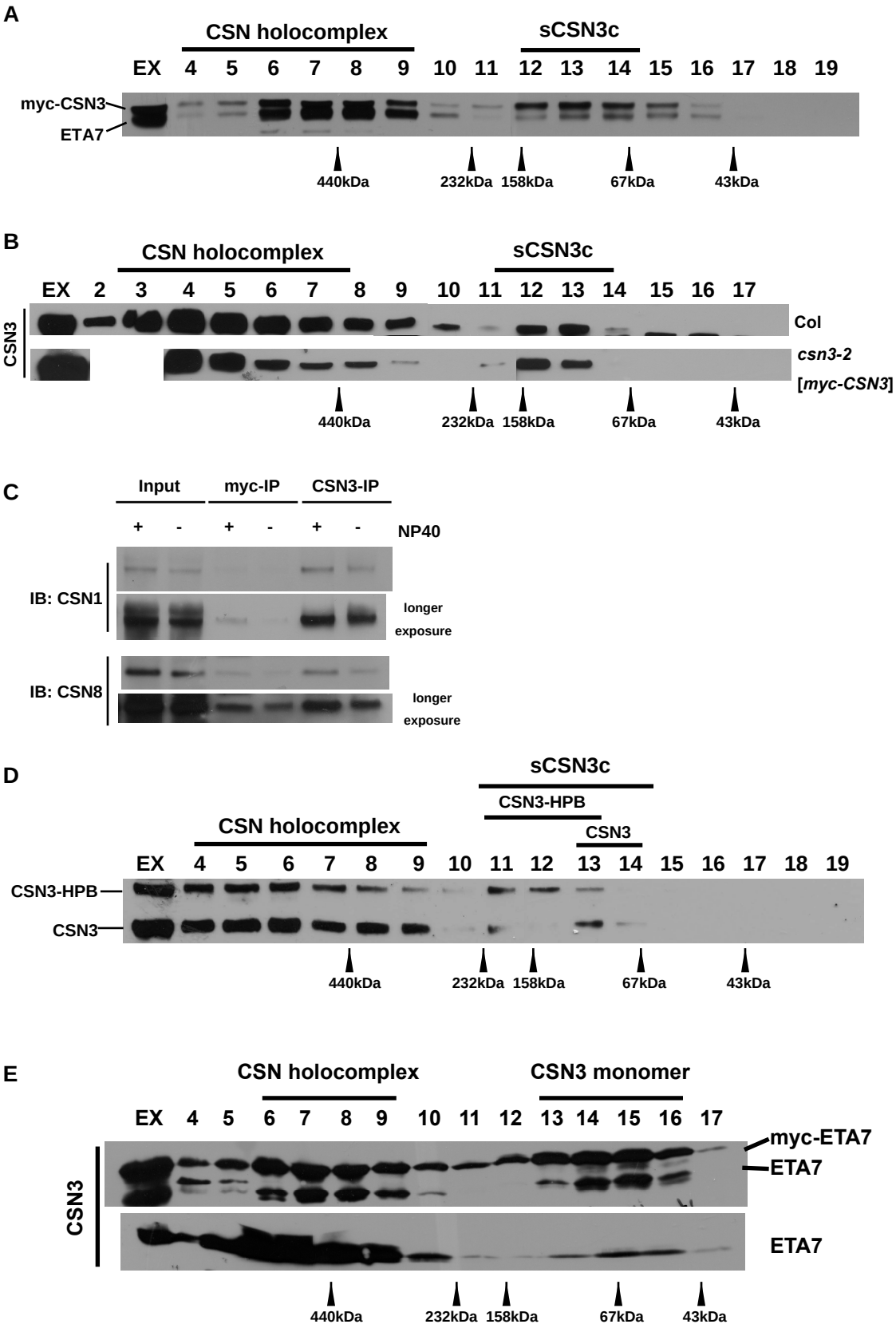
A
CSN holocomplex
sCSN3c
EX 4 5 6 7 8 9 10 11 12 13 14 15 16 17 18 19
myc-CSN3
ETA7
440kDa 232kDa 158kDa 67kDa 43kDa
B
CSN holocomplex
sCSN3c
EX 2 3 4 5 6 7 8 9 10 11 12 13 14 15 16 17
CSN3
Col
csn3-2
[myc-CSN3]
440kDa 232kDa 158kDa 67kDa 43kDa
C
Input
myc-IP
CSN3-IP
+ - + - + -
NP40
IB: CSN1
longer exposure
IB: CSN8
longer exposure
D
sCSN3c
CSN3-HPB
CSN3
CSN holocomplex
EX 4 5 6 7 8 9 10 11 12 13 14 15 16 17 18 19
CSN3-HPB
CSN3
440kDa 232kDa 158kDa 67kDa 43kDa
E
CSN holocomplex
CSN3 monomer
EX 4 5 6 7 8 9 10 11 12 13 14 15 16 17
myc-ETA7
ETA7
CSN3
ETA7
440kDa 232kDa 158kDa 67kDa 43kDa

Figure 26. Tagged-CSN3 proteins are also assembled into a small protein complex besides the CSN holocomplex.

(A) CSN3 detection of GF fractions using protein extracts made from *csn3-3* [*35S:myc-CSN3*] seedlings. The upper band indicates the myc tagged CSN3, while the lower band indicates the endogenous mutated form of CSN3 (ETA7). Molecular mass standards are shown at the bottom of each panel. EX means the extracts before GF.

(B) Leaves of Col and *csn3-2* [*35S:myc-CSN3*] plants were homogenized in buffer containing detergent (Buffer A, 0.5% NP40) to make protein extracts. The extracts were then loaded to a Superdex 200 GF column. Figure shows the CSN3 detection of GF fractions.

(C) Co-immunoprecipitation (co-IP) experiments using the *csn3-2* [*35S:myc-CSN3*] seedling extracts. The endogenous CSN1 and CSN8 can be co-purified by either the myc-IP or the CSN3-IP. Adding detergent (NP40) to the extraction buffer may slightly increase the co-IP efficiency.

(D) similar as in (B), protein extracts made from leaves of *csn3-2+/-* [*35S:CSN3-HPB*] T1 plants were separated on a GF column. CSN3 western of GF fractions shows fractionation patterns of the tagged-CSN3 (upper band) and the endogenous CSN3.

(E) CSN3 detection of GF fractions using *csn3-3* [*35S:myc-ETA7*] and *csn3-3* protein extracts. 7-d.o. seedling extracts were used. Bands of myc-ETA7 and endogenous ETA7 are indicated. Molecular mass standards are labeled at the bottom. EX stands for the extracts before GF.

Affinity purification of tagged CSN3

Cross-linking our homemade α-CSN3 antibody to the protein A matrix caused the loss of the antibody activity (done by William Gray, data not shown). However, A two-step α-CSN3 immunoprecipitation (IP), which used the soluble affinity purified CSN3 antibody followed by adding protein A beads to harvest the CSN3 IP complex, precipitated CSN3 proteins. As shown in **Figure 27A**, α-CSN3 IP worked perfectly to harvest the myc-CSN3 from *csn3-2 [35S:myc-CSN3]* protein extracts. Alternatively, I used the commercially available affinity matrices to purify tagged CSN3 proteins (α-myc-protein A beads for myc-CSN3 or streptavidin-Dynabeads® for CSN3-HPB).

To test the efficiency of myc-IP, leaf protein extracts in buffer A were made from *csn3-2 [35S:myc-CSN3]* homozygous plants and immunoprecipitated with the myc beads. **Figure 27B** showed the α-CSN3 detection of the IP result with the input control. In comparison with the input control, the myc-CSN3 signal found in the IP corresponded to ~7% of the total myc-CSN3, as estimated from the size/darkness of the band (lane 3 to 5, **Figure 27B**). In an analogous experiment using the *csn3-2* segregating population that homozygously express *35S:myc-CSN3*, leaf protein extracts using the IEX equilibration buffer were used for myc-IP. As shown in **Figure 27C**, two forms of CSN3 (myc-CSN3 and endogenous CSN3) were detected by α-CSN3 in the input or after-IP controls, while nothing was detected in the negative controls (lane 2 of protein A IP and lane 4 of myc beads mock IP). Interestingly, both the myc-CSN3 and endogenous CSN3 were detected in the myc IP, indicating the myc-CSN3 interacted with the endogenous CSN3.

In order to test whether the *csn3-3* mutation blocked the CSN3 dimerization. I repeated the myc-IP using the *csn3-3* [*35S:myc-CSN3*] extracts. Interestingly, the endogenous ETA7 could also be weakly co-purified by the myc-IP (**Figure 27D**), suggesting the mutated form of CSN3 might only impair but not totally prevent the heterodimerize with the myc-CSN3. Similar IP results were found in the myc-IP using the extracts of *csn3-2* [*35S:myc-ETA7*] heterozygous plants, in which the concentrated myc-ETA7 IP complex co-purified endogenous CSN3 (**Figure 27E**, right). However, when doing the myc-IP using *csn3-3* [*35S:myc-ETA7*] extracts, I surprisingly found that the ETA7 could not be co-purified with the myc-ETA7, suggesting the mutation within ETA7 blocked the homo-dimerization between two ETA7 molecules. This raised an interesting question of if the sCSN3c is a CSN3 dimer, which will be talked in details in the discussion section.

In the case of CSN3-HPB, leaves of *csn3-2 [35S:CSN3-HPB]* T1 plants were used for making protein extracts. By using the magnetic streptavidin beads that can strongly interact with the biotinylation peptide within the HPB tag, the tagged protein could be enriched by the IP. The α-CSN3 detection of the IP result showed the accumulation of CSN3-HPB in the immunoprecipitates (**Figure 27F**). Loss of the CSN3-HPB signal in the after-IP control (lane 3, **Figure 27F**) indicated that nearly all the tagged CSN3 were harvested by the beads. Interestingly, the endogenous CSN3 could no longer be co-purified in the IP (lane 2, **Figure 27F**), suggesting the C-terminal fusion of a ~30kDa HPB tag to the CSN3 abolished the dimerization of CSN3. However, the aforementioned GF result of CSN3-HPB indicates the tagged protein could still form the sCSN3c (**Figure**

26D). Together with the co-IP result, this strongly suggested that the sCSN3c was not a CSN3 dimer.

To summarize, my IP results suggested that both myc-CSN3 and CSN3-HPB could be purified via an affinity purification step. By using the streptavidin beads, I could purify all the CSN3-HPB from the crude extracts, while the myc-IP or CSN3-IP gave a much lower efficiency for protein enrichment. Interestingly, the N-terminal myc fusion didn't affect the CSN3 dimerization, while the C-terminal HPB fusion abolished it. Additionally, the *csn3-3* mutation did not affect the CSN3 -ETA7 hetero-dimerization but greatly reduced the ETA7 homo-dimerization.

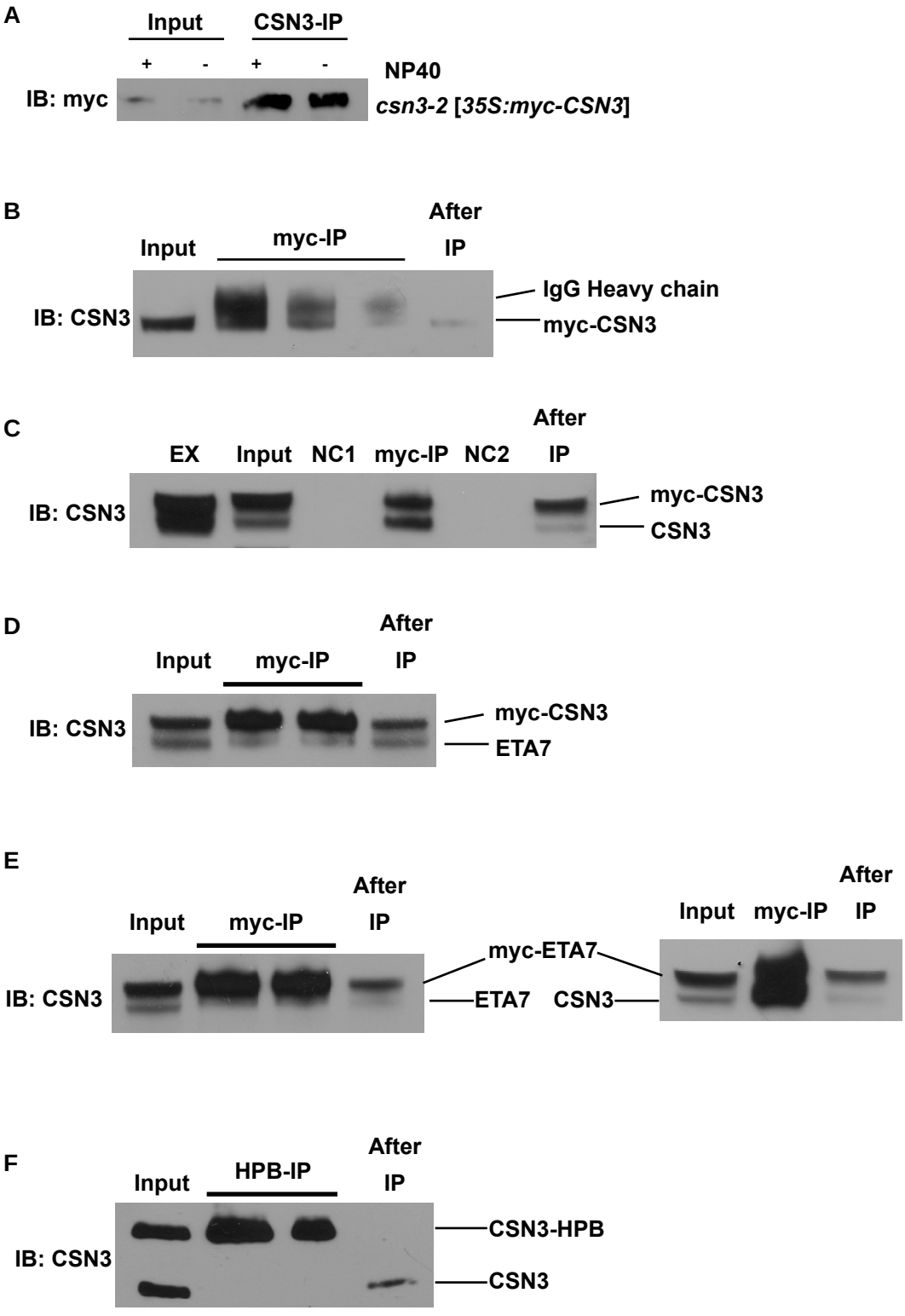
A
Input
CSN3-IP
+
-
+
-
NP40
IB: myc
csn3-2 [35S:myc-CSN3]
B
Input
myc-IP
After IP
IB: CSN3
IgG Heavy chain
myc-CSN3
C
EX
Input
NC1
myc-IP
NC2
After IP
IB: CSN3
myc-CSN3
CSN3
D
Input
myc-IP
After IP
IB: CSN3
myc-CSN3
ETA7
E
Input
myc-IP
After IP
IB: CSN3
myc-ETA7
ETA7
Input
myc-IP
After IP
CSN3
F
Input
HPB-IP
After IP
IB: CSN3
CSN3-HPB
CSN3

Figure 27. Affinity purification of tagged CSN3.

(A) Immunoprecipitation of myc-CSN3 from *csn3-2* [*35S:myc-CSN3*] extracts. Affinity purified CSN3 antibody was added to the extracts to IP myc-CSN3, followed by adding Protein A agarose beads to capture the CSN3 IP complex. The western blotting is done using the myc antibody.

(B~E) myc-IPs using commercial myc-Protein A agarose beads. Extracts were made from plants expressing myc-CSN3 or myc-ETA7 . Immonoblottings (IB) were done using CSN3 antibody.
Seedling (C~E) or leaves (B) protein extracts (2mg) were used for IP. The input and after IP contains 10µl (2%) of the total extracts (500µl). EX indicates 50µg total protein extracts made from *csn3-3* [*35S:myc-CSN3*] seedlings, purpose of which is to indicate the correct size of myc-CSN3/CSN3 bands.

(B) myc-IP using *csn3-2* [*35S:myc-CSN3*] extracts made from leaves of several homozygous plants . The upper band is the heavy chain of IgG.

(C) myc-IP using extracts of *csn3-2* [*35S:myc-CSN3*] heterozygous plants (*csn3-2* segregating). NC1 is a negative control using protein A agarose beads to IP the protein extracts, while NC2 is another negative control using myc-beads to IP the extraction buffer without protein. Notice that the endogenous CSN3 is co-purified with myc-CSN3.

(D) myc-IP was done using *csn3-3* [*35S:myc-CSN3*] extracts. Notice that the endogenous ETA7 is co-purified with myc-CSN3.

(E) Left, myc-IP using *csn3-3* [*35S:myc-ETA7*] extracts. Right, myc-IP using extracts of *csn3-2* [*35S:myc-ETA7*] heterozygous plants (*csn3-2* segregating). Notice that myc-ETA7 heterodimerize with endogenous CSN3 (right) but cannot interact with endogenous ETA7 (left).

(F) Protein extracts for IP were made from leaves of several *csn3-2* [*35S:CSN3-HPB*] T1 plants. Dynabeads® M-280 streptavidin were used to IP CSN3-HPB. Immunobloting was done using the CSN3 antibody.

The overexpression of myc-CSN3 in *csn3-2* cannot restore the wild-type level of auxin sensitivity

The over-expressed myc-CSN3 rescued the *csn3-2* seedling lethal phenotype (data not shown) and migrated into the GF fractions corresponding to the holocomplex and the sCSN3c (**Figure 26A**). However, I am still curious if the tagged proteins are biologically active in the auxin signaling. To answer this question, I tested if the overexpressed myc-CSN3 in *csn3-2* could mimic the wild type-like sensitivity to the auxin induced root growth inhibition. *S*eedlings of *csn3-2 [35S:myc-CSN3]* were used for a root growth assay on 2,4-D plates. While the Col control seedlings were sensitive to 2,4-D, overexpression of myc-CSN3 in *csn3-2* couldn't fully mimic the root growth sensitivity. However, at 0.04μM and 0.05μM 2,4-D treatments, *csn3-2 [35S:myc-CSN3]* (green curve) had a higher value of root growth inhibition than the *csn3-3* control (**Figure 28,** red curve). Compared with previous results that the native promoter driven CSN3 rescued the *csn3-3* mutant root growth phenotype (**Figure 12C**), it is likely that the proper expression pattern of CSN3 is required for the proper auxin response in plants. Ectopic expression of myc-ETA7 also rescued the *csn3-2* seedling lethal phenotype (data not shown). Transgenic plants had a similar root growth curve upon 2,4-D treatments as *csn3-3*, except the 0.04μM 2,4-D data point (**Figure 28**, blue curve).

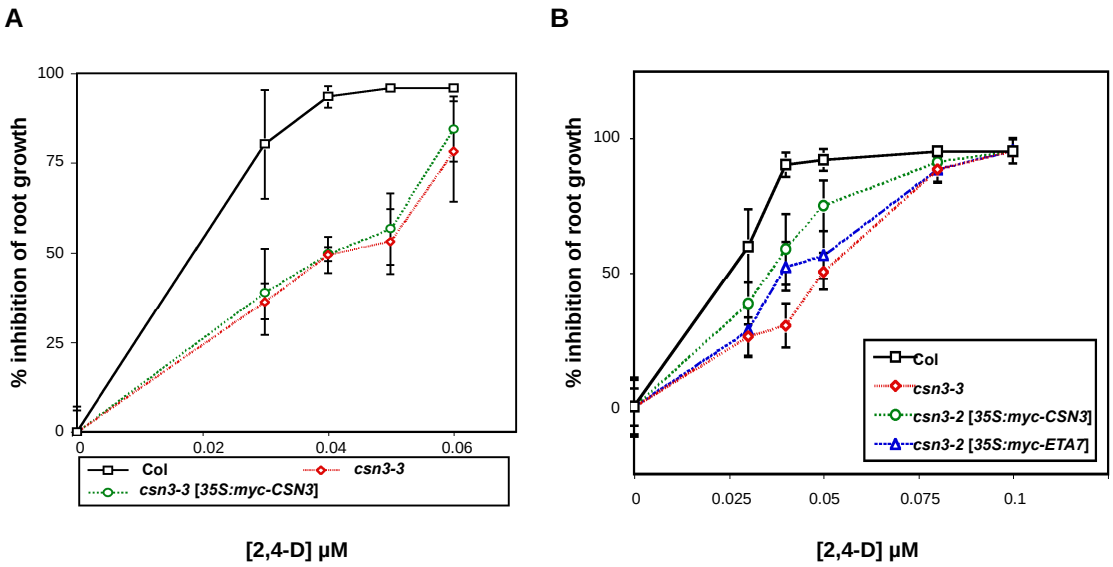

Figure 28. Ectopic expression of myc-CSN3 cannot rescue the root growth phenotype of *csn3-3*.

Root growth assay was done as prior mentioned to test the 2,4-D sensitivity of transgenic plants (seedlings, n≥15). Data are presented as percent inhibition of root growth compared to growth on unsupplemented ATS. Error bars = SD.

(A) 2,4-D induced inhibition on root elongation of Col, *csn3-3* and *csn3-3* [*35S:myc-CSN3*] seedlings.

(B) 2,4-D induced inhibition on root elongation of Col, *csn3-3*, *csn3-2* [*35S:myc-CSN3*] and *csn3-2* [*35S:myc-ETA7*] seedlings.

Scheme of the sCSN3c purification

To combine all data on the sCSN3c purification (IEX, GF and AC), I designed a procedure to purify the sCSN3c (**Figure 29**). The *csn3-2 [35S:CSN3-HPB]* plants will be used for the purification since the HPB tag has a very good IP efficiency. The HiPrep™ 16/10 Q FF (CV=20ml) IEX column will be used in the first capture step to harvest the sCSN3c from seedling or leaves protein extracts. At pH 7, the IEX flow-through fractions containing the sCSN3c will be collected and concentrated to run through the GF column Superdex 200. Then the GF sCSN3c fractions (12 to 14) will be concentrated and incubated with the streptavidin beads for IP. The precipitates will be denatured and saved for future use. For the control group, I am planning to use Col *[35S:GUS-HPB]* plants to run through the same purification steps. Both samples will be separated by a SDS-PAGE and silver stained. Potential candidate bands that are only co purified in the *csn3-2 [35S:CSN3-HPB]* sample will be cut off and trypsin digested for MS/MS analysis (Center for Mass Spectrometry and Proteomics, U of Minnesota).

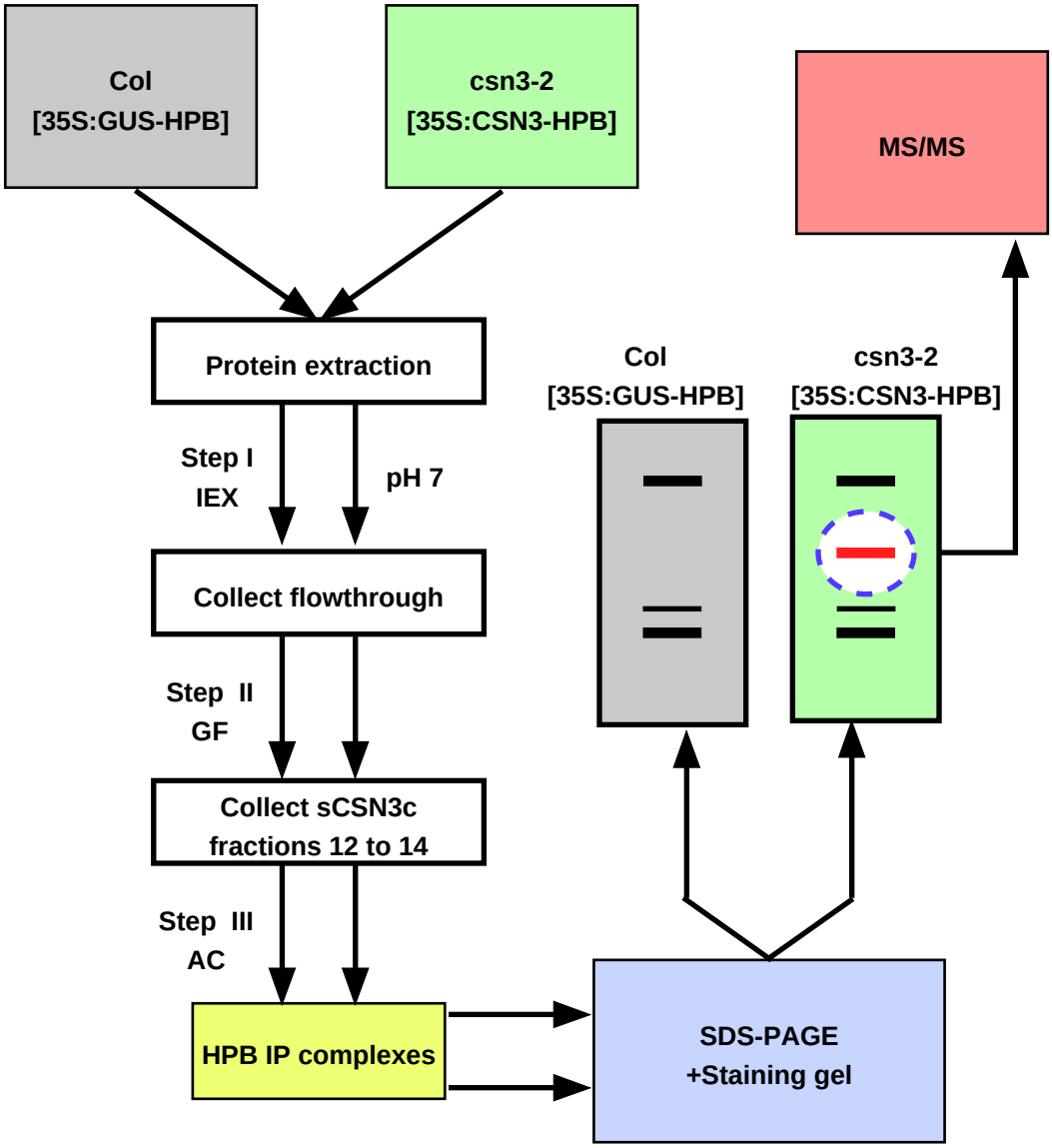

Figure 29. The experimental design for purifying the sCSN3c.

Protein extracts made from *csn3-2* [*35S:CSN3-HPB*] or Col [*35S:GUS-HPB*] plants (seedlings or leaves) will be separated by an anion exchange column at pH 7. The unbound proteins in the IEX flowthrough section will be concentrated and loaded to a GF column. Further separated proteins in GF fractions 12 to 14 are pooled for HPB-IP using the streptavidin beads. The IP complex will be denatured and separated on a gel for staining. Protein bands that specifically appears in the *csn3-2* [*35S:myc-CSN3*] sample (red) will be cleaved and trypsin digested for future MS/MS identification.

Discussion

The predicted size of the sCSN3c

As illustrated in **Figure 18**, proteins eluted into the sCSN3c GF fractions (12 to 14) had the molecular weight ranging from 158kDa (left border of fraction 12) to 79.4kDa (right border of fraction 14) as indicated by the calibration standards and calculation. However, precautions should be considered when using molecular standards for GF. It is not the molecular weight but actually the shape of the protein that determines the GF retention time. If the molecule of interest doesn't have the same shape as the standards, the calculated molecular weight may not be precise. For instance, the CSN5 monomer was eluted into GF fractions 15 to 17, which had a calculated molecular weight of 79.4~40.1kDa according to the marker. However, the calculated molecular weight is bigger than the actual molecular weight of CSN5 (39kDa, TAIR database). Therefore, it is possible that the actual size of the sCSN3c may be less than the value reflected by the molecular marker. If the CSN5 signal detected in GF fractions 15 to 18 represented the CSN5 monomer, as speculated in the previous literature (Kwok et al., 1998), the CSN3 signal detected in fractions 14 to 16 (102~50.7kDa) of the *csn3-3* GF analysis was likely representing the CSN3 monomer (47kDa, TAIR database), while the sCSN3c (GF fractions 12 to 14) probably included CSN3 plus another one or two small proteins.

The sCSN3c contains novel protein/proteins rather than a CSN3 dimer

Yeast two hybrid assays studying the internal-interactions among *Arabidopsis* CSN subunits indicated that CSN3 weakly interacted with itself to form a dimer (Serino

et al., 2003). Consistently, in my IP experiment using plant protein extracts that contain both the tagged (myc-CSN3) and the endogenous CSN3, the endogenous protein could be co-purified by myc-IP (**Figure 27C**), indicating the myc-CSN3 heterodimerized with the native CSN3. In addition, the size of the sCSN3c as indicated by the marker matched the size of a CSN3 dimer. Therefore, it is possible that CSN3 signals found in the sCSN3c GF fractions represent the CSN3-CSN3 dimer, and that the *csn3-3* mutation affects the dimerization, resulting in the accumulation of CSN3 monomer (GF fractions 14 to 16). Consistent to this hypothesis, in the co-IP experiment testing the interaction between myc-ETA7 and endogenous ETA7, I found that the mutation blocked the ETA7 homo-dimerization (**Figure 27E**).

However, the dimer hypothesis may not be true for two reasons. First evidence came from the study of CSN3-HPB. As revealed in **Figure 27F**, the C-terminal fused HPB tag blocked the CSN3 homo-dimerization, as no endogenous CSN3 was co-purified with the CSN3-HPB. Therefore, it is expected that the CSN3-HPB cannot form the sCSN3c, if the sCSN3c is a CSN3 dimer. However, the GF analysis using *csn3-2* [*35S:CSN3-HPB*] T2 plant extracts (**Figure 26D**) clearly showed that the CSN3-HPB was assembled into a small protein complex, the identity of which was most likely the sCSN3c (CSN3-HPB and other proteins within the sCSN3c). Combining both the co-IP and GF results of CSN3-HPB, it is less likely the sCSN3c is a CSN3 dimer.

Second, the isoelectric point (pI) of CSN3 (pI=6.3, TAIR database) suggested that in a neutral equilibration buffer of pH 7, the CSN3 is probably negatively charged and bind an anion exchange column. However, GF fractions containing the sCSN3c did not

bind a strong anion IEX column, with all the CSN3 signal detected in the flow-through fractions at pH 7 (**Figure 12B**). This suggested that other components within the sCSN3c buffered the negative charges of the CSN3 to make the net surface charge of the sCSN3c less negative or even positive. Therefore, it is more likely the sCSN3c contains novel protein/proteins that are probably positively charged at pH 7, rather than another copy of CSN3, which is probably negatively charged at pH 7.

To summarize, my data suggested that CSN3 interacted with a novel protein/proteins that have a different charge property than CSN3 to form the sCSN3c, although the *csn3-3* mutation might affect CSN3 dimerization.

Precautions during the sCSN3c purification

One big challenge for the multi-step purification of a protein complex is to maintain the original composition of the protein complex during each step. The CIPP strategy I am planning to use includes 3 liquid chromatographic steps (IEX, GF and AC) and has the risk of losing the intact sCSN3c. However, my data suggest this won't be a major problem for purifying the sCSN3c for several reasons.

First, the sCSN3c, as reflected by the GF and western detection, seemed relatively stable under my experimental conditions. Similar GF profiles of CSN3 were found in the GF analysis using the cauliflower protein extract (**Figure 20B**), in a scaled GF experiment (**Figure 21**), in GF analyses using IEX eluted proteins (**Figure 24F and 24G**) or using affinity tagged CSN3 proteins (**Figure 26 A, B and D**). The CSN3 signal was readily detected in the sCSN3c GF fractions of all abovementioned cases. Second, all the

buffers used during each step were not dramatically different from each other in case of pH, ionic strength or hydrophobicity (see **Methods** for more details). The buffer exchange step between the IEX and GF didn't reduce the total protein abundance (94% of total proteins remained after running though the PD-10 column for buffer exchange, data not shown), or did it affect the CSN3 GF pattern (**Figure 24F and 24G**). Third, I tried to reduce any unnecessary step that may disrupt the sCSN3c formation. For instance, I removed the 15% PEG precipitation step during the crude extracts preparation, which rendered that all the CSN3 harvested by the IEX was in the holocomplex form (**Figure 24C and 24D**).

However, extra cautions should be considered when using GF to validate the sCSN3c assembly. Since GF is using a size-exclusion column, proteins migrated into the same fraction don't necessarily have the same composition. This could be even worse when using a affinity tagged protein, since adding an extra length of peptide may alter the original properties, such as the surface charge, hydrophobicity, etc., and consequently change the protein complex composition. Therefore I cannot rule out the possibility that the tagged-CSN3 is assembled into another protein complex that has a similar molecular weight as the original sCSN3c. Another issue about the tag is if the sCSN3c containing the tagged CSN3 is still separable from the holocomplex by IEX. Therefore a validation of IEX condition using the tagged protein is needed.

Proteins unspecifically bound to the affinity tag may also cause false positive results. Including a negative control such as overexpressing the tag with a foreign protein (35S:GUS-HPB) (**Figure 29**) may help to rule out proteins copurified with the tag.

However, it still cannot assure that the purified sCSN3c is the original one. Further analyses, such as protein-protein interaction experiments and functional analysis of the CSN3-interacting candidate protein/proteins, are required to confirm that CSN3 interacts with the candidate protein/proteins and functions together in regulating the auxin signaling.

Conclusions

During the last decade, genetic and biochemical studies have revealed the CSN as an important regulator of cullin-RING ubiquitin ligases (CRLs). Although the CSN inactivated CRLs *in vitro* (Yang et al., 2002; Zhou et al., 2003), it was required for the optimal CRL activity *in vivo* (Schwechheimer et al., 2001; Stuttmann et al., 2009). This paradox can be resolved by several explanations. First, the CSN deneddylation activity contributes to the cycling of SCF assembly/disassembly, since the CAND1 protein interacted only with deneddylated CUL1 and promoted the disassembly of an SCF complex (Schmidt et al., 2009). Second, the neddylation/deneddylation status of cullins also affects their stability, with the deneddylated isoforms being more stabile (Wu et al., 2005). Third, studies from fission yeast and human cells indicated that the CSN-associated deubiquitination enzyme Ubp12 protected the substrate adaptors Btb3 and a certain subset of FBPs from autoubiquitination (Zhou et al., 2003; Hetfeld et al., 2005). Therefore, the CSN regulates CRLs through deneddylation and its associated proteins, probably by toggling the CRL assembly/disassembly and protecting the components within a CRL.

Although the CSN may provide a platform for its associated proteins to regulate CRL activity, such as the aforementioned deubiquitination enzyme Ubp12 (Zhou et al., 2003) or a kinase (Uhle et al., 2003), so far the only known biochemical function of the CSN itself is deneddylation (Lyapina et al., 2001). In Arabidopsis, all of the prior reported *csn* mutants were found to exhibit diminished deneddylation activity, resulting

in the accumulation of neddylated CUL1 and delaying the SCF mediated proteolysis of substrates (Peng et al., 2001b; Schwechheimer et al., 2001; Gusmaroli et al., 2007; Dohmann et al., 2008a; Zhang et al., 2008; Stuttmann et al., 2009). Specifically, in auxin signaling, the CSN interacted with $SCF^{TIR1/AFB}$, deneddylated CUL1 and regulated the SCF-mediated degradation of Aux/IAA (Schwechheimer et al., 2001).

However, the dissertation work presented here described an atypical *csn* mutant, *csn3-3*, which conferred quantitatively similar auxin response defects as *csn1-10*, without disturbing the CSN5 recruitment by the CSN holocomplex, the CUL1 neddylation/deneddylation status, or the $SCF^{TIR1/AFB}$-regulated Aux/IAA degradation (**Figure 15 and 17**). My results on *csn3-3* characterizations raised the question of if CSN3 or the CSN holocomplex had novel functions independent of $SCF^{TIR1/AFB}$ in regulating plant auxin responses. Interestingly, the missense mutation affected the assembly of a previously undescribed small CSN3-containing protein complex (sCSN3c). Restoration of the sCSN3c assembly in a complementation line of *csn3-3* rescued the auxin response defects in the mutant. Therefore, I hypothesize that a defective sCSN3c may be the basis of the auxin signaling defects displayed by *csn3-3* mutant plants

csn3-3 defines a novel function of CSN3 in regulating auxin signaling and provides a useful genetic tool

In my dissertation, I applied a series of physiological, biochemical and genetic analyses to identify the defects caused by *csn3-3*, in comparison with a typical *csn* mutant, *csn1-10*. Results on *csn1-10* perfectly fit in with the existing model of auxin

signaling. The mutation decreased the CSN1 protein production, impaired the CSN5 assembly into the CSN holocomplex and consequently resulted in the decreased CUL1 deneddylation, reduced $SCF^{TIR1/AFB}$ activity and defective auxin responses. However, the *csn3-3* mutation did not result in any defects in the CSN holocomplex assembly, deneddylation, or the SCF-mediated proteolysis, but caused quantitatively similar auxin response defects as *csn-10* did. Additional findings that further distinguished *csn3-3* from *csn1-10* came from genetic interaction studies, in which *csn1-10* and *csn3-3* differently interacted with other auxin mutants (*axr1*, *eta1/axr6-3*, *eta2-1/cand1* or *ibr5*). Our results suggested that there might be an SCF-independent pathway that was specifically affected by the *csn3-3* mutation (**Figure 19**).

Studies in fission yeast and Drosophila mutant of individual CSN subunits raised the possibility of subunit functional specialization (Mundt et al., 2002; Oron et al., 2002; Harari-Steinberg et al., 2007; Oron et al., 2007). However, null mutations in any of the eight Arabidopsis CSN subunits conferred identical seedling-lethal phenotypes (Gusmaroli et al., 2007), which probably masked the additional functions of individual CSN individual subunits or CSN subcomplexes in later stages of the plant life cycle. Our *csn3-3* is one of a few viable *csn* mutant reported so far, which can proceed to the mature stage without any severe growth defects. Therefore, *csn3-3* provides a useful genetic tool for better understanding CSN3 or the holocomplex functions in the entire life cycle of Arabidopsis.

A small CSN3-containing protein complex (sCSN3c) is reported for the first time.

In my dissertation, I have reported a previously undescribed ~ 130 kD small CSN3-containing complex (sCSN3c), the assembly of which was affected by the *csn3-3* mutation. Although in a previous study Gusmaroli et al. also found that CSN3 was eluted into a smaller complex of 130 kDa by applying gel-filtration (GF) analyses on the *csn5a-1 csn5b-1* or *csn6a-1 csn6b-1* extracts, the authors proposed that it was either a CSN1-CSN3, or CSN3-CSN4 subcomplex (Gusmaroli et al., 2007). However, the dissertation presented here, together with previous studies on the CSN subcomplex formation suggest that the sCSN3c contains novel protein/proteins, which are supported by several facts.

First, based on my GF data, the sCSN3c did not appear to contain other CSN subunits (CSN1, CSN4, CSN5 and CSN8), suggesting it is less likely the sCSN3c is a CSN subcomplex. Additionally, the yeast two hybrid data on protein-protein interactions among the eight CSN subunits (Serino et al., 2003) and studies on the CSN subcomplex formation using a mass spectrometry approach (Sharon et al., 2009) also suggested that CSN3 does not interact with CSN7. However, I cannot rule out the possibility that CSN2 or CSN6 interact with CSN3 to form the sCSN3c. Second, efforts to purify the sCSN3c also suggest that the small complex is not a CSN3 dimer: a C-terminal HPB tagged CSN3 that lost the dimerization capability was still assembled into the sCSN3c. Additionally, the sCSN3c couldn't bind a strong anion exchange column at pH 7, suggesting CSN3 might recruit a novel protein that was more positively charged at neutral pH to form the sCSN3c. Lastly, my GF analyses also argued against the possibility that the sCSN3c is a breakdown product during the preparation.

Most interestingly, my results also suggest that the loss of sCSN3c correlates with the auxin defects in *csn3-3*. In *csn3-3* GF profile, CSN3 was no longer present in the sCSN3c fractions, but in fractions that correspond to the CSN3 monomer, while expression of a P_{CSN3}*:CSN3* transgene in *csn3-3* rescued both the assembly of sCSN3c and the auxin response defects. These findings raise the possibility that a defective sCSN3c may be the basis of the auxin signaling defects in *csn3-3* (**Figure 19**). One possible role of the sCSN3c in regulating the auxin signaling may be the direct regulation on downstream auxin responsive genes. Indeed, studies in animal systems suggested CSN might have a role in transcriptional regulation (Tsuge et al., 2001; Groisman et al., 2003; Ullah et al., 2007)

Development of a method to purify the sCSN3c from the holocomplex

The CSN holocomplex was originally purified from the cauliflower protein extracts by combining several steps of Ion Exchange Chromatography (IEX), one step of Heparin Affinity purification and one polishing step using gel-filtration (Chamovitz et al., 1996). Published in 2005, Menon et al. also developed a method to purify the Arabidopsis CSN holocomplex from transgenic plants expressing epitope-tagged CSN subunits (CSN3-TAPa and Flag-CSN1) using a tandem affinity purification strategy or a one-step affinity purification strategy (Menon et al., 2005). However, the similar strategy may not apply to the purification of sCSN3c. As revealed by my GF data, the majority of CSN3 were assembled into the CSN holocomplex, while only a small portion of CSN3 (~10%) was in the sCSN3c form. Therefore, the low abundance of the sCSN3c makes it

difficult to purify the complex by directly applying affinity purification of CSN3. A method that can separate the sCSN3c from the holocomplex must be developed first to isolate/enrich the small complex.

In my dissertation, I have developed an IEX purification step that could successfully isolate sCSN3c from the holocomplex. The sCSN3c is less negatively charged at neutral pH than the holocomplex. By applying a strong anion exchange column at pH 7, sCSN3c barely bound the column and could be separated from the CSN holocomplex that firmly bound the column matrix. Additionally, my preliminary data on the affinity purification of sCSN3c using epitope-tagged CSN3 protein showed that the affinity tag didn't prevent CSN3 from forming either the CSN holocomplex or the sCSN3c and that the tagged CSN3 rescued the seedling lethal phenotype of the *csn3-2* null mutants. In summary, my preliminary data have provided useful information on the purification of the sCSN3c from crude protein extracts.

Future Perspectives

Although CSN is involved in a plethora of biological processes, so far the only known biochemical function of CSN is the NEDD8/RUB isopeptidase activity (deneddylation) (Bosu and Kipreos, 2008). However, my dissertation suggests that the deneddylation may not be the only function of CSN, as revealed by the characterization of a viable mutant *csn3-3* in auxin signaling. My data strongly suggest that CSN3 interacts with another unknown protein/proteins to form a small protein complex, which may bypass the $SCF^{TIR1/AFB}$ to regulate plant auxin responses. To validate this hypothesis,

future efforts should be placed on the identification and functional analyses of the CSN3-interacting protein/proteins within the sCSN3c.

Based on my data, the sCSN3c is not likely a CSN subcomplex and may function separately from the holocomplex (deneddylation) in auxin signaling. This raises a new question of whether CSN3, as well as other CSN subunits in Arabidopsis, have specific functions. Studies on *csn* mutants in fission yeast and Drosophila suggested the individual CSN functional specificity (Mundt et al., 2002; Oron et al., 2002; Harari-Steinberg et al., 2007; Oron et al., 2007). However, no such results were found in plants, possibly due to the seedling lethal phenotype of all *csn* null mutants. Studies on viable *csn* mutants, such as *csn3-3*, may help to address this question, assuming each CSN subunit have additional functions in later stages of plant development.

Additionally, it remains unclear if the sCSN3c functions specifically in auxin signaling or provides a more global regulation on many different pathways. The *csn3-3* mutation did not cause obvious phenotypes indicative of defects in other pathways. However, more detailed observation must be done to rule out subtle defects of *csn3-3*. Again, the identification of novel components within the sCSN3c may also shed some light on answering this question.

Lastly, since the residue affected by the *csn3-3* missense mutation is extremely highly conserved across eukaryotes, it seems likely that sCSN3c function may be similarly conserved. Therefore, my studies may also shed some light on the CSN functional studies among species.

Bibliography

Abel, S., and Theologis, A. (1996). Early Genes and Auxin Action. PLANT PHYSIOLOGY 111, 9.

Amerik, A.Y., Swaminathan, S., Krantz, B.A., Wilkinson, K.D., and Hochstrasser, M. (1997). In vivo disassembly of free polyubiquitin chains by yeast Ubp14 modulates rates of protein degradation by the proteasome. Embo Journal 16, 4826-4838.

Bennett, E.J., Rush, J., Gygi, S.P., and Harper, J.W. (2010). Dynamics of Cullin-RING Ubiquitin Ligase Network Revealed by Systematic Quantitative Proteomics. Cell 143, 951-965.

Biswas, K.K., Ooura, C., Higuchi, K., Miyazaki, Y., Van Nguyen, V., Rahman, A., Uchimiya, H., Kiyosue, T., Koshiba, T., Tanaka, A., Narumi, I., and Oono, Y. (2007). Genetic characterization of mutants resistant to the antiauxin p-chlorophenoxyisobutyric acid reveals that AAR3, a gene encoding a DCN1-like protein, regulates responses to the synthetic auxin 2,4-dichlorophenoxyacetic acid in Arabidopsis roots. Plant Physiology 145, 773-785.

Bornstein, G., Ganoth, D., and Hershko, A. (2006). Regulation of neddylation and deneddylation of cullin1 in SCFSkp2 ubiquitin ligase by F-box protein and substrate. Proceedings Of The National Academy Of Sciences Of The United States Of America 103, 11515-11520.

Bosu, D.R., and Kipreos, E.T. (2008). Cullin-RING ubiquitin ligases: global regulation and activation cycles. Cell Division 3.

Calderon Villalobos, L.I.A., Lee, S., De Oliveira, C., Ivetac, A., Brandt, W., Armitage, L., Sheard, L.B., Tan, X., Parry, G., Mao, H., Zheng, N., Napier, R., Kepinski, S., and Estelle, M. (2012). A combinatorial TIR1/AFB-Aux/IAA co-receptor system for differential sensing of auxin. Nature Chemical Biology 8, 477-485.

Callis, J., Carpenter, T., Sun, C.W., and Vierstra, R.D. (1995). Structure And Evolution Of Genes Encoding Polyubiquitin And Ubiquitin-Like Proteins In Arabidopsis-Thaliana Ecotype Columbia. Genetics 139, 921-939.

Chamovitz, D.A., Wei, N., Osterlund, M.T., von Arnim, A.G., Staub, J.M., Matsui, M., and Deng, X.W. (1996). The COP9 complex, a novel multisubunit nuclear regulator involved in light control of a plant developmental switch. Cell 86, 115.

Chen, H., Shen, Y., Tang, X., Yu, L., Wang, J., Guo, L., Zhang, Y., Zhang, H., Feng, S., Strickland, E., Zheng, N., and Deng, X.W. (2006). Arabidopsis CULLIN4 forms an E3 ubiquitin ligase with RBX1 and the CDD complex in mediating light control of development. Plant Cell 18, 1991-2004.

Chew, E.-H., Poobalasingam, T., Hawkey, C.J., and Hagen, T. (2007). Characterization of cullin-based E3 ubiquitin ligases in intact mammalian cells - Evidence for cullin dimerization. Cellular Signalling 19, 1071-1080.

Chini, A., Fonseca, S., Fernandez, G., Adie, B., Chico, J.M., Lorenzo, O., Garcia-Casado, G., Lopez-Vidriero, I., Lozano, F.M., Ponce, M.R., Micol, J.L., and Solano, R. (2007). The JAZ family of repressors is the missing link in jasmonate signalling. Nature 448, 666-U664.

Chuang, H.W., Zhang, W., and Gray, W.M. (2004). Arabidopsis ETA2, an apparent ortholog of the human cullin-interacting protein CAND1, is required for auxin responses mediated by the SCF(TIR1) ubiquitin ligase. The Plant Cell 16, 1883.

Clough, S.J., and Bent, A.F. (1998). Floral dip: a simplified method for Agrobacterium-mediated transformation of Arabidopsis thaliana. Plant Journal 16, 735-743.

Cope, G., Suh, G.B., Aravind, L., Schwarz, S., Zipursky, S.L., Koonin, E., and Deshaies, R. (2002). Role of Predicted Metalloprotease Motif of Jab1/Csn5 in Cleavage of Nedd8 from Cul1. Science 298, 608.

Cope, G.A., and Deshaies, R.J. (2003). COP9 Signalosome: A Multifunctional Regulator of SCF and Other Cullin-Based Ubiquitin Ligases. Cell 114, 663.

Cope, G.A., and Deshaies, R.J. (2006). Targeted silencing of Jab1/Csn5 in human cells downregulates SCF activity through reduction of F-box protein levels. BMC biochemistry 7, 1.

Cyr, D.M., Hohfeld, J., and Patterson, C. (2002). Protein quality control: U-box-containing E3 ubiquitin ligases join the fold. Trends In Biochemical Sciences 27, 368-375.

del Pozo, J.C., and Estelle, M. (1999). The Arabidopsis cullin AtCUL1 is modified by the ubiquitin-related protein RUB1. Proceedings of the National Academy of Sciences of the United States of America 96, 15342.

del Pozo, J.C., Timpte, C., Tan, S., Callis, J., and Estelle, M. (1998). The ubiquitin-related protein RUB1 and auxin response in Arabidopsis. Science 280, 1760-1763.

del Pozo, J.C., Dharmasiri, S., Hellmann, H., Walker, L., Gray, W.M., and Estelle, M. (2002). AXR1-ECR1-dependent conjugation of RUB1 to the Arabidopsis cullin AtCUL1 is required for auxin response. Plant Cell 14, 421-433.

Deshaies, R.J. (1999). SCF and cullin/RING H2-based ubiquitin ligases. Annual Review Of Cell And Developmental Biology 15, 435-467.

Dessau, M., Halimi, Y., Erez, T., Chomsky-Hecht, O., Chamovitz, D.A., and Hirsch, J.A. (2008). The Arabidopsis COP9 signalosome subunit 7 is a model PCI domain protein with subdomains involved in COP9 signalosome assembly. The Plant Cell 20, 2815.

Dharmasiri, N., Dharmasiri, S., and Estelle, M. (2005a). The F-box protein TIR1 is an auxin receptor. Nature 435, 441.

Dharmasiri, N., Dharmasiri, S., Weijers, D., Karunarathna, N., Jurgens, G., and Estelle, M. (2007). AXL and AXR1 have redundant functions in RUB

conjugation and growth and development in Arabidopsis. The Plant Journal: for cell and molecular biology 52, 114.

Dharmasiri, N., Dharmasiri, S., Weijers, D., Lechner, E., Yamada, M., Hobbie, L., Ehrismann, J.S., Jurgens, G., and Estelle, M. (2005b). Plant development is regulated by a family of auxin receptor F box proteins. Developmental Cell 9, 109-119.

Dharmasiri, S., Dharmasiri, N., Hellmann, H., and Estelle, M. (2003). The RUB/Nedd8 conjugation pathway is required for early development in Arabidopsis. Embo Journal 22, 1762-1770.

Dill, A., Thomas, S.G., Hu, J.H., Steber, C.M., and Sun, T.P. (2004). The Arabidopsis F-box protein SLEEPY1 targets gibberellin signaling repressors for gibberellin-induced degradation. Plant Cell 16, 1392-1405.

Doelling, J.H., Yan, N., Kurepa, J., Walker, J., and Vierstra, R.D. (2001). The ubiquitin-specific protease UBP14 is essential for early embryo development in Arabidopsis thaliana. Plant Journal 27, 393-405.

Dohmann, E.M., Kuhnle, C., and Schwechheimer, C. (2005). Loss of the CONSTITUTIVE PHOTOMORPHOGENIC9 signalosome subunit 5 is sufficient to cause the cop/det/fus mutant phenotype in Arabidopsis. The Plant Cell 17, 1967.

Dohmann, E.M., Levesque, M.P., Isono, E., Schmid, M., and Schwechheimer, C. (2008a). Auxin responses in mutants of the Arabidopsis CONSTITUTIVE PHOTOMORPHOGENIC9 signalosome. Plant Physiology 147, 1369.

Dohmann, E.M.N., Nill, C., and Schwechheimer, C. (2010). DELLA proteins restrain germination and elongation growth in Arabidopsis thaliana COP9 signalosome mutants. European Journal Of Cell Biology 89, 163-168.

Dohmann, E.M.N., Levesque, M.P., De Veylder, L., Reichardt, I., Juergens, G., Schmid, M., and Schwechheimer, C. (2008b). The Arabidopsis COP9 signalosome is essential for G2 phase progression and genomic stability. Development 135, 2013-2022.

Doronkin, S., Djagaeva, I., and Beckendorf, S.K. (2003). The COP9 signalosome promotes degradation of Cyclin E during early Drosophila oogenesis. Developmental Cell 4, 699-710.

Duda, D.M., Borg, L.A., Scott, D.C., Hunt, H.W., Hammel, M., and Schulman, B.A. (2008). Structural insights into NEDD8 activation of Cullin-RING ligases: Conformational control of conjugation. Cell 134, 995-1006.

Earley, K.W., Haag, J.R., Pontes, O., Opper, K., Juehne, T., Song, K.M., and Pikaard, C.S. (2006). Gateway-compatible vectors for plant functional genomics and proteomics. Plant Journal 45, 616-629.

Enchev, R.I., Schreiber, A., Beuron, F., and Morris, E.P. (2010). Structural Insights into the COP9 Signalosome and Its Common Architecture with the 26S Proteasome Lid and eIF3. Structure 18, 518-527.

Farras, R., Ferrando, A., Jasik, J., Kleinow, T., Okresz, L., Tiburcio, A., Salchert, K., del Pozo, C., Schell, J., and Koncz, C. (2001). SKP1-SnRK protein kinase

interactions mediate proteasomal binding of a plant SCF ubiquitin ligase. Embo Journal 20, 2742-2756.

Feng, S., Ma, L., Wang, X., Xie, D., Dinesh-Kumar, S.P., Wei, N., and Deng, X. (2003). The COP9 Signalosome Interacts Physically with SCFCOI1 and Modulates Jasmonate Responses. THE PLANT CELL 15, 1083.

Feng, S.H., Shen, Y.P., Sullivan, J.A., Rubio, V., Xiong, Y., Sun, T.P., and Deng, X.W. (2004). Arabidopsis CAND1, an unmodified CUL1-interacting protein, is involved in multiple developmental pathways controlled by ubiquitin/proteasome-mediated protein degradation. Plant Cell 16, 1870-1882.

Fischer, E.S., Scrima, A., Bohm, K., Matsumoto, S., Lingaraju, G.M., Faty, M., Yasuda, T., Cavadini, S., Wakasugi, M., Hanaoka, F., Iwai, S., Gut, H., Sugasawa, K., and Thoma, N.H. (2011). The Molecular Basis of CRL4(DDB2/CSA) Ubiquitin Ligase Architecture, Targeting, and Activation. Cell 147, 1024-1039.

Gagne, J.M., Downes, B.P., Shiu, S.H., Durski, A.M., and Vierstra, R.D. (2002). The F-box subunit of the SCF E3 complex is encoded by a diverse superfamily of genes in Arabidopsis. Proceedings Of The National Academy Of Sciences Of The United States Of America 99, 11519-11524.

Galan, J.M., and Peter, M. (1999). Ubiquitin-dependent degradation of multiple F-box proteins by an autocatalytic mechanism. Proceedings Of The National Academy Of Sciences Of The United States Of America 96, 9124-9129.

Geyer, R., Wee, S., Anderson, S., Yates, J., and Wolf, D.A. (2003). BTB/POZ domain proteins are putative substrate adaptors for cullin 3 ubiquitin ligases. Molecular Cell 12, 783-790.

Glickman, M.H., Rubin, D.M., Coux, O., Wefes, I., Pfeifer, G., Cjeka, Z., Baumeister, W., Fried, V.A., and Finley, D. (1998). A subcomplex of the proteasome regulatory particle required for ubiquitin-conjugate degradation and related to the COP9-signalosome and eIF3. Cell 94, 615-623.

Goldenberg, S.J., Cascio, T.C., Shumway, S.D., Garbutt, K.C., Liu, J.D., Xiong, Y., and Zheng, N. (2004). Structure of the Cand1-Cul1-Roc1 complex reveals regulatory mechanisms for the assembly of the multisubunit cullin-dependent ubiquitin ligases. Cell 119, 517-528.

Gong, L.M., and Yeh, E.T.H. (1999). Identification of the activating and conjugating enzymes of the NEDD8 conjugation pathway. Journal Of Biological Chemistry 274, 12036-12042.

Gray, W.M., Hellmann, H., Dharmasiri, S., and Estelle, M. (2002). Role of the Arabidopsis RING-H2 protein RBX1 in RUB modification and SCF function. Plant Cell 14, 2137-2144.

Gray, W.M., Muskett, P.R., Chuang, H.W., and Parker, J.E. (2003). Arabidopsis SGT1b is required for SCF(TIR1)-mediated auxin response. The Plant Cell 15, 1310.

Gray, W.M., Ostin, A., Sandberg, G., Romano, C.P., and Estelle, M. (1998). High temperature promotes auxin-mediated hypocotyl elongation in Arabidopsis.

Proceedings of the National Academy of Sciences of the United States of America 95, 7197.

Gray, W.M., Kepinski, S., Rouse, D., Leyser, O., and Estelle, M. (2001). Auxin regulates SCF(TIR1)-dependent degradation of AUX/IAA proteins. Nature 414, 271.

Gray, W.M., del Pozo, J.C., Walker, L., Hobbie, L., Risseeuw, E., Banks, T., Crosby, W.L., Yang, M., Ma, H., and Estelle, M. (1999). Identification of an SCF ubiquitin-ligase complex required for auxin response in Arabidopsis thaliana. Genes & development 13, 1678.

Greenham, K., Santner, A., Castillejo, C., Mooney, S., Sairanen, I., Ljung, K., and Estelle, M. (2011). The AFB4 Auxin Receptor Is a Negative Regulator of Auxin Signaling in Seedlings. Current Biology 21, 520-525.

Groisman, R., Polanowska, J., Kuraoka, I., Sawada, J., Saijo, M., Drapkin, R., Kisselev, A.F., Tanaka, K., and Nakatani, Y. (2003). The ubiquitin ligase activity in the DDB2 and CSA complexes is differentially regulated by the COP9 signalosome in response to DNA damage. Cell 113, 357-367.

Guilfoyle, T.J., and Hagen, G. (2007). Auxin response factors. Current Opinion In Plant Biology 10, 453-460.

Gusmaroli, G., Feng, S., and Deng, X.W. (2004). The Arabidopsis CSN5A and CSN5B subunits are present in distinct COP9 signalosome complexes, and mutations in their JAMM domains exhibit differential dominant negative effects on development. The Plant Cell 16, 2984.

Gusmaroli, G., Figueroa, P., Serino, G., and Deng, X.W. (2007). Role of the MPN subunits in COP9 signalosome assembly and activity, and their regulatory interaction with Arabidopsis Cullin3-based E3 ligases. The Plant Cell 19, 564.

Hakenjos, J.P., Richter, R., Dohmann, E.M.N., Katsiarimpa, A., Isono, E., and Schwechheimer, C. (2011). MLN4924 Is an Efficient Inhibitor of NEDD8 Conjugation in Plants. Plant Physiology 156, 527-536.

Haracska, L., Torres-Ramos, C.A., Johnson, R.E., Prakash, S., and Prakash, L. (2004). Opposing effects of ubiquitin conjugation and SUMO modification of PCNA on replicational bypass of DNA lesions in Saccharomyces cerevisiae. Mol. Cell. Biol. 24, 4267-4274.

Harari-Steinberg, O., Cantera, R., Denti, S., Bianchi, E., Oron, E., Segal, D., and Chamovitz, D.A. (2007). COP9 signalosome subunit 5 (CSN5/Jab1) regulates the development of the Drosophila immune system: effects on Cactus, Dorsal and hematopoiesis. Genes To Cells 12, 183-195.

Hardtke, C.S., and Berleth, T. (1998). The Arabidopsis gene MONOPTEROS encodes a transcription factor mediating embryo axis formation and vascular development. Embo Journal 17, 1405-1411.

Hardtke, C.S., Ckurshumova, W., Vidaurre, D.P., Singh, S.A., Stamatiou, G., Tiwari, S.B., Hagen, G., Guilfoyle, T.J., and Berleth, T. (2004). Overlapping and non-redundant functions of the Arabidopsis auxin response factors

MONOPTEROS and NONPHOTOTROPIC HYPOCOTYL 4. Development 131, 1089-1100.

He, Q., Cheng, P., He, Q.Y., and Liu, Y. (2005). The COP9 signalosome regulates the Neurospora circadian clock by controlling the stability of the SCFFWD-1 complex. Genes & Development 19, 1518-1531.

Hellmann, H., Hobbie, L., Chapman, A., Dharmasiri, S., Dharmasiri, N., del Pozo, C., Reinhardt, D., and Estelle, M. (2003). Arabidopsis AXR6 encodes CUL1 implicating SCF E3 ligases in auxin regulation of embryogenesis. The EMBO journal 22, 3314.

Hershko, A., and Ciechanover, A. (1998). The ubiquitin system. Annual Review Of Biochemistry 67, 425-479.

Hetfeld, B.K.J., Helfrich, A., Kapelarl, B., Scheel, H., Hofmann, K., Guterman, A., Glickman, M., Schade, R., Kloetzel, P.M., and Dubiel, W. (2005). The zinc finger of the CSN-associated deubiquitinating enzyme USP15 is essential to rescue the E3 ligase Rbx1. Current Biology 15, 1217-1221.

Hobbie, L., McGovern, M., Hurwitz, L.R., Pierro, A., Liu, N.Y., Bandyopadhyay, A., and Estelle, M. (2000). The axr6 mutants of Arabidopsis thaliana define a gene involved in auxin response and early development. Development 127, 23-32.

Hoege, C., Pfander, B., Moldovan, G.L., Pyrowolakis, G., and Jentsch, S. (2002). RAD6-dependent DNA repair is linked to modification of PCNA by ubiquitin and SUMO. Nature 419, 135-141.

Imaizumi, T., Schultz, T.F., Harmon, F.G., Ho, L.A., and Kay, S.A. (2005). FKF1F-BOX protein mediates cyclic degradation of a repressor of CONSTANS in Arabidopsis. Science 309, 293-297.

Ito, H., and Gray, W.M. (2006). A gain-of-function mutation in the Arabidopsis pleiotropic drug resistance transporter PDR9 confers resistance to auxinic herbicides. Plant Physiology 142, 63.

Joazeiro, C.A.P., Wing, S.S., Huang, H.K., Leverson, J.D., Hunter, T., and Liu, Y.C. (1999). The tyrosine kinase negative regulator c-Cbl as a RING-type, E2-dependent ubiquitin-protein ligase. Science 286, 309-312.

Kelley, L.A., and Sternberg, M.J. (2009). Protein structure prediction on the Web: a case study using the Phyre server. Nature protocols 4, 363.

Kepinski, S., and Leyser, O. (2005). The Arabidopsis F-box protein TIR1 is an auxin receptor. Nature 435, 446.

Kim, J., Harter, K., and Theologis, A. (1997). Protein-protein interactions among the Aux/IAA proteins. Proceedings Of The National Academy Of Sciences Of The United States Of America 94, 11786-11791.

Kim, T.H., Hofmann, K., von Arnim, A.G., and Chamovitz, D.A. (2001). PCI complexes: pretty complex interactions in diverse signaling pathways. Trends In Plant Science 6, 379-386.

Komander, D., Clague, M.J., and Urbe, S. (2009). Breaking the chains: structure and function of the deubiquitinases. Nature Reviews Molecular Cell Biology 10, 550-563.

Kurz, T., Chou, Y.-C., WillemS, A.R., Meyer-Schaller, N., Hecht, M.-L., Tyers, M., Peter, M., and Sicheri, F. (2008). Dcn1 functions as a scaffold-type E3 ligase for cullin neddylation. Molecular Cell 29, 23-35.

Kurz, T., Ozlu, N., Rudolf, F., O'Rourke, S.M., Luke, B., Hofmann, K., Hyman, A.A., Bowerman, B., and Peter, M. (2005). The conserved protein DCN-1/Dcn1p is required for cullin neddylation in C-elegans and S-cerevisiae. Nature 435, 1257-1261.

Kwok, S.F., Solano, R., Tsuge, T., Chamovitz, D.A., Ecker, J.R., Matsui, M., and Deng, X.W. (1998). Arabidopsis homologs of a c-Jun coactivator are present both in monomeric form and in the COP9 complex, and their abundance is differentially affected by the pleiotropic cop/det/fus mutations. Plant Cell 10, 1779-1790.

Lam, Y.A., Xu, W., DeMartino, G.N., and Cohen, R.E. (1997). Editing of ubiquitin conjugates by an isopeptidase in the 26S proteasome. Nature 385, 737-740.

Lechner, E., Achard, P., Vansiri, A., Potuschak, T., and Genschik, P. (2006). F-box proteins everywhere. Current Opinion In Plant Biology 9, 631-638.

Lechner, E., Xie, D.X., Grava, S., Pigaglio, E., Planchais, S., Murray, J.A.H., Parmentier, Y., Mutterer, J., Dubreucq, B., Shen, W.H., and Genschik, P. (2002). The AtRbx1 protein is part of plant SCF complexes, and its down-regulation causes severe growth and developmental defects. Journal Of Biological Chemistry 277, 50069-50080.

Leitner, J., Petrasek, J., Tomanov, K., Retzer, K., Parezova, M., Korbei, B., Bachmair, A., Zazimalova, E., and Luschnig, C. Lysine63-linked ubiquitylation of PIN2 auxin carrier protein governs hormonally controlled adaptation of Arabidopsis root growth. Proceedings of the National Academy of Sciences of the United States of America 109, 8322-8327.

Li, H., Hagen, G., and Guilfoyle, T.J. (2011a). Do some IAA proteins have two repression domains? Plant signaling & behavior 6, 858-860.

Li, H.B., Tiwari, S.B., Hagen, G., and Guilfoyle, T.J. (2011b). Identical Amino Acid Substitutions in the Repression Domain of Auxin/Indole-3-Acetic Acid Proteins Have Contrasting Effects on Auxin Signaling. Plant Physiology 155, 1252-1263.

Liakopoulos, D., Doenges, G., Matuschewski, K., and Jentsch, S. (1998). A novel protein modification pathway related to the ubiquitin system. Embo Journal 17, 2208-2214.

Lincoln, C., Britton, J.H., and Estelle, M. (1990). Growth and Development of the axr1 Mutants of Arabidopsis. THE PLANT CELL 2, 1071.

Liu, F.Q., Ni, W.M., Griffith, M.E., Huang, Z.Y., Chang, C.Q., Peng, W., Ma, H., and Xie, D.X. (2004). The ASK1 and ASK2 genes are essential for Arabidopsis early development. Plant Cell 16, 5-20.

Liu, J.D., Furukawa, M., Matsumoto, T., and Xiong, Y. (2002). NEDD8 modification of CUL1 dissociates p120(CAND1), an inhibitor of CULl-SKP1 binding and SCIF ligases. Molecular Cell 10, 1511-1518.

Lo, S.C., and Hannink, M. (2006). CAND1-mediated substrate adaptor recycling is required for efficient repression of Nrf2 by Keap1. Mol. Cell. Biol. 26, 1235-1244.

Lur, H.S., and Setter, T.L. (1993). Role of Auxin in Maize Endosperm Development (Timing of Nuclear DNA Endoreduplication, Zein Expression, and Cytokinin). Plant Physiology 103, 273.

Lyapina, S., Cope, G., Shevchenko, A., Serino, G., Tsuge, T., Zhou, C., Wolf, D., Wei, N., Shevchenko, A., and Deshaies, R. (2001). Promotion of NEDD8-CUL1 Conjugate Cleavage by COP9 Signalosome. Science 292, 1382.

Lykke-Andersen, K., Schaefer, L., Menon, S., Deng, X.W., Miller, J.B., and Wei, N. (2003). Disruption of the COP2 signalosome Csn2 subunit in mice causes deficient cell proliferation, accumulation of p53 and cyclin E, and early embryonic death. Mol. Cell. Biol. 23, 6790-6797.

Maraschin, F.D., Memelink, J., and Offringa, R. (2009). Auxin-induced, SCFTIR1-mediated poly-ubiquitination marks AUX/IAA proteins for degradation. Plant Journal 59, 100-109.

Menon, S., Rubio, V., Wang, X., Deng, X.W., and Wei, N. (2005). Purification of the COP9 signalosome from porcine spleen, human cell lines, and Arabidopsis thaliana plants. Methods in enzymology 398, 468.

Menon, S., Chi, H., Zhang, H., Deng, X.W., Flavell, R.A., and Wei, N. (2007). COP9 signalosome subunit 8 is essential for peripheral T cell homeostasis and antigen receptor-induced entry into the cell cycle from quiescence. Nature immunology.

Merlet, J., Burger, J., Gomes, J.E., and Pintard, L. (2009). Regulation of cullin-RING E3 ubiquitin-ligases by neddylation and dimerization. Cell. Mol. Life Sci. 66, 1924-1938.

Min, K.W., Hwang, J.W., Lee, J.S., Park, Y., Tamura, T., and Yoon, J.B. (2003). TIP120A associates with cullins and modulates ubiquitin ligase activity. Journal Of Biological Chemistry 278, 15905-15910.

Miyauchi, Y., Kato, M., Tokunaga, F., and Iwai, K. (2008). The COP9/signalosome increases the efficiency of von hippel-lindau protein ubiquitin ligase-mediated hypoxia-inducible factor-alpha ubiquitination. Journal Of Biological Chemistry 283, 16622-16631.

Mockaitis, K., and Estelle, M. (2008). Auxin Receptors and Plant Development: A New Signaling Paradigm. In Annual Review Of Cell And Developmental Biology (Palo Alto: Annual Reviews), pp. 55-80.

Mundt, K.E., Liu, C., and Carr, A.M. (2002). Deletion Mutants in COP9/Signalosome Subunits in Fission Yeast Schizosaccharomyces pombe Display Distinct Phenotypes. Mol. Biol. Cell %R 10.1091/mbc.01-10-0521 13, 493-502.

Mundt, K.E., Porte, J., Murray, J.M., Brikos, C., Christensen, P.U., Caspari, T., Hagan, I.M., Millar, J.B.A., Simanis, V., Hofmann, K., and Carr, A.M. (1999). The COP9/signalosome complex is conserved in fission yeast and has a role in S phase. Current Biology 9, 1427-1430.

Murase, K., Hirano, Y., Sun, T.-p., and Hakoshima, T. (2008). Gibberellin-induced DELLA recognition by the gibberellin receptor GID1. Nature 456, 459-U415.

Nagpal, P., Walker, L.M., Young, J.C., Sonawala, A., Timpte, C., Estelle, M., and Reed, J.W. (2000). AXR2 encodes a member of the Aux/IAA protein family. Plant Physiology 123, 563-573.

Nijman, S.M.B., Luna-Vargas, M.P.A., Velds, A., Brummelkamp, T.R., Dirac, A.M.G., Sixma, T.K., and Bernards, R. (2005). A genomic and functional inventory of deubiquitinating enzymes. Cell 123, 773-786.

Okushima, Y., Overvoorde, P.J., Arima, K., Alonso, J.M., Chan, A., Chang, C., Ecker, J.R., Hughes, B., Lui, A., Nguyen, D., Onodera, C., Quach, H., Smith, A., Yu, G.X., and Theologis, A. (2005). Functional genomic analysis of the AUXIN RESPONSE FACTOR gene family members in Arabidopsis thaliana: Unique and overlapping functions of ARF7 and ARF19. Plant Cell 17, 444-463.

Olma, M.H., Roy, M., Le Bihan, T., Sumara, I., Maerki, S., Larsen, B., Quadroni, M., Peter, M., Tyers, M., and Pintard, L. (2009). An interaction network of the mammalian COP9 signalosome identifies Dda1 as a core subunit of multiple Cul4-based E3 ligases. Journal of cell science 122, 1035.

Oono, Y., Chen, Q.G., Overvoorde, P.J., Kohler, C., and Theologis, A. (1998). age Mutants of Arabidopsis exhibit altered auxin-regulated gene expression. The Plant Cell 10, 1649.

Oron, E., Mannervik, M., Rencus, S., Harari-Steinberg, O., Neuman-Silberberg, S., Sega, D., and Chamovitz, D.A. (2002). COP9 signalosome subunits 4 and 5 regulate multiple pleiotropic pathways in Drosophila melanogaster. Development 129, 4399-4409.

Oron, E., Tuller, T., Li, L., Rozovsky, N., Yekutieli, D., Rencus-Lazar, S., Segal, D., Chor, B., Edgar, B.A., and Chamovitz, D.A. (2007). Genomic analysis of COP9 signalosome function in Drosophila melanogaster reveals a role in temporal regulation of gene expression. Molecular Systems Biology 3.

Ouellet, F., Overvoorde, P.J., and Theologis, A. (2001). IAA17/AXR3: Biochemical insight into an auxin mutant phenotype. Plant Cell 13, 829-841.

Pan, Z.Q., Kentsis, A., Dias, D.C., Yamoah, K., and Wu, K. (2004). Nedd8 on cullin: building an expressway to protein destruction. Oncogene 23, 1985-1997.

Parry, G., Calderon-Villalobos, L.I., Prigge, M., Peret, B., Dharmasiri, S., Itoh, H., Lechner, E., Gray, W.M., Bennett, M., and Estelle, M. (2009). Complex regulation of the TIR1/AFB family of auxin receptors. Proceedings Of The National Academy Of Sciences Of The United States Of America 106, 22540-22545.

Patton, E.E., Willems, A.R., and Tyers, M. (1998). Combinatorial control in ubiquitin-dependent proteolysis: don't Skp the F-box hypothesis. Trends in Genetics 14, 236.

Peng, Z., Serino, G., and Deng, X.W. (2001a). A role of Arabidopsis COP9 signalosome in multifaceted developmental processes revealed by the

characterization of its subunit 3. Development (Cambridge, England) 128, 4277.

Peng, Z.H., Serino, G., and Deng, X.W. (2001b). Molecular characterization of subunit 6 of the COP9 signalosome and its role in multifaceted developmental processes in Arabidopsis. Plant Cell 13, 2393-2407.

Peters, J.M. (2002). The anaphase-promoting complex: Proteolysis in mitosis and beyond. Molecular Cell 9, 931-943.

Petroski, M.D., and Deshaies, R.J. (2005). Function and regulation of Cullin-RING ubiquitin ligases. Nature Reviews Molecular Cell Biology 6, 9-20.

Pickart, C.M. (2001). MECHANISMS UNDERLYING UBIQUITINATION. Annual Review of Biochemistry 70, 503.

Pintard, L., Kurz, T., Glaser, S., Willis, J.H., Peter, M., and Bowerman, B. (2003). Neddylation and deneddylation of CUL-3 is required to target MEI-1/katanin for degradation at the meiosis-to-mitosis transition in C-elegans. Current Biology 13, 911-921.

Podust, V.N., Brownell, J.E., Gladysheva, T.B., Luo, R.S., Wang, C.H., Coggins, M.B., Pierce, J.W., Lightcap, E.S., and Chau, V. (2000). A Nedd8 conjugation pathway is essential for proteolytic targeting of p27(Kip1) by ubiquitination. Proceedings Of The National Academy Of Sciences Of The United States Of America 97, 4579-4584.

Pringle, J.R., Preston, R.A., Adams, A.E.M., Stearns, T., Drubin, D.G., Haarer, B.K., and Jones, E.W. (1989). Fluorescence microscopy methods for yeast 31, 357-435.

Qi, Y.P., and Katagiri, F. Purification of Resistance Protein Complexes Using a Biotinylated Affinity (HPB) Tag. In Plant Immunity: Methods And Protocols, pp. 21-30.

Quint, M., Ito, H., Zhang, W., and Gray, W.M. (2005). Characterization of a novel temperature-sensitive allele of the CUL1/AXR6 subunit of SCF ubiquitin-ligases. The Plant Journal: for cell and molecular biology 43, 371.

Quint, M., Barkawi, L.S., Fan, K.-T., Cohen, J.D., and Gray, W.M. (2009). Arabidopsis IAR4 Modulates Auxin Response by Regulating Auxin Homeostasis. Plant Physiology 150, 748-758.

Ramos, J.A., Zenser, N., Leyser, O., and Callis, J. (2001). Rapid degradation of auxin/indoleacetic acid proteins requires conserved amino acids of domain II and is proteasome dependent. Plant Cell 13, 2349-2360.

Read, M.A., Brownell, J.E., Gladysheva, T.B., Hottelet, M., Parent, L.A., Coggins, M.B., Pierce, J.W., Podust, V.N., Luo, R.S., Chau, V., and Palombella, V.J. (2000). Nedd8 modification of Cul-1 activates SCF beta(TrCp)-dependent ubiquitination of I kappa B alpha. Mol. Cell. Biol. 20, 2326-2333.

Remington, D.L., Vision, T.J., Guilfoyle, T.J., and Reed, J.W. (2004). Contrasting modes of diversification in the Aux/IAA and ARF gene families. Plant Physiology 135, 1738-1752.

Risseeuw, E.P., Daskalchuk, T.E., Banks, T.W., Liu, E., Cotelesage, J., Hellmann, H., Estelle, M., Somers, D.E., and Crosby, W.L. (2003). Protein interaction

analysis of SCF ubiquitin E3 ligase subunits from Arabidopsis. Plant Journal 34, 753-767.

Ruegger, M., Dewey, E., Gray, W., Hobbie, L., Turner, J., and Estelle, M. (1998). The TIR1 protein of Arabidopsis functions in auxin response and is related to human SKP2 and yeast Grr1p. Genes and Development 12, 198.

Saha, A., and Deshaies, R.J. (2008). Multimodal Activation of the Ubiquitin Ligase SCF by Nedd8 Conjugation. Molecular Cell 32, 21-31.

Samach, A., Klenz, J.E., Kohalmi, S.E., Risseeuw, E., Haughn, G.W., and Crosby, W.L. (1999). The UNUSUAL FLORAL ORGANS gene of Arabidopsis thaliana is an F-box protein required for normal patterning and growth in the floral meristem. Plant Journal 20, 433-445.

Sasaki, A., Itoh, H., Gomi, K., Ueguchi-Tanaka, M., Ishiyama, K., Kobayashi, M., Jeong, D.H., An, G., Kitano, H., Ashikari, M., and Matsuoka, M. (2003). Accumulation of phosphorylated repressor for gibberellin signaling in an F-box mutant. Science 299, 1896-1898.

Schmidt, M.W., McQuary, P.R., Wee, S., Hofmann, K., and Wolf, D.A. (2009). F-Box-Directed CRL Complex Assembly and Regulation by the CSN and CAND1. Molecular Cell 35, 586-597.

Schwechheimer, C., and Deng, X.W. (2001). COP9 signalosome revisited: a novel mediator of protein degradation. Trends In Cell Biology 11, 420-426.

Schwechheimer, C., Serino, G., Callis, J., Crosby, W.L., Lyapina, S., Deshaies, R.J., Gray, W.M., Estelle, M., and Deng, X.W. (2001). Interactions of the COP9 signalosome with the E3 ubiquitin ligase SCFTIRI in mediating auxin response. Science (New York, N.Y.) 292, 1379.

Serino, G., and Deng, X.W.m. (2003). THE COP9 signalosome: Regulating plant development through the control of proteolysis. Annual Review Of Plant Biology 54, 165-182.

Serino, G., Tsuge, T., Kwok, S., Matsui, M., Wei, N., and Deng, X.W. (1999). Arabidopsis cop8 and fus4 mutations define the same gene that encodes subunit 4 of the COP9 signalosome. The Plant Cell 11, 1967.

Serino, G., Su, H., Peng, Z., Tsuge, T., Wei, N., Gu, H., and Deng, X.W. (2003). Characterization of the last subunit of the Arabidopsis COP9 signalosome: implications for the overall structure and origin of the complex. The Plant Cell 15, 719.

Sharon, M., Mao, H., Erba, E.B., Stephens, E., Zheng, N., and Robinson, C.V. (2009). Symmetrical Modularity of the COP9 Signalosome Complex Suggests its Multifunctionality. Structure 17, 31-40.

Sheard, L.B., Tan, X., Mao, H.B., Withers, J., Ben-Nissan, G., Hinds, T.R., Kobayashi, Y., Hsu, F.F., Sharon, M., Browse, J., He, S.Y., Rizo, J., Howe, G.A., and Zheng, N. (2010). Jasmonate perception by inositol-phosphate-potentiated COI1-JAZ co-receptor. Nature 468, 400-U301.

Shen, W.H., Parmentier, Y., Hellmann, H., Lechner, E., Dong, A.W., Masson, J., Granier, F., Lepiniec, L., Estelle, M., and Genschik, P. (2002). Null mutation

of AtCUL1 causes arrest in early embryogenesis in Arabidopsis. Molecular Biology Of The Cell 13, 1916-1928.

Smalle, J., and Vierstra, R.D. (2004). The ubiquitin 26S proteasome proteolytic pathway. Annual Review Of Plant Biology 55, 555-590.

Soucy, T.A., Smith, P.G., Milhollen, M.A., Berger, A.J., Gavin, J.M., Adhikari, S., Brownell, J.E., Burke, K.E., Cardin, D.P., Critchley, S., Cullis, C.A., Doucette, A., Garnsey, J.J., Gaulin, J.L., Gershman, R.E., Lublinsky, A.R., McDonald, A., Mizutani, H., Narayanan, U., Olhava, E.J., Peluso, S., Rezaei, M., Sintchak, M.D., Talreja, T., Thomas, M.P., Traore, T., Vyskocil, S., Weatherhead, G.S., Yu, J., Zhang, J., Dick, L.R., Claiborne, C.F., Rolfe, M., Bolen, J.B., and Langston, S.P. (2009). An inhibitor of NEDD8-activating enzyme as a new approach to treat cancer. Nature 458, 732-U767.

Stasinopoulos, T.C., and Hangarter, R.P. (1990). Preventing Photochemistry In Culture Media By Long-Pass Light Filters Alters Growth Of Cultured-Tissues. Plant Physiology 93, 1365-1369.

Staub, J.M., Wei, N., and Deng, X.W. (1996). Evidence for FUS6 as a component of the nuclear-localized COP9 complex in Arabidopsis. Plant Cell 8, 2047-2056.

Stelter, P., and Ulrich, H.D. (2003). Control of spontaneous and damage-induced mutagenesis by SUMO and ubiquitin conjugation. Nature 425, 188-191.

Strader, L.C., Monroe-Augustus, M., and Bartel, B. (2008). The IBR5 phosphatase promotes Arabidopsis auxin responses through a novel mechanism distinct from TIR1-mediated repressor degradation. BMC plant biology 8, 41.

Stuttmann, J., Lechner, E., Guerois, R., Parker, J.E., Nussaume, L., Genschik, P., and Noel, L.D. (2009). COP9 signalosome- and 26S proteasome-dependent regulation of SCFTIR1 accumulation in Arabidopsis. The Journal of biological chemistry 284, 7920.

Sun, Z.W., and Allis, C.D. (2002). Ubiquitination of histone H2B regulates H3 methylation and gene silencing in yeast. Nature 418, 104-108.

Szemenyei, H., Hannon, M., and Long, J.A. (2008). TOPLESS mediates auxin-dependent transcriptional repression during Arabidopsis embryogenesis. Science 319, 1384-1386.

Tan, X., Calderon-Villalobos, L.I., Sharon, M., Zheng, C., Robinson, C.V., Estelle, M., and Zheng, N. (2007). Mechanism of auxin perception by the TIR1 ubiquitin ligase. Nature 446, 640.

Tang, X., Orlicky, S., Lin, Z., Willems, A., Neculai, D., Ceccarelli, D., Mercurio, F., Shilton, B.H., Sicheri, F., and Tyers, M. (2007). Suprafacial orientation of the SCFCdc4 dimer accommodates multiple geometries for substrate ubiquitination. Cell 129, 1165-1176.

Terrell, J., Shih, S., Dunn, R., and Hicke, L. (1998). A function for monoubiquitination in the internalization of a G protein-coupled receptor. Molecular Cell 1, 193-202.

Thines, B., Katsir, L., Melotto, M., Niu, Y., Mandaokar, A., Liu, G., Nomura, K., He, S.Y., Howe, G.A., and Browse, J. (2007). JAZ repressor proteins are

targets of the SCFCO11 complex during jasmonate signalling. Nature 448, 661-U662.

Tian, Q., Nagpal, P., and Reed, J.W. (2003). Regulation of Arabidopsis SHY2/IAA3 protein turnover. Plant Journal 36, 643-651.

Tiwari, S.B., Hagen, G., and Guilfoyle, T. (2003). The roles of auxin response factor domains in auxin-responsive transcription. Plant Cell 15, 533-543.

Tiwari, S.B., Hagen, G., and Guilfoyle, T.J. (2004). Aux/IAA Proteins Contain a Potent Transcriptional Repression Domain. THE PLANT CELL 16, 533.

Tsuge, T., Matsui, M., and Wei, N. (2001). The subunit 1 of the COP9 signalosome suppresses gene expression through its N-terminal domain and incorporates into the complex through the PCI domain. Journal of Molecular Biology 305, 1.

Uhle, S., Medalia, O., Waldron, R., Dumdey, R., Henklein, P., Bech-Otschir, D., Huang, X., Berse, M., Sperling, J., Schade, R., and Dubiel, W. (2003). Protein kinase CK2 and protein kinase D are associated with the COP9 signalosome. Embo Journal 22, 1302-1312.

Ullah, Z., Buckley, M.S., Arnosti, D.N., and Henry, R.W. (2007). Retinoblastoma protein regulation by the COP9 signalosome. Molecular Biology Of The Cell 18, 1179-1186.

Ulmasov, T., Hagen, G., and Guilfoyle, T.J. (1999a). Dimerization and DNA binding of auxin response factors. Plant Journal 19, 309-319.

Ulmasov, T., Hagen, G., and Guilfoyle, T.J. (1999b). Activation and repression of transcription by auxin-response factors. Proceedings Of The National Academy Of Sciences Of The United States Of America 96, 5844-5849.

Ulmasov, T., Liu, Z.B., Hagen, G., and Guilfoyle, T.J. (1995). Composite Structure Of Auxin Response Elements. Plant Cell 7, 1611-1623.

Ulmasov, T., Murfett, J., Hagen, G., and Guilfoyle, T.J. (1997). Aux/IAA Proteins Repress Expression of Reporter Genes Containing Natural and Highly Active Synthetic Auxin Response Elements. THE PLANT CELL 9, 1963.

Vierstra, R.D. (2003). The ubiquitin/26S proteasome pathway, the complex last chapter in the life of many plant proteins. Trends In Plant Science 8, 135-142.

Voges, D., Zwickl, P., and Baumeister, W. (1999). The 26S proteasome: A molecular machine designed for controlled proteolysis. Annual Review Of Biochemistry 68, 1015-1068.

Wang, X.P., Feng, S.H., Nakayama, N., Crosby, W.L., Irish, V., Deng, X.W., and Wei, N. (2003). The COP9 signalosome interacts with SCFUFO and participates in Arabidopsis flower development. Plant Cell 15, 1071-1082.

Wee, S., Geyer, R.K., Toda, T., and Wolf, D.A. (2005). CSN facilitates Cullin-RING ubiquitin ligase function by counteracting autocatalytic adapter instability. Nature cell biology 7, 387.

Wei, N., and Deng, X.W. (1996). The role of the COP/DET/FUS genes in light control of arabidopsis seedling development. Plant Physiology 112, 871-878.

Wei, N., Chamovitz, D.A., and Deng, X.-W. (1994). Arabidopsis COP9 is a component of a novel signaling complex mediating light control of development. Cell 78, 117.

Wei, N., Tsuge, T., Serino, G., Dohmae, N., Takio, K., Matsui, M., and Deng, X.W. (1998). The COP9 complex is conserved between plants and mammals and is related to the 26S proteasome regulatory complex. Current Biology 8, 919-922.

Welchman, R.L., Gordon, C., and Mayer, R.J. (2005). Ubiquitin and ubiquitin-like proteins as multifunctional signals. Nature Reviews Molecular Cell Biology 6, 599-609.

Wilmoth, J.C., Wang, S.C., Tiwari, S.B., Joshi, A.D., Hagen, G., Guilfoyle, T.J., Alonso, J.M., Ecker, J.R., and Reed, J.W. (2005). NPH4/ARF7 and ARF19 promote leaf expansion and auxin-induced lateral root formation. Plant Journal 43, 118-130.

Wimuttisuk, W., and Singer, J.D. (2007). The Cullin3 ubiquitin ligase functions as a Nedd8-bound heterodimer. Molecular Biology Of The Cell 18, 899-909.

Wing, S.S.c. (2003). Deubiquitinating enzymes - the importance of driving in reverse along the ubiquitin-proteasome pathway. International Journal Of Biochemistry & Cell Biology 35, 590-605.

Wingfield, P. 2001. Protein Precipitation Using Ammonium Sulfate. Current Protocols in Protein Science. A.3F.1–A.3F.8.

Wong, L.M., Abel, S., Shen, N., delaFoata, M., Mall, Y., and Theologis, A. (1996). Differential activation of the primary auxin response genes, PS-IAA4/5 and PS-IAA6, during early plant development. Plant Journal 9, 587-599.

Woo, H.R., Chung, K.M., Park, J.H., Oh, S.A., Ahn, T., Hong, S.H., Jang, S.K., and Nam, H.G. (2001). ORE9, an F-box protein that regulates leaf senescence in Arabidopsis. Plant Cell 13, 1779-1790.

Wu, G., Xu, G.Z., Schulman, B.A., Jeffrey, P.D., Harper, J.W., and Pavletich, N.P. (2003). Structure of a beta-TrCP1-Skp1-beta-catenin complex: Destruction motif binding and lysine specificity of the SCF beta-TrCP1 ubiquitin ligase. Molecular Cell 11, 1445-1456.

Wu, J.T., Chan, Y.R., and Chien, C.T. (2006). Protection of cullin-RING E3 ligases by CSN-UBP12. Trends in cell biology 16, 362.

Wu, J.T., Lin, H.C., Hu, Y.C., and Chien, C.T. (2005). Neddylation and deneddylation regulate Cul1 and Cul3 protein accumulation. Nature Cell Biology 7, 1014-U1123.

Wu, K., Chen, A., and Pan, Z.-Q. (2000). Conjugation of Nedd8 to CUL1 Enhances the Ability of the ROC1-CUL1 Complex to Promote Ubiquitin Polymerization. Journal of Biological Chemistry 275, 32317.

Xu, L.H., Liu, F.Q., Lechner, E., Genschik, P., Crosby, W.L., Ma, H., Peng, W., Huang, D.F., and Xie, D.X. (2002). The SCFCOl1 ubiquitin-ligase complexes are required for jasmonate response in Arabidopsis. Plant Cell 14, 1919-1935.

Yang, M., Hu, Y., Lodhi, M., McCombie, W.R., and Ma, H. (1999). The Arabidopsis SKP1-LIKE1 gene is essential for male meiosis and may control homologue separation. Proceedings Of The National Academy Of Sciences Of The United States Of America 96, 11416-11421.

Yang, X., Menon, S., Lykke-Andersen, K., Tsuge, T., Di, X., Wang, X., Rodriguez-Suarez, R.J., Zhang, H., and Wei, N. (2002). The COP9 Signalosome Inhibits p27kip1 Degradation and Impedes G1-S Phase Progression via Deneddylation of SCF Cul1. Current Biology 12, 667.

Zhang, W., Ito, H., Quint, M., Huang, H., Noel, L.D., and Gray, W.M. (2008). Genetic analysis of CAND1-CUL1 interactions in Arabidopsis supports a role for CAND1-mediated cycling of the SCFTIR1 complex. Proceedings of the National Academy of Sciences of the United States of America 105, 8470.

Zhao, D.Z., Ni, W.M., Feng, B.M., Han, T.F., Petrasek, M.G., and Ma, H. (2003). Members of the Arabidopsis-SKP1-like gene family xhibit a variety of expression patterns and may play diverse roles in Arabidopsis. Plant Physiology 133, 203-217.

Zheng, J.Y., Yang, X.M., Harrell, J.M., Ryzhikov, S., Shim, E.H., Lykke-Andersen, K., Wei, N., Sun, H., Kobayashi, R., and Zhang, H. (2002a). CAND1 binds to unneddylated CUL1 and regulates the formation of SCF ubiquitin E3 ligase complex. Molecular Cell 10, 1519-1526.

Zheng, N., Schulman, B.A., Song, L.Z., Miller, J.J., Jeffrey, P.D., Wang, P., Chu, C., Koepp, D.M., Elledge, S.J., Pagano, M., Conaway, R.C., Conaway, J.W., Harper, J.W., and Pavletich, N.P. (2002b). Structure of the Cul1-Rbx1-Skp1-F box(Skp2) SCF ubiquitin ligase complex. Nature 416, 703-709.

Zhou, C.S., Wee, S., Rhee, E., Naumann, M., Dubiel, W., and Wolf, D.A. (2003). Fission yeast COP9/signalosome suppresses cullin acivity through recruitment of the deubiquitylating enzyme Ubp12p. Molecular Cell 11, 927-938.

Zhou, P.B., and Howley, P.M. (1998). Ubiquitination and degradation of the substrate recognition subunits of SCF ubiquitin-protein ligases. Molecular Cell 2, 571-580.

Appendix: Additional Figures

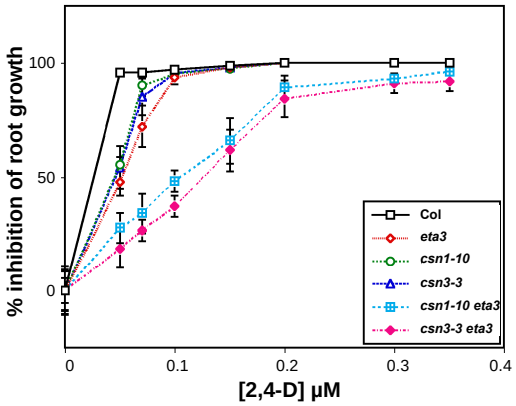

Figure 30. *csn1-10* and *csn3-3* enhance the *eta3* root growth resistance to 2,4-D.

The *eta3* mutation causes loss-of-function of the *SGT1b* gene (Gray et al., 2003). Inhibition of root elongation by increasing concentrations of the synthetic auxin 2,4-D was measured using 5-day-old (d.o.) seedlings of Col, *eta3, csn1-10*, *csn3-3*, *csn1-10 eta3* and *csn3-3 eta3*.
Seedlings (n≥15) grown on ATS medium were transferred to medium containing 2,4-D and grown for another four days. Data are presented as percent inhibition of root growth compared to growth on unsupplemented ATS. Error bars = SD.

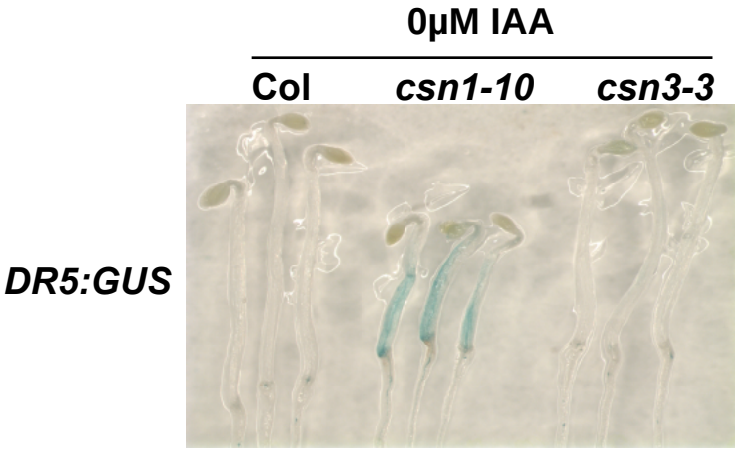

Figure 31. Endogenous auxin induced reporter expression in etiolated seedlings. 5-d.o. dark-grown transgenic Col, *csn1-10* and *csn3-3* carrying the DR5:GUS reporter were histochemical stained for GUS signal. Showing the hypocotyl region of etiolated seedlings and the endogenous auxin triggered *DR5:GUS* expression.

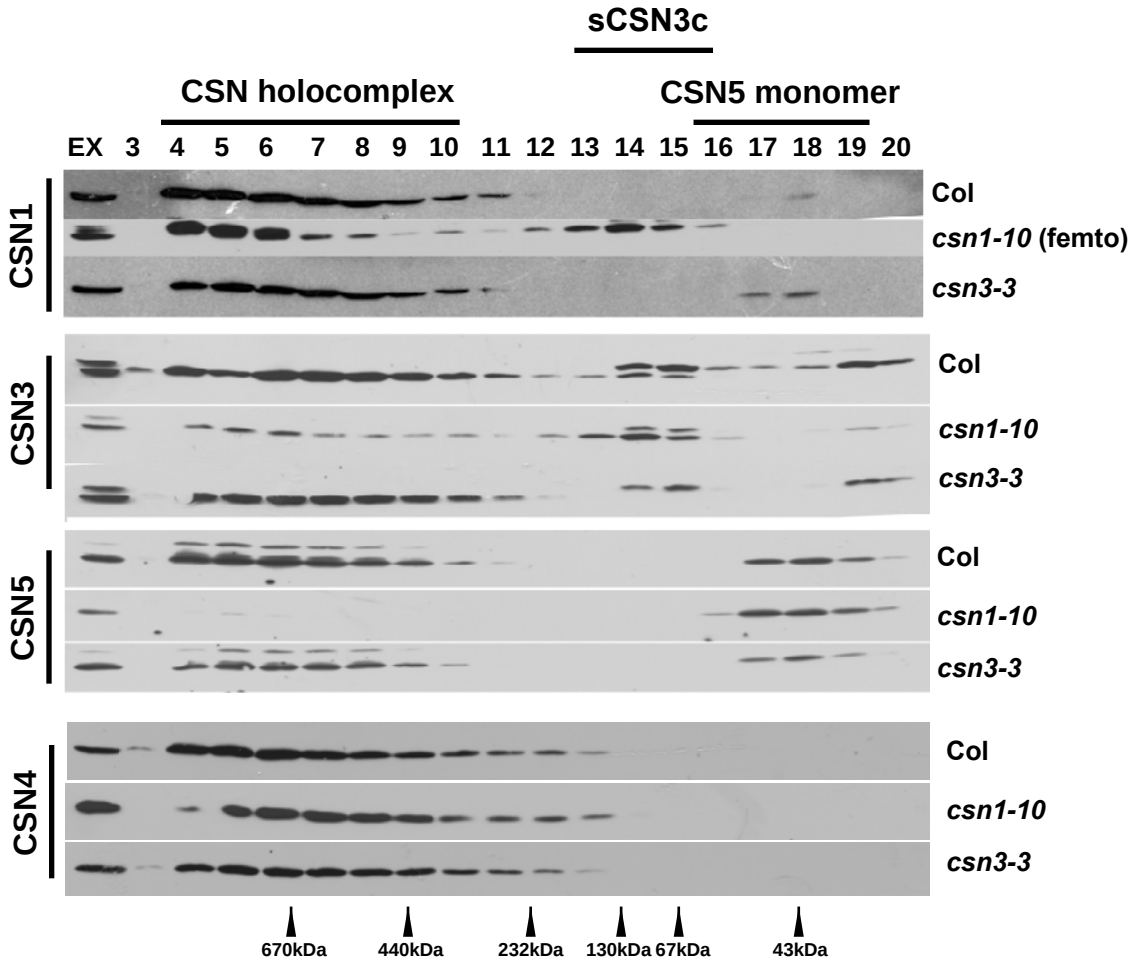

Figure 32. GF profilings of Col, *csn1-10* and *csn3-3* using extracts made in buffer containing detergent.

Showing CSN1, CSN3, CSN4 and CSN5 detections of gel-filtration (GF) fractions. 7-day-old Col, *csn1-10* and *csn3-3* seedling extracts were made using the GF buffer plus 0.5% NP40. The GF analyses were operated on a Pharmacia FPLC system with manually switching of the flow-path. Molecular mass standards are labeled at the bottom. EX stands for the extracts before GF. The CSN1 detection of *csn1-10* GF fractions was done using a femto ECL detection kit.

A

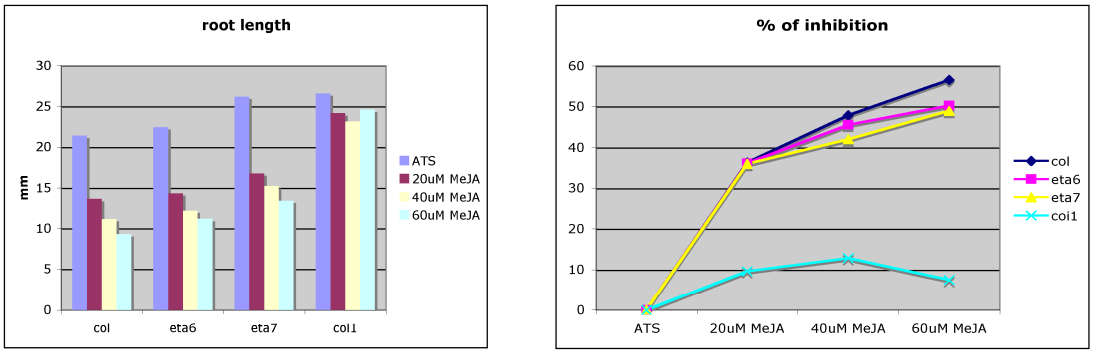

B

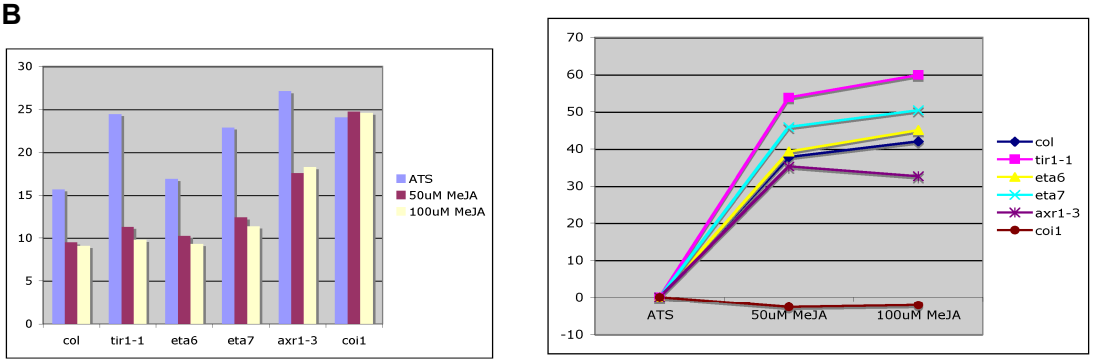

Figure 33. Me-JA induced root growth inhibition using seedlings of different genetic back-grounds.

Data presented here were done only once.

(A) Col, *eta6/csn1-10*, *eta7/csn3-3* and *coi1* mutants were grown horizontally on plates with Me-JA of indicated concentrations. After 8 days, seedlings were carefully pulled off the plates and the root lengths were measured (mm). Left shows the root lengths. Right shows the percentage of root growth inhibition.

(B) Col, *eta6/csn1-10*, *eta7/csn3-3*, *tir1-1*, *axr1-3* and *coi1* mutants were grown vertically on ATS plates for 6 days. Then the seedlings were transferred to Me-JA plates of indicated concentrations and grown partly horizontally (plates were placed at 45 degree angle, so that the root will go into the agar). After another 3 days, seedlings were carefully pulled off the plates and the root growth after transfer were measured (mm). Left shows the root lengths. Right shows the percentage of root growth inhibition.

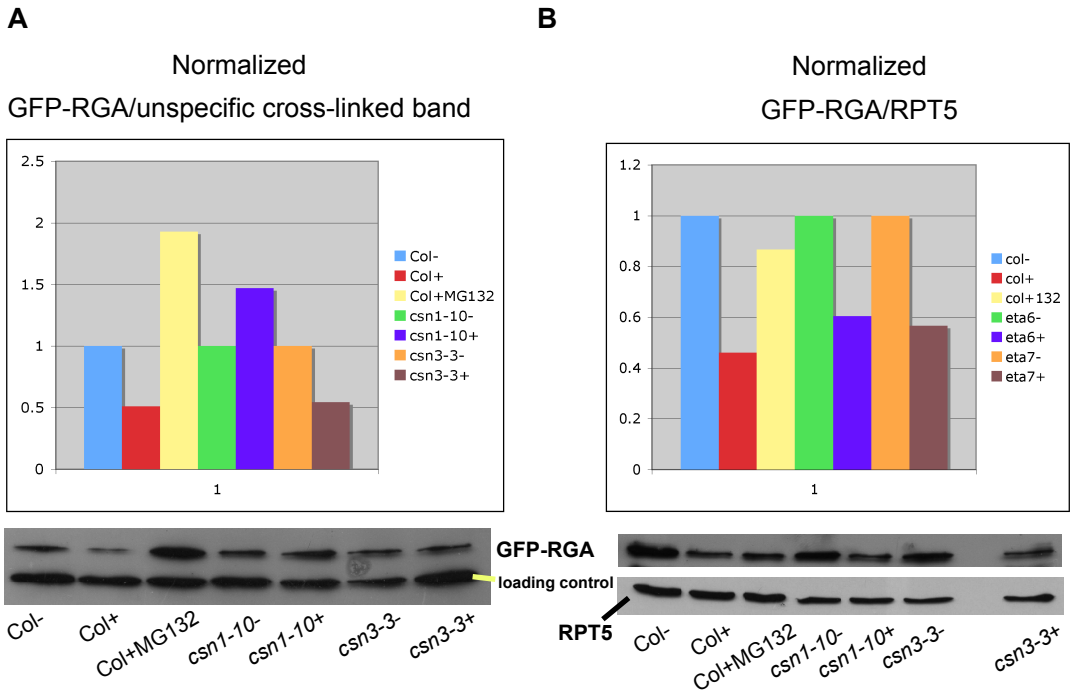

Figure 34. Gibberellin (GA) induced GFP-RGA degradation assays.

(A) Relative GFP-RGA (under 35S promoter) signal of Col, *csn1-10* and *csn3-3* with 20μM GA treatment for 1hr. 6-d.o. seedlings were soaked into liquid ATS with or without GA. Protein extracts were made after 1hr treatment. For mock treatment, seedlings were incubated in ATS. The GFP western signal was quantitatively measured using Photoshop (darkness density of the bands), and normalized using a unspecific cross-linked band as a loading control (lower band). Data were then normalized to the untreated sample accordingly (e.g. Col +GA/Col -GA, all the -GA samples are 100%). The graph was generated from two biological repeats. Bottom shows the GFP western result of one repeat.

(B) Similar as in (A), 6-d.o. seedlings were pre-treated with PAC for 48hrs to decrease endogenous GA production. During the 20μM GA treatment (1hr), 100ug/ml CHX was added to the ATS liquid, too. RPT5 was used as a loading control. The graph was generated from two biological repeats. Bottom shows one of the repeats (GFP and RPT5 western results)

The GFP signal or GFP/RPT5 value was all normalized to the untreated sample accordingly. Therefore the data I presented here ignored the fact that *csn1-10* or *csn3-3* seedlings may have more GFP-RGA to begin with, compared to that of Col. Also data were inconsistent among repeats.

A

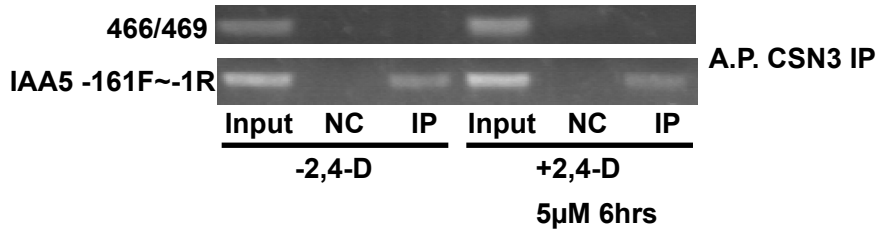

B

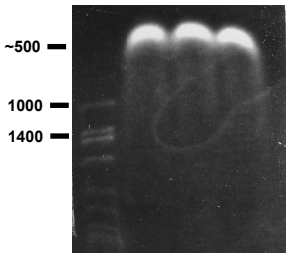

C

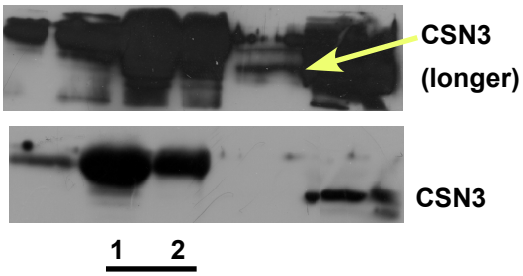

D

Ct value

		466/469	Repeat 1	Repeat 2	Repeat 3
-2,4-D	input	20.21	24.17	19.73	20.45
	NC	na	na	29.13	29.66
	IP	na	34.05	29.3	29.36
+2,4-D 1hr	input	20.58		20.03	
	NC	na		29.68	
	IP	na		27.98	
+2,4-D 6hr	input	20.91	23.4	20.57	20.81
	NC	na	na	33.57	32.24
	IP	na	34.37	27.06	29.07

E

Ct value

		IAA5 -161F~-1R		UBQ5	
		Col [DR5]	eta7 [DR5]	Col [DR5]	eta7 [DR5]
-2,4-D	Input	20.45	21.23		
	NC	29.66	29.96	26.87	26.71
	IP	29.36	29.59	27.5	27.31
+2,4-D 6hr	Input	20.81	21.5		
	NC	32.24	30.2	27.6	27.01
	IP	29.07	28.85	27.39	27.06

$$\text{Fold Enrichment} = \frac{2^{\text{Ct(IAA5 NC)-Ct(IAA5 IP)}}}{2^{\text{Ct(UBQ5 NC)-Ct(UBQ5 IP)}}}$$

Col -2,4-D	1.91
Col +2,4-D 6hr	7.78
eta7 -2,4-D	1.96
eta7 +2,4-D 6hr	2.64

Figure 35. Chromatin Immunoprecipitation (ChIP) experiments using IAA5 promoter primers.

The experiments were carried out as described in Saleh's paper (Nature Protocols, 2008). About 1g Col [DR5] seedlings were used for cross-linking. The chromatins were isolated and sonicated using the sonicator in Dr. Bob Brambl's lab at power 1.5~2, 20s 4 times. The IPs were done using affinity purified CSN3 antibody (at least 3hrs incubation). The salmon sperm DNA/protein Aagarose beads were used to pre-clean the sheared chromatins/protein extracts, as well as to harvest the CSN3 IP complexes (2hrs incubation). After reverse cross-linking and protein digestion, DNAs that were embedded by CSN3 were released. One pair of primers spanning the IAA5 promoter region (-161F~-1R) was used for quantitative PCR.

(A) The PCR results of one ChIP experiment using the IAA5 promoter specific primers. Input means the sheared DNA, NC means DNAs from mock IP without antibody. For more details, please refer to the nature protocol. The bands have been sequenced to be IAA5 fragments. 466/469 primers were mapping primers serving as a negative control.

(B) Testing the DNA shearing efficiency. Chromatins isolated from 2,4-D untreated, 1hr treated (5μM) and 6hr treated (5μM) samples were loaded to a 0.8% LE gel. Most DNAs were sheared into ~500bp fragments.

(C) Testing the CSN3 IP efficiency. CSN3 western detection of IP results from one experiment, showing the IP efficiency is very low. GF-EX(Col) is used to indicate the position of CSN3. The bands in IP samples are probably the heavy chain of IgG.

(D) Ct value of quantitative PCR using ChIP samples of Col [DR5] seedlings without/with 5μM 2,4-D treatment (1hr and 6hrs). The PCRs were done using IAA5 promoter primers (-161F~-1R), notice the decreased Ct value in IP samples (enrichment). Data contain 3 repeats, with repeat 1 represented in (A).

(E) Fold enrichment measured in Col [DR5] and eta7 [DR5], 2,4-D treated/untreated ChIP samples. Ct values of IAA5 and UBQ5 were used to normalize the data and calculate the fold enrichment. Notice that the 2,4-D treatment enhanced the association of CSN3 to the IAA5 promoter region, while in eta7, this association is reduced. Data was from only one biological repeat. Another one cannot repeat this result.

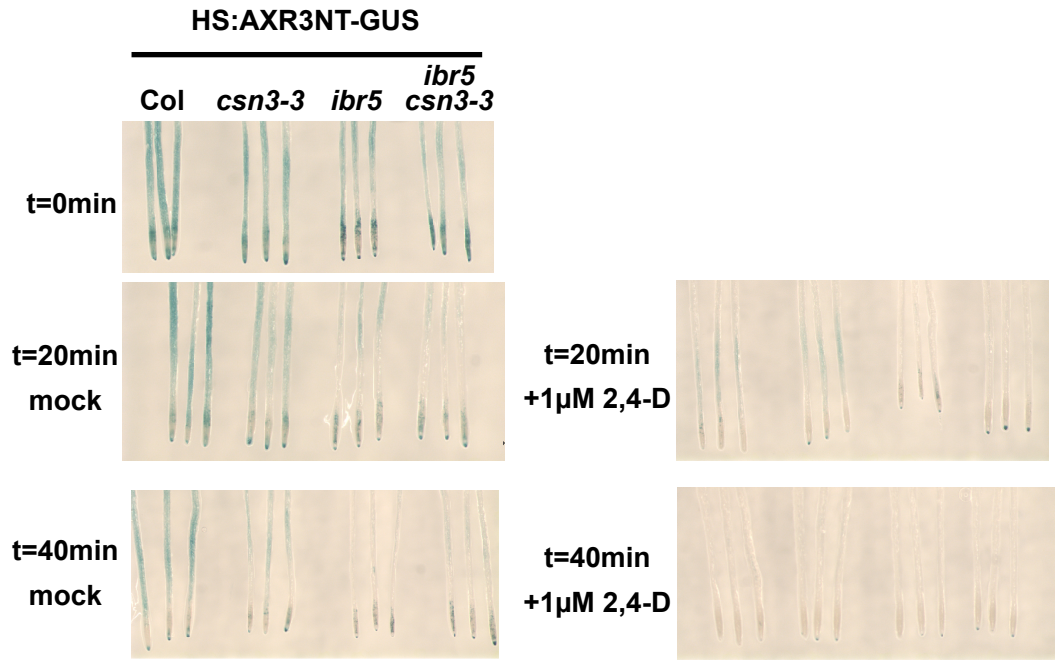

Figure 36. HS:AXR3NT-GUS degradation assay in Col, *csn3-3*, *ibr5* and *ibr5 csn3-3*.

5-d.o. seedlings of different genetic backgrounds containing the reporter were heat-shocked for 2hrs and stained for GUS signal at 0min, 20min and 40min, without or with 1μM 2,4-D treatment.

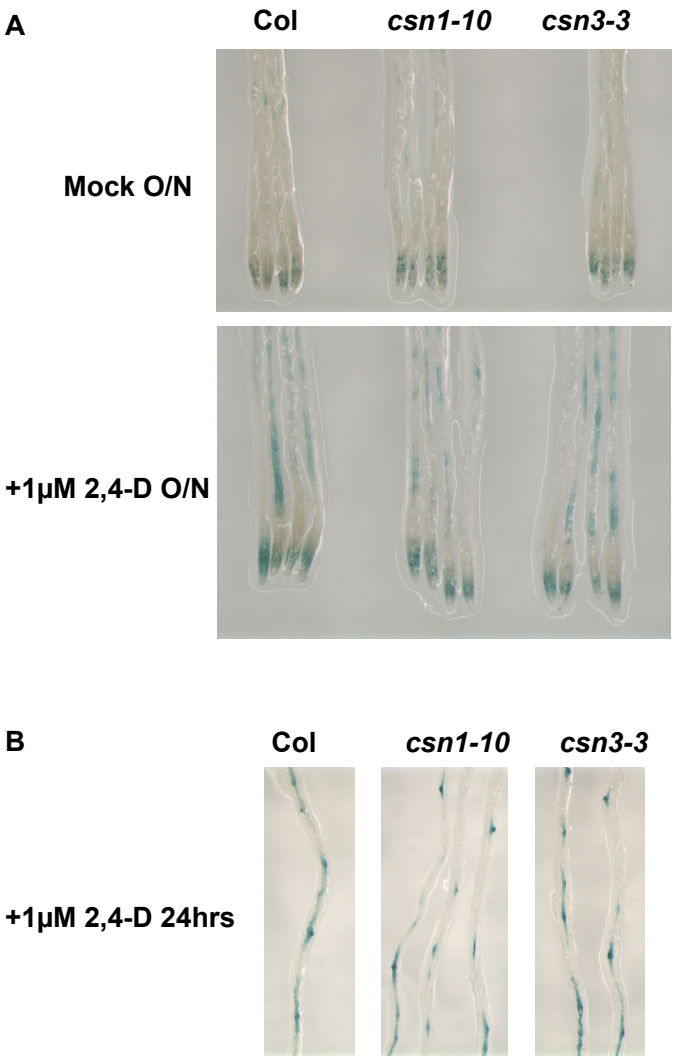

Figure 37. FA4 (CYCB:GUS) reporter expression in Col, *csn1-10* and *csn3-3.*
(A) 7-d.o. seedlings of different genetic backgrounds containing the reporter were incubated with or without 1μM 2,4-D overnight and stained for GUS signals. No obvious differences were found among different genetic backgrounds.
(B) No obvious differences in the FA4 reporter expression were found in the lateral root primordia region among different genetic backgrounds. 7-d.o. seedlings were 2,4-D treated for 24hrs and stained for GUS signals. Pictures were taken in the upper part of the root.

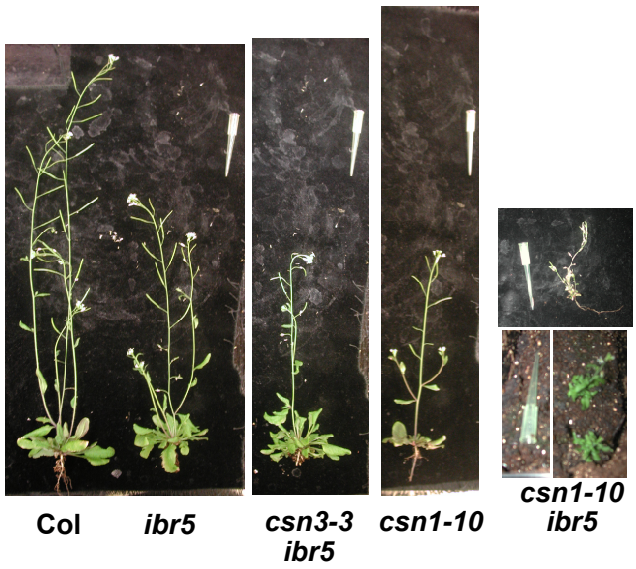

Figure 38. Adult plants of Col, *ibr5, csn3-3 ibr5*, *csn1-10* and *csn1-10 ibr5.*
45-d.o. plants were used for this figure. However, in a more recent repeating experiment, double mutants of *csn3-3 ibr5* and *csn1-10 ibr5* didn't look so different from the single *ibr5* mutant. The double mutants also need further genotyping and sequencing to confirm.

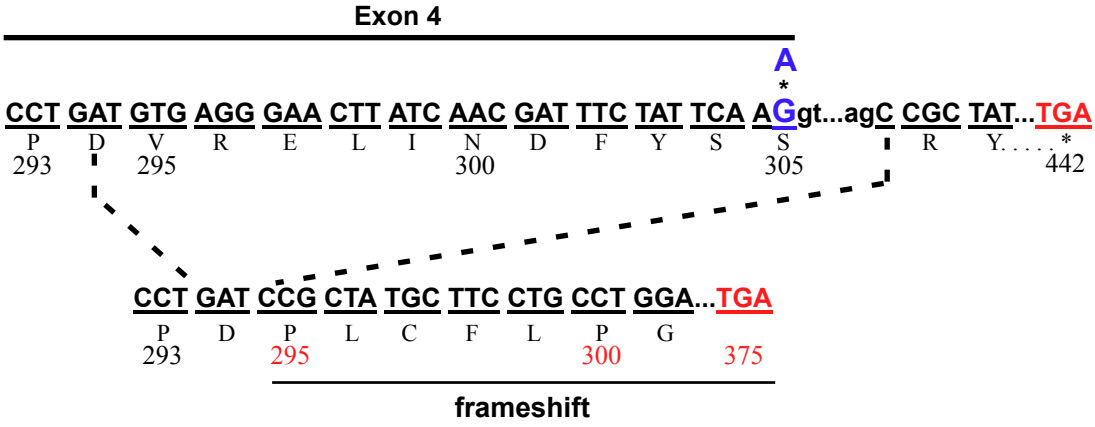

Figure 39. The *csn1-10* mutation causes an alternative splicing event on *AtCSN1* mRNA transcription.

The G to A point mutation occurs in the last base of *AtCSN1* exon 4 and affects mRNA splicing, in addition to the missense mutation (Ser to Asn at position 305). Sequencing the RT-PCR product shown in **Figure 14C** detected two mRNA species; one was correctly spliced cDNA containing the S305N substitution (top), while another one was produced from using an errant splice site 32 bases upstream, resulting a short deletion followed by a frameshift that truncates the protein (bottom). Capital letters stand for DNA base within exons, while lower-case letters are for introns.

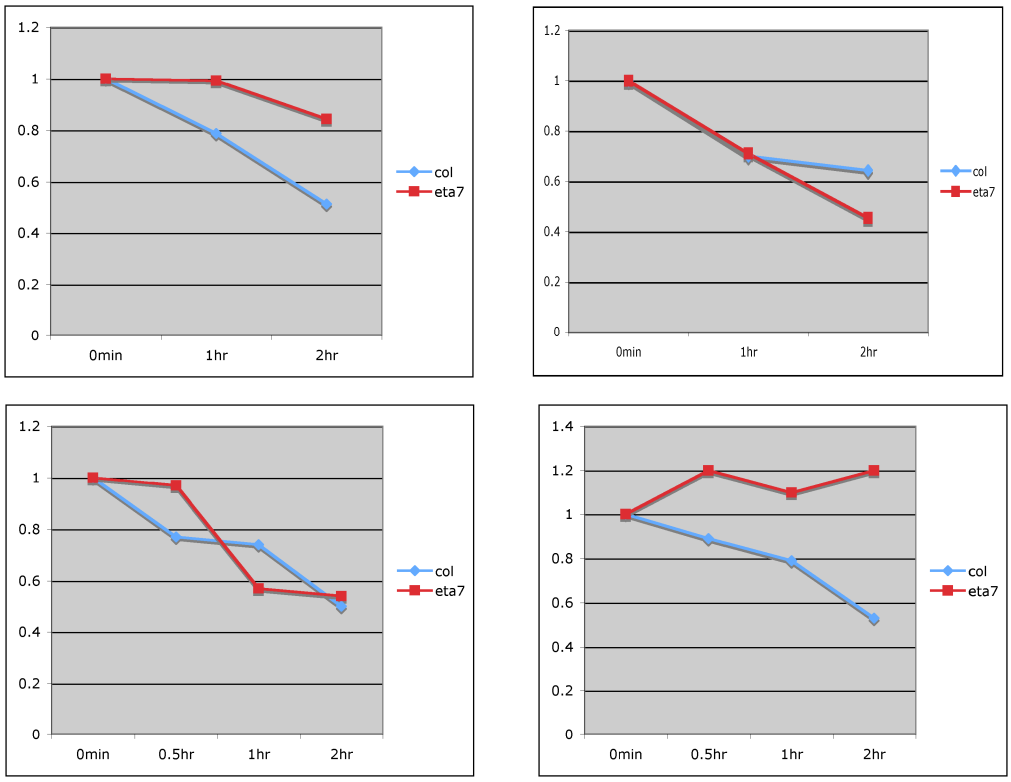

Figure 40. HS:AXR3NT-GUS degradation in 2,4-D untreated Col and *eta7/csn3-3* seedlings.

Figure shows 4 repeats of quantitative measurement (GUS-MUG assay) of HS:AXR3NT-GUS degradation in Col and *eta7/csn3-3*. 6-d.o. seedlings were heat shocked for 2 hours in liquid ATS, transferred to new ATS media of room temperature for 1hr (cooling down), and then sampled at 0, 0.5, 1 and 2 hrs. Protein extractions as well as GUS-MUG fluorescence (FU) measurements were done as described in the methods. 6 technical repeats each contains more than 15 seedlings for each timepoint. The value of FU/protein was then calculated and averaged among technical repeats. Data were presented as percentage of remaining GUS signal compared to the 0 timepoint.

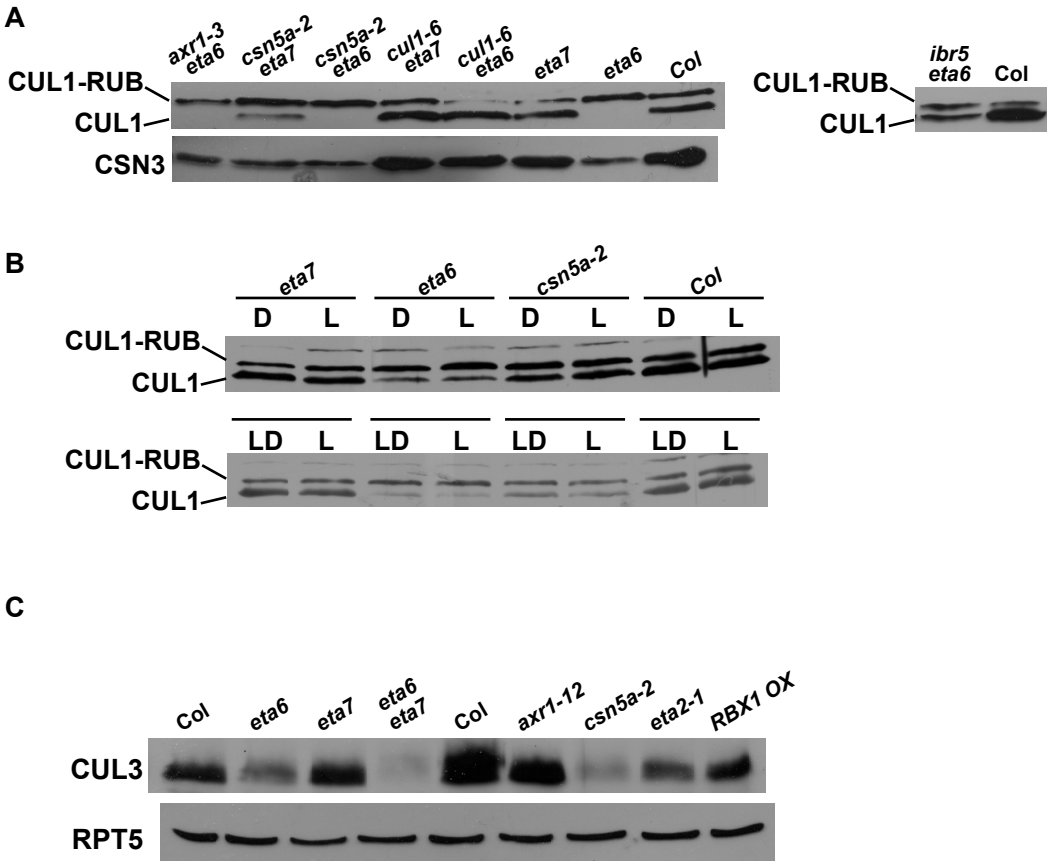

Figure 33. Cullin western detections of seedling extracts made from different genetic backgrounds.

Protein extracts were made from mutant seedlings in Buffer A (0.5% NP-40).

(A) CUL1 western was done using Col, *eta6*, *eta7*, *cul1-6 eta6*, *cul1-6 eta7*, *csn5a-2 eta6*, *csn5a-2 eta7* and *axr1-3 eta6* samples.

(B) CUL1 western was done using Col, *eta6*, *eta7* and *csn5a-2* samples made from light grown (7-d.o., "L"), dark grown (1 day under light condition, 6 days under dark condition, "D") and light to dark transferred (6 days under light condition, then transferred to dark for 1 day, "LD") seedlings

(C) CUL3 western was done using Col, *eta6*, *eta7*, *eta6 eta7, csn5a-2, eta2-1, axr1-12* and RBX1 overexpression line (*RBX1 OX*). RPT5 was used as a loading control.

A

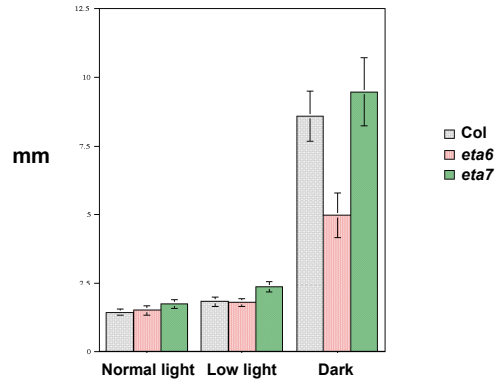

	col	col sd	eta6	eta6 sd	eta7	eta7 sd
normal light	1.43	0.11	1.51	0.17	1.73	0.16
low light	1.81	0.18	1.78	0.15	2.37	0.19
dark	8.57	0.91	4.99	0.81	9.47	1.24

B

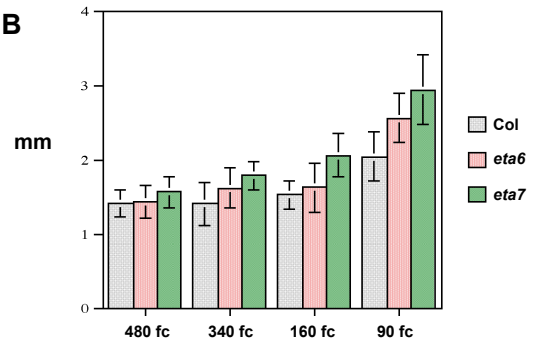

	col	col sd	eta6	eta6 sd	eta7	eta7 sd
480fc	1.42	0.18	1.44	0.22	1.58	0.21
340fc	1.42	0.29	1.63	0.27	1.8	0.19
160fc	1.54	0.19	1.64	0.33	2.07	0.29
90fc	2.05	0.33	2.5	0.33	2.95	0.47

C

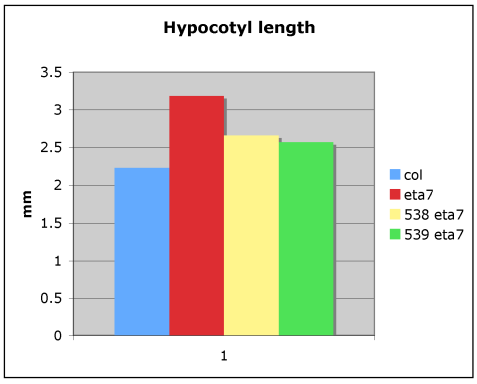

col	eta7	538 eta7	539 eta7	
2.23	3.18	2.66	2.57	ave
0.34	0.55	0.47	0.49	sd

col	eta7	569 L2	569 L4	
1.92	2.39	1.84	1.88	ave
0.27	0.28	0.22	0.16	sd

D

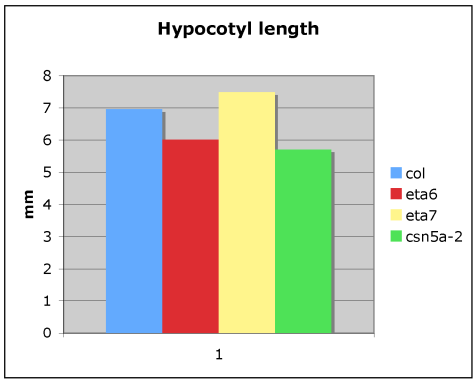

col	eta6	eta7	csn5a-2	
6.95	6.01	7.48	5.71	ave
1.1	1.11	0.89	1.09	sd

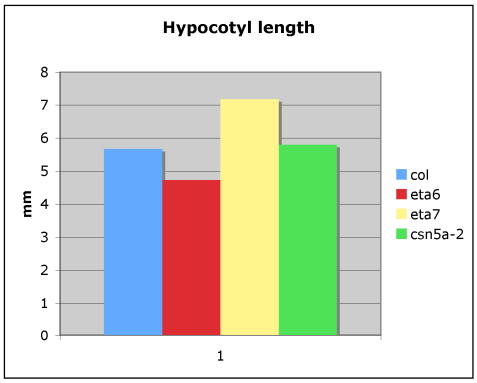

col	eta6	eta7	csn5a-2	
5.67	4.73	7.18	5.8	ave
0.8	0.66	1	0.83	sd

Figure 42. Hypocotyl lengths of *eta6* and *eta7* seedlings under different light conditions.
(A) Hypocotyl lengths of 6-d.o. Col, *eta6* and *eta7* seedlings (n≥15) grown under normal light, dim light (one film on top of the plates) and dark conditions. Seedlings were grown horizontally. Error bars indicate the standard deviation (sd).
(B) Hypocotyl lengths of 6-d.o. Col, *eta6* and *eta7* seedlings (n≥15) grown under dim light conditions. Seedlings were grown horizontally. A film was placed on top of each plate, which was then kept a certain distance from the light source. By using a illumination meter (Weston, Model 756), the light intensities were determined (480 foot candle (fc), 340 fc, 160 fc and 90fc).
(C) Hypocotyl lengths of 6-d.o. Col, *eta7, eta7* [*35S:myc-CSN3*] (538), *eta7* [*35S:myc-ETA7*] (539) and two independent complementation lines of *eta7* [g*CSN3*] (569, Line2 and Line 4) seedlings (n≥15) grown under dim light condition (90fc). Left, Col, eta7, 538 and 539. Right, Col, eta7, 569 L2 and 569 L4.
(D) Hypocotyl lengths of 6-d.o. Col, *eta6, eta7* and *csn5a-2* seedlings (n≥15) grown under red light or far-red light condition. Left, red light treatment. Right, far-red light treatment.